August 2007

Wireless Multiple Access Communication over Collision Frequency Shift Channels

Chen Xia
University of Nebraska-Lincoln, chenxia@mariner.unl.edu

Wireless Multiple Access Communication

over Collision Frequency Shift Keyed Channels

A Dissertation

by

Chen Xia

Presented to the Faculty of

The Graduate College at the University of Nebraska

In Partial Fulfillment of Requirements

for the Degree of Doctor of Philosophy

Major: Engineering

(Electrical Engineering)

Under the Supervision of Professor Lance C. Pérez

Lincoln, Nebraska

August, 2007

WIRELESS MULTIPLE ACCESS COMMUNICATION OVER COLLISION FREQUENCY SHIFT KEYED CHANNELS

Chen Xia, Ph.D.

University of Nebraska, 2007

Advisor: Lance C. Pérez

A collision frequency shift keyed system (CFSK) using M-ary FSK signaling is investigated. CFSK is a wireless multiple access system in which users access a channel without cooperation. This results in collisions when users simultaneously transmit signals in the same frequency band. However, analysis has shown that the CFSK system has the potential to achieve greater capacities than binary multiple access systems.

In this dissertation, bounds on the multiuser capacity of the noisy synchronous and asynchronous CFSK channel are derived. Analytical models are designed for investigating these capacity results. It is shown that the capacity of the noisy synchronous CFSK channel is greater than the capacity of multiuser direct-squence (DS) and frequency-hopping (FH) CDMA systems. The capacity of the asynchronous CFSK channel is significantly high in the over-loaded case and this capacity is greater than most asynchronous CDMA systems.

Multiuser detection on the CFSK channel is then investigated. Due to the ex-

tremely high complexity of the optimal multiuser detector, iterative multiuser detectors are considered. Three simplified iterative multiuser detectors are derived, the wide sense most probable (WSMP) combinations detector, the narrow sense most probable (NSMP) combinations detector and the relaxation detector. The WSMP detector utilizes the K-most probable combinations (K-MPC) and the k-most probable frequencies (k-MPF) metric. Simulations show that these detectors can achieve near single-user performance under a variety of load conditions. The relaxation detector, in particular, offers excellent performance.

Randomly generated convolutional codes are considered for use in the CFSK system. The choice of code parameters for different detectors and different transmission rates are discussed. Simulation results show that with the proper choice of code parameters, it is possible to achieve performance near that of uniquely decodable codes. In addition, the achieved rates surpass the rates for most CDMA systems.

ACKNOWLEDGEMENTS

First I would like to express my gratitude to Dr. Lance C. Pérez for his direction and encouragement throughout this research. His kindest support is the most important reason that I can complete this dissertation. Special thanks are given to my supervisor committee for their valuable comments in the development of this dissertation.

I would like to thank Dr. Fan Jiang. I enjoy talking with him about error control coding and the Houston Rockets. Also, thanks are given to all my labmates. They bring me a fulfilling and fun experience in the MC^2 lab. I learned a lot in talking with Shuo Shen and Robert Sprick about sensor networks. I am grateful to Paul Kavan who helped me setup my computer again and again. Also, it is fun to talk with Peter Lavin about music.

At last, I owe a debt of gratitude to my dear family. My wife and my parents keep on supporting me throughout these years. Their love is the warmest thing in my life and provides me the motivation to complete my doctoral study.

DEDICATION

To my grandmother, Suqiong Li.

Contents

List of Figures

List of Tables

List of Abbreviations and Symbols

aPEP	*a Priori* enumeration polynomial
AWGN	Additive white Gaussian noise
BER	Bit error rate
CDMA	Code division multiple access
CFSK	Collision frequency shift-keyed
CTEP	Channel transition enumeration polynomial
DS-SSMA	Direct sequence spreading spectrum multiple access
FDMA	Frequency division multiple access
FH-SSMA	Frequency hop spreading spectrum multiple access
GSM	Globe system for mobile communication

IC	Interference Cancellation
ID	Iterative detection
K-MPC	K most probable combinations
k-MPF	k most probable frequencies
KS	Kautz Singleton code
MAP	Maximum *a posteriori*
MLSD	Most likelihood sequence detection
NSMP	Narrow sense most probable combinations
P.D.F.	Probability density function
P.S.D.	Power spectral density
RSC	Recursive systematic convolutional code
RS	Reed Solomon
SNR	Signal to noise ratio
SSMA	Spreading spectrum multiple access
TC	Turbo Code

TCMA	Trellis-coded multiple access
TDMA	Time division multiple access
UDBC	Uniquely decodable block code
UDC	Uniquely decodable code
WSMP	Wide sense most probable combinations
α	Forward metric of MAP algorithm
A_1	The *a priori* information input to the metric computation
A_2	The *a priori* information input to the MAP decoders
$A(W)$	The distance enumerating function for a super-trellis code
A_d	The number of code word pairs on the super-trellis with Hamming distance d
β	Backward metric of MAP algorithm
C_0	The set of all possible frequency combinations in computing the channel metric of the 0^{th} user
C_0'	The set of most probable frequency combinations in computing the channel metric of the 0^{th} user in narrow sense or wide sense

C_0''	A super set of C_0 containing frequency combinations accord two Constraint 2
$d_{\min}$	Minimum distance of the super-trellis code
D_j	Binary difference matrix in the j^{th} iteration in the construction of UDBC
$\tilde{D}$	Binary difference matrix for the construction of binary UDBC
$\tilde{D}^*$	Non-binary difference matrix for the construction of non-binary UDBC
E_1	The extrinsic information output from the metric computation
E_2	The extrinsic information output from the MAP decoders
E_s	Symbol energy
$\Phi_j^{(i_k)}$	Asynchronous phase for user $U^{(i_k)}$ to transmit frequency f_j
f_j	The j^{th} frequency
$f_{j_i}^{(i)}$	The frequency with index j_i and transmitted by the i^{th} user
$\bar{F}$	Received frequency block consisting of frequency vectors from time 0 to $T-1$
$\bar{F}_t$	Received frequency block consisting of frequency vector at time t
$\mathcal{F}$	The set of M frequencies $\{f_0, \ldots, f_{M-1}\}$
γ	Branch transition probability for a symbol

i	Index, counting the users, range: $0 \cdots T-1$
j	Index, counting the frequencies, range: $0 \cdots M-1$
K	Number of combinations used in K-MPC or k-MPF
κ	Spectral efficiency
Λ	Real numbers between 0 and 1, i.e. $\lambda = [0,1] \in \mathbb{R}$
M	Number of frequencies
M_{aPEP}	The number of multiplications needed for computing the aPEP in the relaxation metric
M_{CTEP}	The number of multiplications needed for computing the CTEP in the relaxation metric
N	Length of a coding block
N_o	Noise power defined as one-sided power spectrum
N_{NSMP}	The total of computation needed for NSMP in the first iteration
N_{aPEP}	The number of additions needed for computing the aPEP in the relaxation metric

N_{CTEP} The number of additions needed for computing the CTEP in the relaxation metric

Ω Bandwidth expansion factor

$p_{j_u}^{(u)}$ A priori probability for frequency f_{j_u} for user U_u

$P^{(u)}$ A priori probability block for all frequencies of user U_u

$P(\bar{F}_t|f_{j_i}^{(i)})$ The channel metric for the i^{th} user that denotes the probability of the received signal vector given that the i^{th} user transmits the frequency $f_{j_i}^{(i)}$

P_{dist} The distance between a frequency combination and the received signal vector $\bar{F}_t$

P_{NSMP} The channel measurement in searching the narrow sense most probable combinations

P_{WSMP} The channel measurement in searching the wide sense most probable combinations

q Order of the Galois Field GF(2^q).

Q The number of quantization levels in the function $\mathcal{S}$

Q_j Quantization level of frequency f_j in the function $\mathcal{S}$

ρ_j	Received energy for frequency j
R	Rate of the convolutional codes
R_c	Transmission rate in bits/symbol achieved by a user
S_t	The state of trellis at time t
$\bar{s}_t$	The set of symbols sent by all the users at time t
$\hat{\bar{s}}_t$	The set of symbols estimated for all the users at time t
$\mathcal{S}$	A function that maps a M-dimensional vector in Λ^M to a subset of integers Ξ
Ξ	A subset of integers
T	Number of users
$T_j(D)$	The channel transition enumeration polynomial for the frequency f_j
$T(D)$	The channel transition enumeration polynomial
$T_{\max}$	The maximal umber of users to achieve the spectral efficiency for a given transmission rate and number of frequencies
$U^{(i)}$	The i^{th} user that access to the system
μ_j	Multiplicity of frequency f_j, denotes the number of transmissions on f_j

$\bar{\mu}$	Pattern of a frequency combination
$\bar{\mu}_{\max}$	The pattern of the most probable frequency combination
$\hat{v}_i$	Output symbol of the consensus decoder for the i^{th} user
$V_j(D)$	The *a priori* enumeration polynomial for frequency f_j
$V_j^{(i)}(D)$	The *a priori* enumeration polynomial for frequency f_j of user $U^{(i)}$
ξ_x	The approximated in-phase component of the demodulation output
ξ_y	The approximated quadrature component of the demodulation output

Chapter 1

Introduction

In the last several decades, the world has witnessed the rapid development and widespread application of multiple access communication systems, especially in mobile communication systems. A great deal of effort has been made to more efficiently utilize the limited resources of the wireless channels in these systems.

In a multiple access system, multiple users communicate with a common receiver over the same communication channel and the receiver recovers each user's information by allocating channel resources to different users. In frequency division multiple access (FDMA) systems, time division multiple access (TDMA) systems [1], and code division multiple access (CDMA) systems [2], different frequency bands, time slots and code spaces are assigned to the users, respectively.

Many multiple access mobile communication systems are based on a philosophy

that treats every user except for the current user of interest as unwanted noise, called multiple access interference (MAI). These systems are called single-user receiver systems. The presence of MAI prevents these systems from more efficiently utilizing the channel. Much research [3]-[8] has shown that the signals from other users are useful and can be utilized to improve the performance and capacity of these systems. Techniques that do this are generally called multiuser detection and a multiple access system with multiuser detection is called a multiuser system. Instead of making the signals uncorrelated, systems using multiuser detection attempt to manipulate the correlation among the users' signals.

Much research has focused on multiuser CDMA systems, even though another category of multiple access systems based on collision-type channels has been shown [10]-[14] to be more efficient. This dissertation focuses on the performance and design of a particular multiple access system with a collision-type channel called collision frequency shift-keying (CFSK). A diagram of a CFSK system is shown in Figure 1.1.

Suppose that there are T users accessing the system, each of whom generate and transmit signals independently. Each transmitter uses M-ary FSK modulation and all users share the same set of frequencies $\mathcal{F}$ denoted by

$$\mathcal{F} = \{f_0, \ldots, f_{M-1}\}.$$

Since there is no cooperation among the T users, collisions occur when two or more of the users send the same frequency at the same time. At the receiver, a non-coherent

detector outputs a vector $\bar{F}$ denoted by

$$\bar{F} = [\rho_0, \rho_1, \ldots, \rho_{M-1}]. \tag{1.1}$$

If the entry ρ_j denotes the energy level of frequency f_j, and thus indicates the number of transmissions on this frequency, then the channel is called the CFSK channel with intensity information. If $\rho_j \in \{0, 1\}$, where $\rho_j = 1$ when there is energy detected on frequency f_j, and $\rho_j = 0$ when there is no energy detected, then the channel is called the CFSK channel without intensity information. The multiuser detector performs multiuser detection on the vector $\bar{F}$, and outputs an estimate of each user's transmitted information.

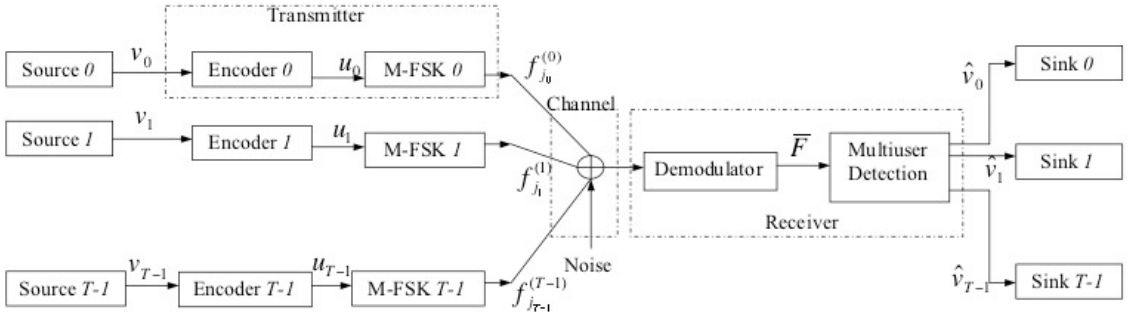

Figure 1.1: Block diagram of a CFSK system.

1.1 Motivation for CFSK

The high spectral efficiency of the CFSK channel provides the primary motivation for investigating this system. Chang and Wolf [13] derived the capacity of the noiseless T-user, M-frequency multiple-access channel with and without intensity information in 1982. In [14], Grant and Schlegel compared the results of Chang and Wolf and the capacity of a CDMA system given in [15, 16, 9]. This comparison is shown in Figure 1.2. Note that the number of chips in the CFSK system is defined as the number of frequencies and the spreading factor is defined as the ratio of the number of chips to the number of users.

The results in Figure 1.2 show that the CFSK channel with or without intensity information has a higher sum rate, or capacity, than conventional CDMA and CDMA with multiuser detection for moderate to large spreading factors. The sum rate is defined as a summation of the maximal allowable transmission rates of all the users that access the channel. In Figure 1.2, the capacity is normalized by the number of chips so that this capacity is fair for all spreading factors. For large spreading factors, the convergence of the two capacity curves for each system suggests that single user detectors are sufficient. For low spreading factors, that is when a large number of users are sharing the same bandwidth, the CFSK system with intensity information has a greater capacity than both conventional CDMA and CDMA with multiuser detection. However, the advantage of the CFSK system with intensity information

is not as high as it is for moderate spreading factors. For the CFSK system without intensity information, the capacity drops dramatically for low spreading factors, since the "0 or 1" detection of each frequency causes a large loss of channel information in heavily loaded systems. These results suggest that the CFSK channel with intensity information has more potential than CDMA for achieving high information rates, especially when the spreading factor is moderate, say, between 1 and 10.

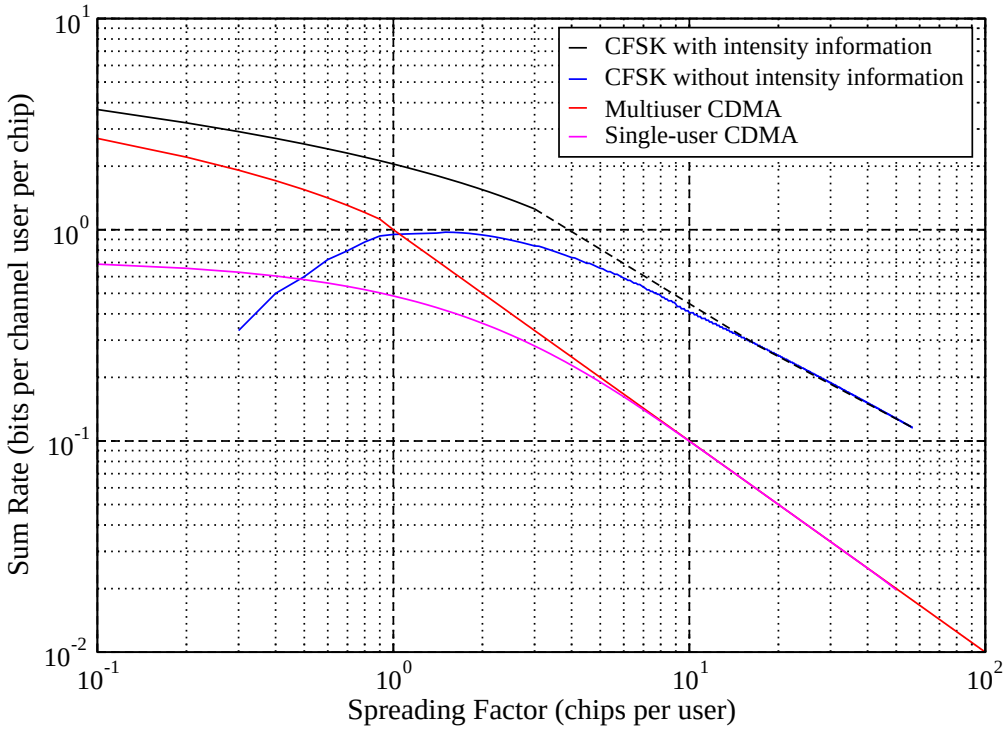

Figure 1.2: A comparison of the sum rates of CDMA and CFSK systems.

In addition to increased multiuser capacity, there are many other attractive features of the CFSK system with intensity information. First, it is resistant to the near-far effect, as the receiver performs multiuser detection. The near-far effect occurs when some interfering users have a much higher received power than the received power from the user of interest. This can significantly degrade the performance of a single-user detector since single-user detectors generally treat all the interfering users' signals as noise. With multiuser detection, the received signals from the interfering users are utilized in detecting the information from the user of interest. Thus, though the received power from the interfering users may be much higher than the received power from the user of interest in multiuser detectors, the detection results for interfering users can be helpful for the detection of the user of interest.

In [3], Verdú proved that the optimal multiuser detector in a CDMA system with orthogonal spreading codes can provide perfect resistance to the near-far effect. That is, the received power among the users maybe highly unbalanced, but the performance of the detector is not affected by the near-far effect as long as the received signal-noise-ratio (SNR) for each of the users is above a threshold. For suboptimal multiuser detectors and non-orthogonal spreading codes, Verdú showed that the multiuser detector can still tolerate an imbalance in the received power to some extent. Capacity results for the CFSK system show that the CFSK system with multiuser detection is also resistant to the near-far effect.

Second, because of the inherent frequency diversity of the CFSK system, its performance over frequency selective-fading channels may be better than that of a conventional multiple access system. In addition, the CFSK system may be resistant to inter-symbol interference (ISI) since the individual frequency symbols can be chosen to be longer than the delay spread of many fading channels. The reason for this is that the detection is done in the frequency domain. If the delay spread of a frequency symbol is longer than the delay spread of the fading channel, no symbol entirely overlaps an adjacent symbol in the time domain. By choosing the appropriate sampling time, the frequency spectrum of each individual frequency symbol can be recovered.

The third feature of the CFSK system is that the system can adjust the users' transmission rates by simply changing the size of the modulation alphabet. Thus, the CFSK system can be extended to a multi-rate system in which users use different size alphabets. This feature makes the CFSK system very attractive in multimedia applications over wireless networks, especially over ad hoc wireless networks with various Quality of Service (QoS) requirements.

Finally, the non-binary nature of the CFSK system enables better bit error performance than binary systems. In an uncoded single-user system, analytical results show that the bit error rate (BER) of FSK modulation improves as the size of the alphabet gets larger. This suggests that the CFSK system has the potential of achieving better BER performance than systems using binary modulation schemes. Note that the im-

provement in BER performance is at the cost of increased bandwidth. However, the CFSK system with multiuser detection can achieve greater spectral efficiency than other multiple access systems as shown in Figure 1.2, where the normalized sum rate is equivalent to the spectral efficiency.

No implementation of the CFSK receiver exist so far to achieve a near capacity rate and decent BER performance with low complexity. The optimal CFSK receiver using maximum likelihood sequence detection (MLSD) has an exponential complexity with the number of the users that is impractical [11]. Chang and Wolf's code design requires specific receiver structure that has poor BER performance on noisy channels [13]. Grant and Schlegel designed a consensus receiver for the CFSK system without intensity information that can not approach the capacity of the CFSK system with intensity information [14]. In [17], the channel metric of the CFSK channel with intensity information requires an iterative multiuser detector with exponential complexity with the number of users that is impractical. Thus, efforts are made in this dissertation to design simplified iterative multiuser detectors with near capacity rate and decent BER performance.

1.2 Overview

This dissertation focuses on three important aspects of the the CFSK system: i) theoretical bounds on the channel capacity, ii) the design of multiuser detection techniques

and iii) channel code design for the CFSK system with multiuser detection.

In Chapter 2, the performance of the CFSK channel under several channel conditions is discussed. Previous results on the CFSK channel with intensity information focus on the synchronized noiseless case [13]. In [9], capacity bounds for the noisy CFSK channel without intensity information are derived. In Chapter 2 new capacity bounds for the CFSK channel with intensity information under both synchronous and asynchronous situations are derived. To obtain these capacity results, an optimal multiuser detector is assumed. These bounds show that the capacity of the asynchronous CFSK channel is unaffected by the near-far effect or fading and the capacity is above a constant level even when the system is over-loaded.

In Chapter 3, detection strategies for the CFSK channel are investigated. The implementation of an optimal multiuser detector based on Maximum Likelihood Sequence Detection (MLSD) is discussed. It is shown that this approach is an NP-hard problem, and thus impractical for applications. Iterative detection techniques are proposed that provide a suboptimal solution for multiuser detection of the CFSK channel with intensity information. In the iterative detectors, an optimal multiuser channel metric that considers all the possible combinations of the users' choices is first derived. The complexity of this metric is an exponential function of the number of users and is not practical for heavily loaded systems. As a result, further simplifications of the iterative multiuser channel metric are required. These simplifications

reduce or enlarge the size of the set of the possible combinations of the users' choices such that the computational complexity is polynomial with the number of users.

In Chapter 4, the performance of several iterative multiuser detectors is studied. The effectiveness of the metric simplifications given in Chapter 3 is shown via simulation. EXIT analysis of the iterative detectors shows that multiaccess code design is very important to achieving higher rates and to improve the system performance for heavily loaded systems.

In Chapter 5, the design of multiacccess codes for the CFSK system is investigated. Distance properties and unique decodability of multiaccess codes are defined. It is shown that it is extremely difficult to find an effective method to construct uniquely decodable multiaccess codes for the CFSK channel with intensity information. Thus, randomly generated convolutional codes are used and are shown to be nearly unique decodable. The choice of code parameters is investigated in detail. Simulation results are presented to demonstrate that the random codes approach the performance of nearly uniquely decodable codes.

In Chapter 6, performance comparisons of CFSK and CDMA, including DS/CDMA and FH/CDMA, are given. The results show that the CFSK system has advantages over the CDMA system in some cases. Finally, conclusions and comments for future research are given.

Chapter 2

Theoretical Performance of the CFSK Channel

2.1 Introduction

In [13], Chang and Wolf derived the capacity of the noiseless CFSK channel with and without intensity information. Subsequently, Grant [9] derived an approximate expression for the channel capacity of the noiseless CFSK channel without intensity information and showed that it asymptotically approaches Chang and Wolf's result. Furthermore, Grant provided upper and lower bounds on the capacity of the CFSK channel without intensity information in the presence of noise and undetected interference. These results established a theoretical basis for the design of a multiple-

access communication system over the CFSK channel. Grant, however, did not find the capacity of the noisy CFSK channel with intensity information. Moreover, all of the aforementioned capacity results are for synchronous systems, i.e, the symbols are transmitted with the same phase. In many practical applications, synchronization is hard to achieve.

In an asynchronous CFSK system the phase of the FSK signal sent by one user is different from those sent by other users. Destructive interference of the signals from different users makes it extremely difficult to estimate the number of users in each frequency band. Thus, different capacity results for the asynchronous CFSK channel are anticipated, especially for the case with intensity information.

In this chapter, mathematical models for the synchronous and asynchronous CFSK channels are given that enable an analysis of the asynchronous CFSK system. In deriving the capacity results, an optimal multiuser detector is assumed. The capacities of the CFSK channel with and without intensity information, in synchronous and asynchronous scenarios, are then studied numerically. Finally, a comparison is made between the capacity results for CFSK systems and CDMA systems.

2.2 Channel Models

For convenience of discussion, the diagram of the CFSK system described in Chapter 1 is reproduced in Figure 2.1. In this system, it is assumed that the received signal

energy for each of the users at the receiver is E_s. This assumption neglects the near-far effect which will be discussed later. It is also assumed that each user must choose one of the frequencies to transmit at each time since Chang and Wolf's derived the sum rates for the T-user M-frequency multiple access system based on this assumption [13].

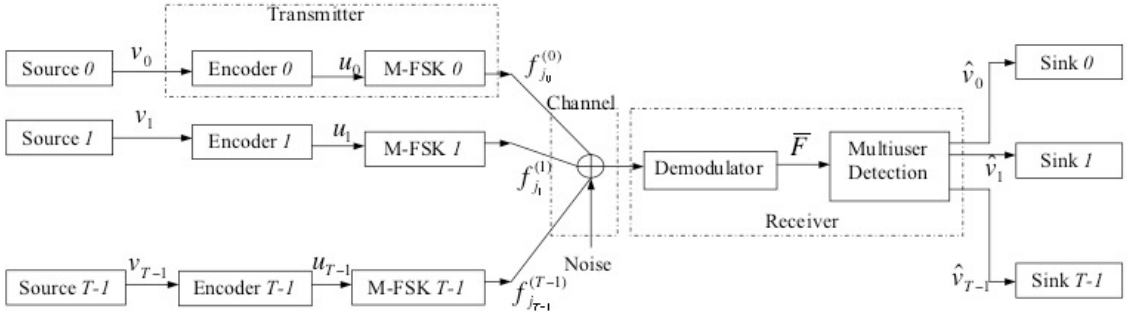

Figure 2.1: Block diagram of a CFSK system.

2.2.1 Synchronous Channel

Assuming that all users transmit with the same phase, the output signal of the demodulator on frequency f_j is given by

$$\begin{aligned} x_j &= \mu_j \sqrt{E_s} \cos(\phi_j) + n_x, \\ y_j &= \mu_j \sqrt{E_s} \sin(\phi_j) + n_y, \end{aligned}$$

where μ_j is the number of users that transmit frequency f_j, ϕ_j is the phase, and n_x and n_y are Gaussian random variables with variance $\frac{N_o}{2}$. Thus,

$$\rho_j = x_j^2 + y_j^2 \tag{2.1}$$

is the detected output energy of the channel on frequency f_j. When $\mu_j \neq 0$, the distribution of $\sqrt{\rho_j}$ is a Rician distribution that can be approximated by

$$f_{\sqrt{\rho_j}}(\rho) \approx \frac{1}{N_o} \exp\left(- \frac{(\mu_j \sqrt{E_s} - \sqrt{\rho})^2}{N_o} \right). \tag{2.2}$$

In [17] it is shown that this approximation is tight enough to investigate the capacity of this channel. When $\mu_j = 0$, the distribution of $\sqrt{\rho_j}$ is given by the Rayleigh distribution

$$f_{\sqrt{\rho_j}}(\rho) = \frac{2\sqrt{\rho}}{N_o} \exp\left(- \frac{\rho}{N_o} \right). \tag{2.3}$$

The distributions in (2.2) and (2.3) are plotted in Figure 2.2 for $\mu_j = 0, 1, \ldots, 5$, for a signal-to-noise ratio (SNR) of 8 dB. Clearly, the distributions of $\sqrt{\rho_j}$ for one or more transmissions are uniformly spaced along the $\sqrt{\rho}$ axis. Thus, optimal detection of the number of transmissions requires a series of thresholds that are uniformly spaced along the $\sqrt{\rho}$ axis, except for the threshold between 0 transmissions and 1 transmission.

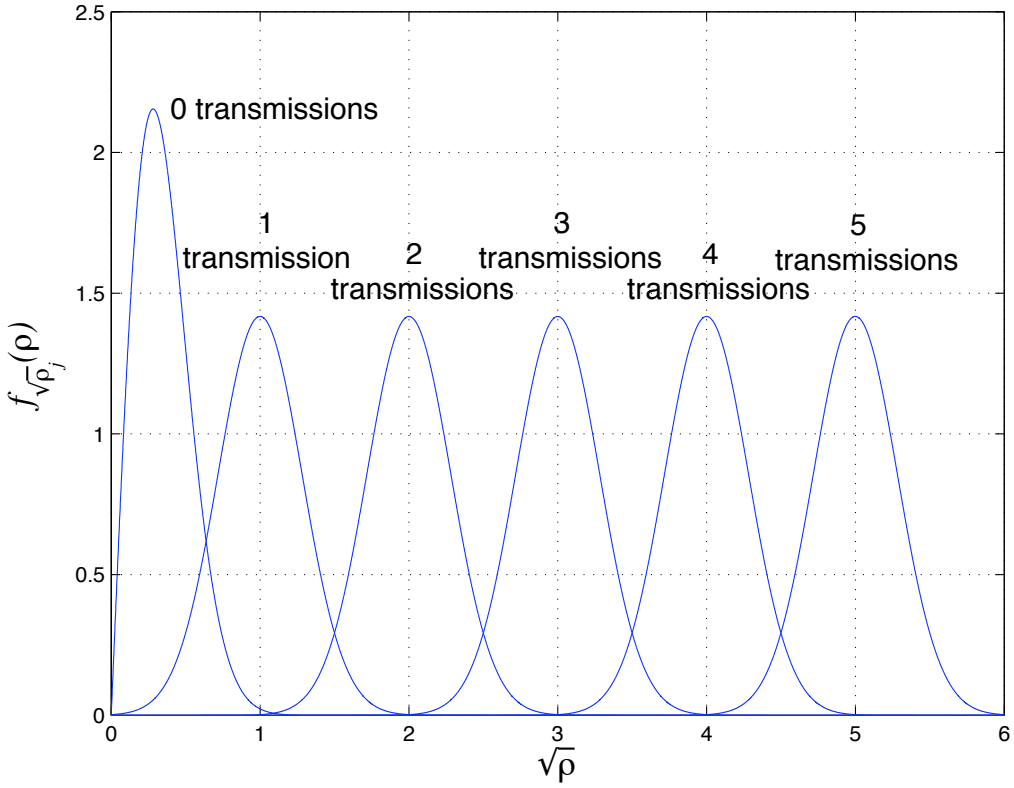

Figure 2.2: Probability density functions for the received symbol energy on the noisy synchronous CFSK channel at 8 dB.

2.2.2 Asynchronous Channel

For the asynchronous CFSK channel, the detector output for frequency j is given by

$$\begin{aligned} x_j &= \sqrt{E_s}\sum_{k=1}^{\mu_j}\cos(\phi_j^{(i_k)}) + n_x, \\ y_j &= \sqrt{E_s}\sum_{k=1}^{\mu_j}\sin(\phi_j^{(i_k)}) + n_y, \end{aligned} \tag{2.4}$$

where $\phi_j^{(i_k)}$ denotes the phase with which the i_k^{th} user transmits frequency f_j. The detected energy level for this channel is still given by (2.1). Since all users transmit asynchronously and independently, the distribution of the phase $\phi_j^{(i_k)}$ can be assumed to be uniform between 0 and 2π, i.e.,

$$f_{\phi_j^{(i_k)}}(\phi) = \begin{cases} \frac{1}{2\pi} & 0 \le \phi \le 2\pi, \\ 0 & \text{otherwise.} \end{cases}$$

The following proposition gives a tight approximation on the distribution of asynchronous signals for large number of users.

Proposition 2.2.1 *When $\mu_j \gg 1$, x_j and y_j can be approximated by two independent Gaussian random variables: $\xi_x \sim \mathcal{N}[0, \frac{\mu_j E_s + N_o}{2}]$ and $\xi_y \sim \mathcal{N}[0, \frac{\mu_j E_s + N_o}{2}]$, respectively.*

Proof: In the absence of Gaussian noise, the detector outputs are given by

$$x_j = \sqrt{E_s}\sum_{k=1}^{\mu_j}\cos(\phi_j^{(i_k)}),$$

and

$$y_j = \sqrt{E_s}\sum_{k=1}^{\mu_j}\sin(\phi_j^{(i_k)}).$$

Assuming the phase $\phi_j^{(i_k)}$ is uniformly distributed between 0 and 2π,

$$E(x_j) = E\big(\sum_{k=1}^{\mu_j} \sqrt{E_s}\cos(\phi_j^{(i_k)})\big) = 0,$$

and

$$E(y_j) = E\big(\sum_{k=1}^{\mu_j} \sqrt{E_s}\sin(\phi_j^{(i_k)})\big) = 0.$$

Since the phases of different users are independent, the variance of x_j is given by

$$\begin{aligned}
\sigma^2(x_j) &= E(x_j^2) \\
&= E\Big(\textstyle\sum_{k=1}^{\mu_j} E_s\cos(\phi_j^{(i_k)})^2 + E_s\sum_{u=1}^{\mu_j}\sum_{k=1}^{\mu_j}\cos(\phi_j^{(i_u)})\cos(\phi_j^{(i_k)})\Big) \\
&= \textstyle\sum_{k=1}^{\mu_j} E_s E\big(\cos(\phi_j^{(i_k)})^2\big) + E_s E\big(\sum_{u=1}^{\mu_j}\sum_{k=1}^{\mu_j}\cos(\phi_j^{(i_u)})\cos(\phi_j^{(i_k)})\big) \\
&= \textstyle\sum_{k=1}^{\mu_j} E_s E\big(\cos(\phi_j^{(i_k)})^2\big) + E_s E\big(\sum_{u=1}^{\mu_j}\cos(\phi_j^{(i_u)})\big)E\big(\sum_{k=1}^{\mu_j}\cos(\phi_j^{(i_k)})\big) \\
&= \textstyle\sum_{k=1}^{\mu_j} \frac{E_s}{2} \\
&= \frac{\mu_j E_s}{2}.
\end{aligned}$$

Similarly, we have $\sigma^2(y_j) = \frac{\mu_j E_s}{2}$. Since the transmissions of the users are independent and identically distributed, when μ_j is large, both x_j and y_j can be approximated by Gaussian distributions by the central limit theorem with zero mean and variance $\frac{\mu_j E_s}{2}$.

The correlation between x_j and y_j is given by

$$E(x_j y_j) = E(\sum_{u=1}^{\mu_j}\sum_{k=1}^{\mu_j} E_s\cos(\phi_j^{(i_u)})\sin(\phi_j^{(i_k)})) = 0.$$

In the limit of the number of users, x_j and y_j are Gaussian and the correlation $E(x_j y_j)$ is zero, so x_j and y_j are independent. If Gaussian noise with zero mean and variance

$\frac{N_o}{2}$ is considered, the detector outputs in (2.4) can be approximated by Gaussian distributions, with zero mean and variance $\frac{\mu_j E_s + N_o}{2}$. Denote the independent effective Gaussian noises by $\xi_x \sim \mathcal{N}(0, \frac{\mu_j E_s + N_o}{2})$ and $\xi_y \sim \mathcal{N}(0, \frac{\mu_j E_s + N_o}{2})$. Then,

$$x_j \approx \xi_x,$$

and

$$y_j \approx \xi_y.$$

□

An immediate result from the proof is that

$$E(\rho_j) = E(x_j^2 + y_j^2) = \mu_j E_s + N_0,$$

when x_j and y_j are independent. Thus, the distribution of $\sqrt{\rho_j}$ for the noisy asynchronous CFSK channel can be approximated by the Rayleigh distribution

$$f_{\sqrt{\rho_j}}(\rho) \approx \frac{2\sqrt{\rho}}{\mu_j E_s + N_o} \exp\left(- \frac{\rho}{\mu_j E_s + N_o} \right). \tag{2.5}$$

The distribution in (2.5) is plotted in Figure 2.3 for $\mu_j = 0, \ldots, 5$ at an SNR of 8dB. In Figure 2.3, the distributions are the same as for the synchronous case when $\mu_j = 0$ and 1 , since there is no collision on frequency f_j when μ_j is 0 or 1.

Based on the approximate distribution given in (2.5), the thresholds for the optimal detector of the noiseless asynchronous CFSK channel are shown in Table 2.1

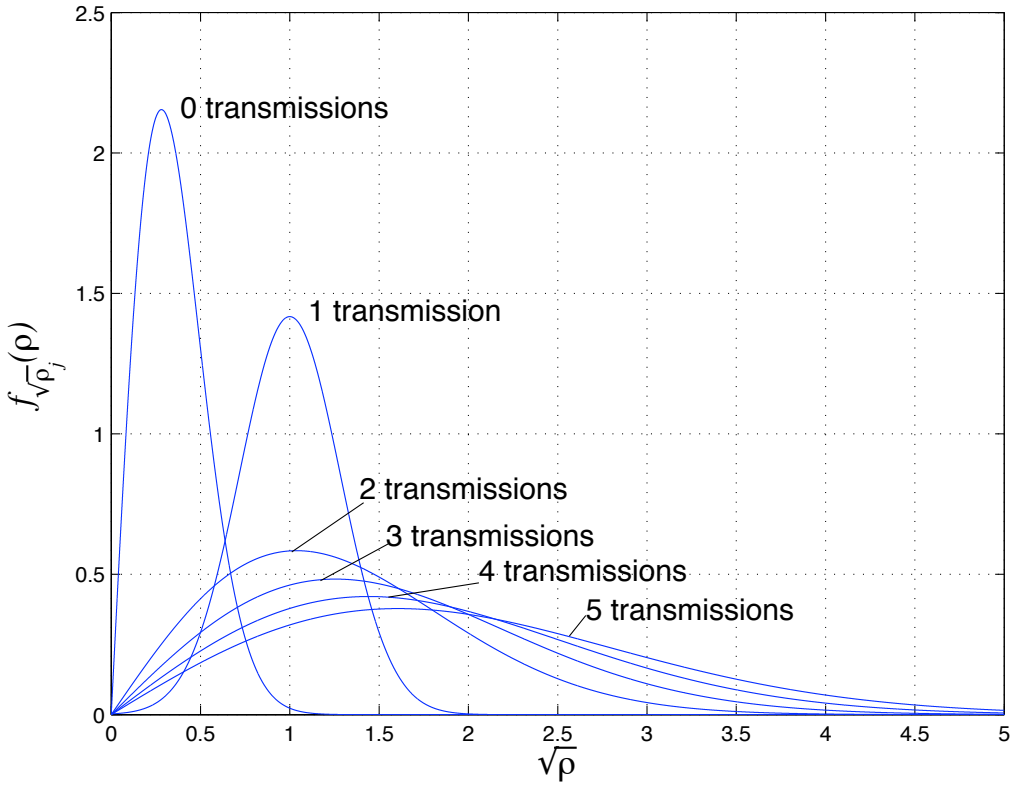

Figure 2.3: Probability density functions for the symbol received energy of the noisy asynchronous CFSK channel at 8 dB.

Table 2.1: Thresholds for detection of u_j over the noiseless asynchronous CFSK channel.

$u_j = 0$	$\sqrt{\rho_j} = 0$
$u_j = 1$	$\sqrt{\rho_j} = 1$
$u_j = 2$	$\sqrt{\rho_j} \leq 1.299, \sqrt{\rho_j} \neq 0, 1$
$u_j = 3$	$1.299 < \sqrt{\rho_j} \leq 1.547$
$u_j = 4$	$1.547 < \sqrt{\rho_j} \leq 1.759$
$u_j = 5$	$\sqrt{\rho_j} > 1.759$

for the 5-user case. In this case, the distributions of $\sqrt{\rho_j}$ are not uniformly spaced along the $\sqrt{\rho}$ axis and the curves of $f_{\sqrt{\rho_j}}(\rho)$ significantly overlap each other when $\mu_j \geq 2$. Though a series of thresholds on the $\sqrt{\rho}$ axis can be found and the detector can distinguish between different numbers of transmissions for $\mu_j \geq 2$, there will be many detection errors on the asynchronous channel. If the number of transmissions is not required, one can find a single threshold for $\sqrt{\rho_j}$ that determines whether or not at least a single transmission has occurred. For example, in the noiseless case, if no energy is detected on the j^{th} frequency, the detector outputs a 0, otherwise, the detector outputs a 1 indicating a transmission has occurred.

Thus, for the CFSK channel, asynchronous transmission results in highly inaccurate intensity information, but still indicates whether or not a transmission has

occurred. It is reasonable to expect that the capacity of the asynchronous CFSK channel without intensity information provides a lower bound for the channel with intensity information. It is also expected that the capacity of the CFSK channel without intensity information is not seriously affected by asynchronous transmission.

2.2.3 Optimal Multiuser Detection

Before presenting the capacity results, it is necessary to describe the optimal multiuser detector used in the derivations. Let the signals sent by the users at time t be denoted by

$$\bar{s}_t = [f_{j_0}^{(0)}, \ldots, f_{j_{T-1}}^{(T-1)}], \tag{2.6}$$

where $f_{j_i}^{(i)}$ denotes that the i^{th} user transmits frequency f_{j_i}. The sequence of signals received by the multiuser detector is given by $[\bar{F}_0, \ldots, \bar{F}_{N-1}]$, where $\bar{F}_t$ for $t = 0, 1, \ldots, N-1$ is of the form given by (1.1). The optimal multiuser detector based on the *maximum a posteriori* criterion uses

$$\hat{\bar{s}}_t = \text{argmax}_{\bar{s}_t} P(\bar{F}_0, \ldots, \bar{F}_{N-1} | \bar{s}_t) \tag{2.7}$$

to estimate the vector of signals transmitted by the users. To separate the users' information from the received signal, an optimal coding scheme that uses uniquely decodable channel codes [18, 19, 20] is assumed. In Chapter 3, details of the implementation of the optimal multiuser detector are discussed and code design is discussed in Chapter 5.

2.3 Capacity of the Noisy Synchronous CFSK Channel with Intensity Information

The size of the output alphabet from the noisy CFSK channel with intensity information can be extremely large since the energy level output from the channel on each frequency is proportional to the number of users. This makes computing the exact capacity of the noisy CFSK channel with intensity information very complex when the numbers of frequencies and users are large.

Let X and U be the input and output alphabets of the noisy channel and let M be the number of frequencies. Each element of X and U is a $1 \times M$ vector in which each entry denotes the number of transmissions on the corresponding frequency. For all $x \in X$, let

$$x = \{x_1, x_2, \ldots, x_M\}.$$

Since x is the input to the noisy channel, it is straightforward to see that $x_j = \mu_j$ for $j = 1, 2, \ldots, M$. For all $u \in U$, let

$$u = \{u_1, u_2, \ldots, u_M\},$$

where u_j is the number of transmissions detected on the j^{th} frequency at the output of the noisy channel.

When M is small, it is possible to compute the exact capacity using

$$C_{\text{s,w}} = \max_{P_X(x)} \big[I(U;X)big] = \max_{P_X(x)} \big[H(U) - H(U|X)\big],$$

where the maximum is over the input distribution $P_X(x)$, $H(U)$ is given by

$$H(U) = \sum_{u \in U} -p_U(u) \log(p_U(u)),$$

and the conditional entropy $H(U|X)$ is given by

$$\begin{aligned} H(U|X) &= \sum_{u \in U, x \in X} p_{U,X}(u,x) I(u|x) \\ &= \sum_{u \in U, x \in X} -p_X(x) p_{U|X}(u|x) \log(p_{U|X}(u|x)). \end{aligned}$$

The probability of the output symbols can be computed using

$$p_U(u) = \sum_{x \in X} p_X(x) p_{U|X}(u|x).$$

The probability $p_{U|X}(u|x)$ is given by

$$p_{U|X}(u|x) = \prod_{j=0}^{M-1} P(u_j|x_j),$$

where the channel transition probabilities $P(u_j|x_j)$ for frequency f_j can be computed from the detector thresholds for the synchronous channel and the distributions in (2.2) and (2.3).

It was proven in [13] that if all the users send the frequencies with equal probability $\frac{1}{M}$, then channel capacity can be achieved. In this case, the probability of an input

symbol x is

$$\begin{aligned} p_X(x) &= \binom{T}{x_1}\binom{T-x_1}{x_2}\cdots\binom{T-x_1-\ldots-x_{M-1}}{x_M}\frac{1}{M^T} \\ &= \frac{T!}{x_1!x_2!\ldots x_M!}\frac{1}{M^T}. \end{aligned}$$

By exhaustively constructing the set of all input symbols X, the set U can also be found.

When M and the number of users, T, are not very large, it is possible to construct X and U by computer search. In Figure 2.4, the exact capacities are shown for SNR's of 6 dB, 8 dB and 12 dB. For high SNR's, the capacity of the noisy channel approaches the capacity of the noiseless channel. When there are 2 frequencies and 2 users, the sum rate for the noiseless channel is less than 2 bits/channel use, the rate achieved by the FDMA system with 2 frequencies and on-off keying signaling. This is because that when Chang and Wolf computed this sum rate [13], they assumed that each user must choose one of the frequencies to transmit at each time. When the number of users is higher than the number of frequencies, more information can be obtained from the collision of frequencies and thus the sum rates achieved by the CFSK system is higher than that achieved by the FDMA system.

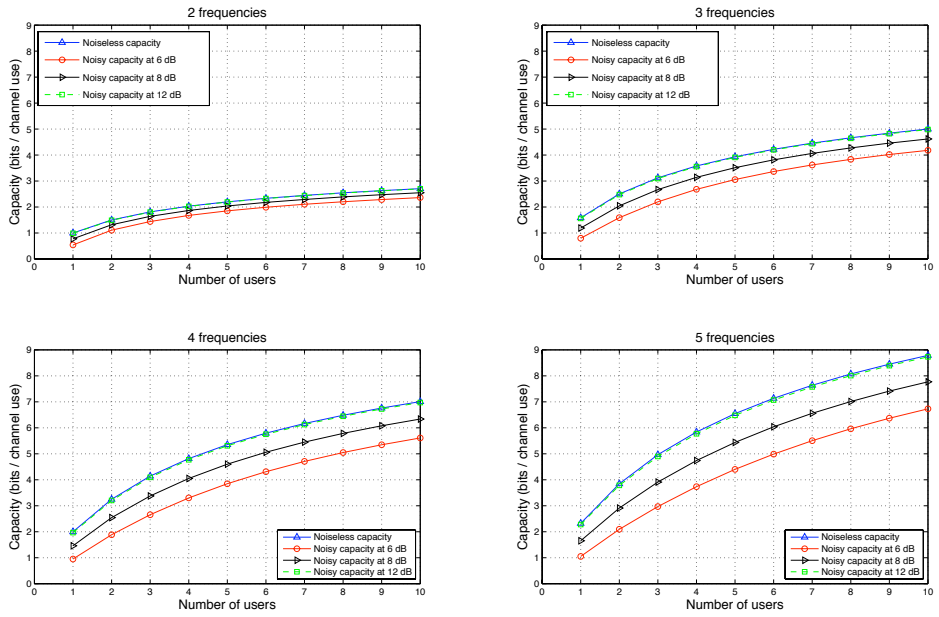

Figure 2.4: Exact capacities of the noisy synchronous CFSK channel with intensity information at 6 dB, 8 dB and 12 dB.

2.4 Capacity of the Noiseless Asynchronous CFSK Channels

It is interesting to study the noiseless asynchronous CFSK channel since it provides an upper bound on the capacity of the noisy channel. In order to analyze the capacity of the noiseless asynchronous CFSK channel, the analytical model proposed in Figure 2.5 is used. The asynchronous transmission and the non-coherent detection at the receiver results in the non-coherent channel in Figure 2.5. By dropping the intensity information, the non-zero intensity information from the non-coherent channel becomes 1 at the output of the second subchannel in Figure 2.5. In this model, the optimal detector uses 0 for the threshold between 0 and 1 since the channel is noiseless.

Following the data processing inequality [21],

$$C_{\mathrm{a,w}} = \max_{P_X(x)} \big[I(U;X)\big] \geq C_{\mathrm{a,wo}} = \max_{P_X(x)} \big[I(V;X)\big], \tag{2.8}$$

where $C_{\mathrm{a,w}}$ is the capacity of the noiseless asynchronous channel with intensity information and $C_{\mathrm{a,wo}}$ is the capacity of the noiseless asynchronous channel without intensity information. For the asynchronous channel without intensity information, it is clear that the noiseless capacity is equal to that in the synchronous case. In the absence of noise, the synchronous and asynchronous channels without intensity information behave exactly the same, since the signal energy can always be detected

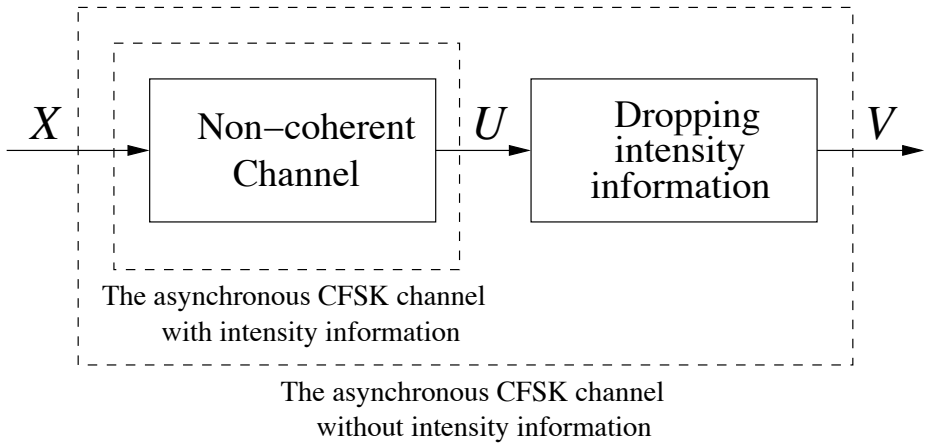

Figure 2.5: The analytical model for the noiseless asynchronous CFSK channel without intensity information.

if there is at least one transmission over the channel regardless of whether or not the transmissions are synchronous. For example, using the thresholds from Table 2.2.,

$$P(\text{Inactive}|\text{Inactive}) = P(u_j = 0|x_j = 0) = 1,$$

$$P(\text{Active}|\text{Inactive}) = \sum_{k=1}^{T} P(u_j = k|x_j = 0) = 0,$$

$$P(\text{Active}|\text{Active}) = \sum_{k=1}^{T-1} P(u_j = k|x_j = n) = 1,$$

and

$$P(\text{Inactive}|\text{Active}) = P(u_j = 0|x_j = n) = 0,$$

where $0 < n < M$. Thus, $C_{\text{a,wo}}$ in (2.8) is equal to the capacity of the noiseless synchronous channel without intensity information that has been found in [13]. It is

worth noting that the transition probabilities for the noiseless asynchronous channel without intensity information are not affected by the near-far effect or fading.

To compute the capacity of the noiseless asynchronous CFSK channel with intensity information, the channel transition probabilities $p(u_j|x_j)$ are computed from the distribution in (2.5) and the thresholds in Table 2.1. In Table 2.2, the channel transition probabilities are given for the 5-user case.

Table 2.2: Transition probabilities $P_{U|X}(u_j|x_j)$ for the noiseless asynchronous CFSK channel.

	$u_j = 0$	$u_j = 1$	$u_j = 2$	$u_j = 3$	$u_j = 4$	$u_j = 5$
$x_j = 0$	1.000	0	0	0	0	0
$x_j = 1$	0	1.000	0	0	0	0
$x_j = 2$	0	0	0.570	0.128	0.089	0.213
$x_j = 3$	0	0	0.430	0.120	0.093	0.357
$x_j = 4$	0	0	0.344	0.106	0.088	0.462
$x_j = 5$	0	0	0.286	0.094	0.081	0.539

Unfortunately, it is extremely difficult to find the optimal input distributions required to achieve the channel capacity since this is a T-dimensional optimization problem. Consequently, in the following discussion specific distributions of the input frequencies for the users are assumed in order to achieve a high sum rate. The sum

rates obtained in this manner are lower bounds on the channel capacity.

In order to find a "good" distribution for the input frequencies, comparisons are made between the asynchronous channels with and without intensity information.When $T \gg M$, the number of transmissions of each frequency is large and the distributions $f_{\sqrt{\rho_j}}(\rho)$ significantly overlap each other. Thus, the intensity information becomes less and less important and it is reasonable to assume that the capacity grows in a similar manner as the channel without intensity information. Based on this, we use the same input distributions that achieve capacity on the channel without intensity information. When $T \leq M$, all users use a uniform distribution, $P(f_j^{(i)}) = \frac{1}{M}$, and when $T > M$, all users use the same distribution that puts higher weight on one of the frequencies and distributes the remaining weight evenly over the other frequencies.

Given the input distribution, the corresponding sum rate can be found using the same approach for the noisy synchronous channel with intensity information. Figure 2.6 shows the resulting sum rates. It is clear from these results that the channels with and without intensity information behave similarly when the number of users is large. In particular, the sum rate approaches a constant non-zero level as M increases. However, the capacity of the channel with intensity information is much higher than that of the channel without intensity information. This is because intensity information is useful even when the number of users is high.

Take the 10-user case as an example. The distributions for 9 and 10 transmissions overlap each other significantly and almost no useful information can be obtained by distinguishing between 9 and 10 transmissions. However, the distributions for 1 transmission (or 2 transmissions) and 9 (or 10) transmissions are relatively far from each other and useful information can be obtained by distinguishing the two cases.

Another observation from Figure 2.6 is that for a small number of users, the capacities of the synchronous channel and the asynchronous channel are close to each other. This is due to the fact that for a small number of users most of the frequencies are occupied by 0, 1 or 2 transmissions and asynchronous transmission does not significantly affect the receiver output.

2.5 Asynchronous Capacity: CFSK vs. CDMA

From the capacity bounds derived in this chapter, it can be concluded that the asynchronous CFSK channel with intensity information offers good performance even in over-loaded situations. In fact, the capacity approaches a non-zero value when the number of users is much higher than the number of frequencies and thus promises non-zero sum rates for all the users. The asynchronous channel with intensity information allows a higher transmission rate than the channel without intensity information in the over-loaded situation. Moreover, this rate will not go to zero under the near-far effect or fading since the capacity of the channel without intensity information pro-

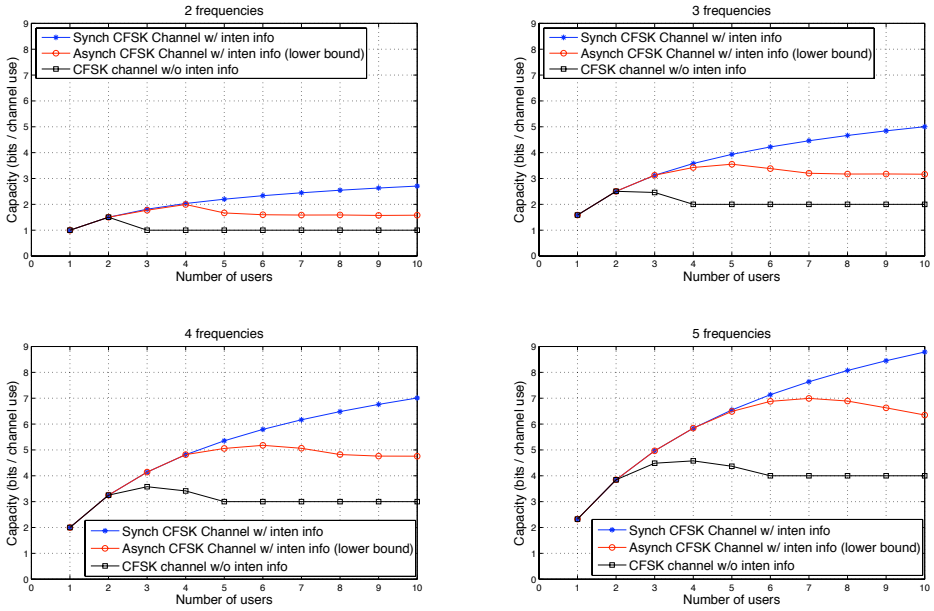

Figure 2.6: Capacity of noiseless asynchronous CFSK channels.

vides a lower bound for the channel with intensity information and the performance of the channel without intensity information is robust under the near-far effect and fading.

To determine the performance gain in practical applications, it is interesting to compare the capacity results for the CFSK systems with those of CDMA systems in the symbol asynchronous case. For a direct-sequence (DS) CDMA system, the single-user capacity results derived in [15] assume symbol asynchronous transmission. For the multiuser capacity provided in [9], synchronous transmission is assumed. Though there is no explicit result given for the multiuser capacity for the asynchronous DS-CDMA system, the results in [22] prove that for a symbol asynchronous (but chip synchronous) DS-CDMA system, the capacity equals that of the symbol synchronous system under the constraint that all the users have the same transmission power and the optimality is achieved with a specific spreading code construction. Thus, the sum capacity of the symbol synchronous multiuser DS-CDMA system provides an upper bound for that of the asynchronous system.

For frequency-hopping (FH) CDMA systems, there is no result for the multiuser capacity. The single-user capacity for the noiseless FH-CDMA system is first discussed in [23], where slow frequency-hopping with M-ary modulation is assumed. In [24], two types of FH-CDMA systems are discussed: on-off keying (OOK) and M-ary frequency-shift-keying (MFSK). The single-user capacity results are extended to the

symbol asynchronous noisy channel, and both the slow and fast FH-CDMA systems are considered. It is shown that the fast FH-CDMA system with BFSK modulation is more bandwidth efficient than a system with MFSK modulation for $M > 2$. Thus, BFSK FH-CDMA is chosen for this comparison.

In Figure 2.7, capacity results are compared between the asynchronous CFSK systems and the asynchronous CDMA systems according to the results given in [15, 9, 22, 24]. In this comparison, 5 is chosen as the chip number for simple computations. The results show that the CFSK systems have the highest capacity for moderately loaded systems. When the load is small, the OOK FH-CDMA system with single-user detection is the most bandwidth efficient. For the highly load conditions, the multiuser CDMA system has the highest capacity. However, this capacity can only be achieved with a very special spreading code construction that is impractical in heavily-loaded systems.

The CFSK system without intensity information also has a relative high capacity over a wide range of loads. This capacity assumes uniquely decodable codes which are very difficult to construct such codes in general. The performance of this system with random codes is discussed in detail in Chapter 5. In Chapters 3 and 4, we focus on the analysis of the synchronous CFSK system for ease of exposition and the results are easily extended to the asynchronous CFSK system.

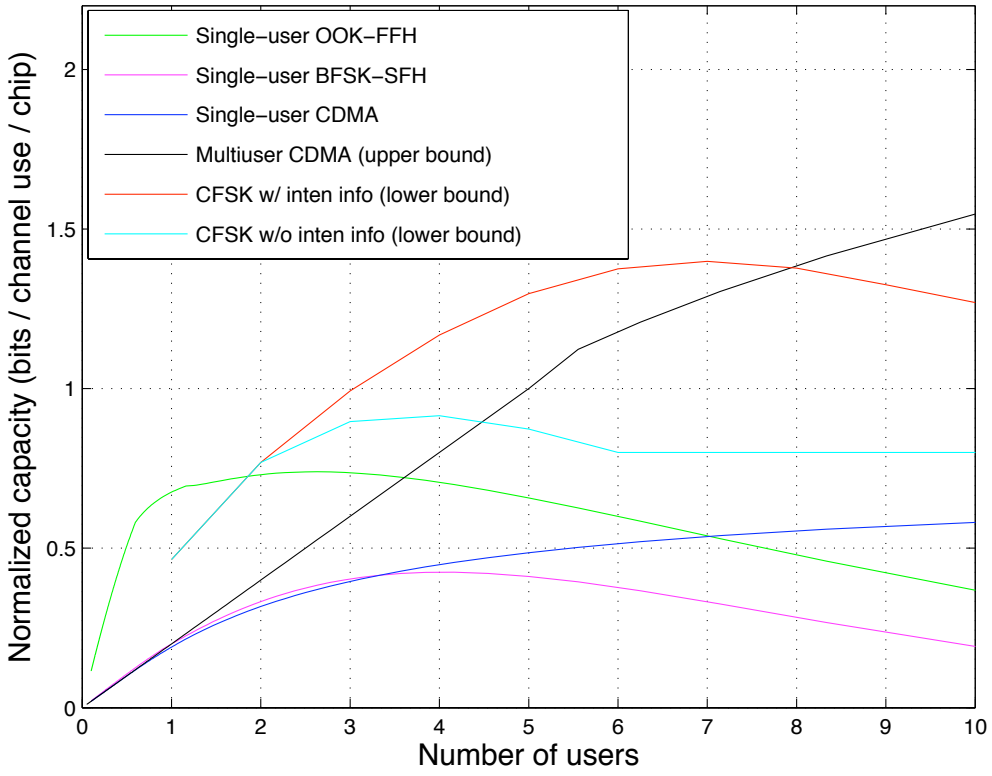

Figure 2.7: Normalized capacity for noiseless asynchronous CFSK and CDMA systems.

Chapter 3

Multiuser Detection over the CFSK Channel

3.1 Introduction

Multiuser detection is one of the most popular topics for contemporary multiple-access systems, such as CDMA and TCMA, due to its significant performance gain [3, 9, 11]. Most of the efforts in this area are contributed to developing simplified multiuser detectors due to the prohibitively high complexity of optimal multiuser detectors [25, 26, 12]. The iterative multiuser detectors have been shown to be an effective method to achieve near optimal performance with reduced complexity [27, 6].

In [27], an optimal iterative multiuser detector for a synchronous coded CDMA

system was proposed based on the *a posteriori* probability (APP) CDMA detector and a list of single-user APP channel decoders. This APP CDMA detector has exponential complexity and is impractical. Thus, various form of iterative CDMA detectors were developed [28, 29, 30, 31] in order to achieve near single-user performance with practical complexity. In [28], the APP CDMA detector is replaced by an interference canceler and a single-user minimum-mean square error (MMSE) filter. The resulting detector achieves performance approaching that of the APP detector. In [29, 30], a suboptimal maximum *a posteriori* (MAP) probability CDMA detector was investigated whose complexity is linear with the number of users. Gamal, et al. [31] proposed an iterative MMSE detector whose performance is better than all the the above iterative multiuser detectors, and whose the complexity is polynomial with the number of users.

From the analysis in Chapter 2, it is obvious that multiuser detection can provide huge performance gains over the CFSK channel. Based on the principles of optimal multiuser detection given in Section 2.2.3, a detector using maximal likelihood sequence detection (MLSD) is introduced in this chapter. This receiver provides a performance benchmark for the CFSK channel with intensity information. However, the complexity of this detector is not practical and suboptimal detectors are required. The optimal iterative multiuser detector for the CFSK system based on an optimal iterative multiuser channel metric is discussed in [17]. Unfortunately, the proposed

optimal metric has non-polynomial complexity. This chapter investigates simplifications to the optimal metric proposed in [17]. Several metrics are proposed and their performance and complexity are evaluated.

3.2 Optimal Multiuser Detection

In principle, the CFSK system can be regarded as a single-user trellis-coded modulation system, in which the single-user trellis is a *super-trellis*. The super-trellis can be constructed from all the users' trellis information as follows. The super-trellis code takes the input bits of the users as input. The states of the users' trellises are concatenated to form the state of the super-trellis. The output of the super-trellis is the channel symbol output from the M-FSK modulator, which has the form of $\bar{s}_t$ given by (2.6). The optimal multiuser detection criterion given in (2.7) makes decisions on the symbol vector $\bar{s}_t$ at each stage by considering N trellis sections in the super-trellis. Maximum likelihood sequence detection (MLSD) [11] can be used to implement the optimal detector.

For example, a 2-user 4-frequency CFSK system is described by the super-trellis in Figure 3.1. Each user uses a rate 1/2, memory 1 convolutional code. Thus, the super-trellis code has 2 input bits and 4 states. The output is $\bar{s}_t = [\mu_0, \mu_1, \mu_2, \mu_3]$, where μ_j denotes the number of transmissions on frequency f_j, and $\sum_{j=0}^{3} \mu_j = 2$.

For decoding, the channel metric is the conditional probability of the received

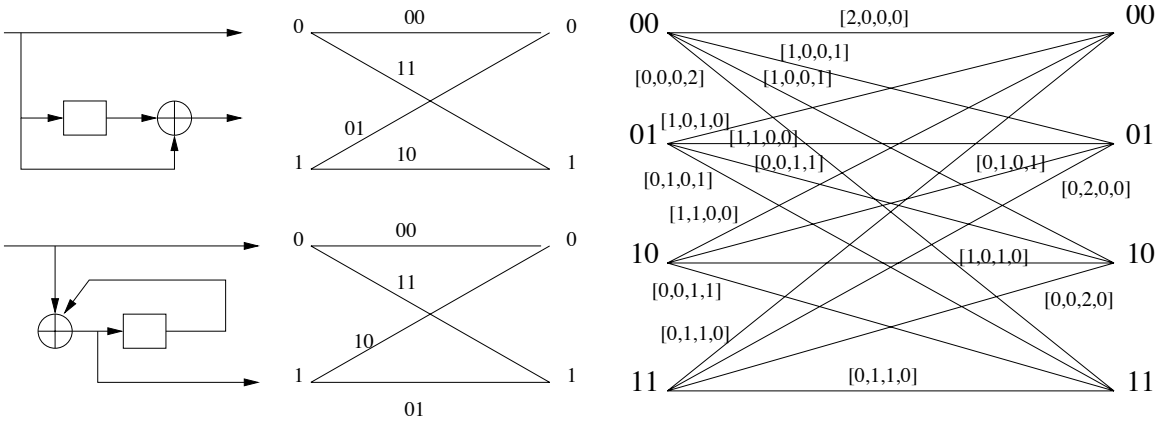

Figure 3.1: A two-user super-trellis.

signal vector $\bar{F}_t$ given the trellis output $\bar{s}_t$,

$$P(\bar{F}_t|\bar{s}_t) = \left(\frac{1}{N_o}\right)^M \prod_{j=0}^{M-1} e^{\left(-\frac{(\mu_j\sqrt{E_s}-\sqrt{\rho_j})^2}{N_0}\right)}. \tag{3.1}$$

Using this metric, an estimate of the symbol vector $\hat{\bar{s}}_t$ can be made based on the criterion given in (2.7). Assuming that the inputs to the super-trellis are equally likely, MLSD can be implemented using the Viterbi algorithm [32].

A limitation of the MLSD detector is that the complexity of the super-trellis is very high when there are a large number of users. Though the number of input bits k and memory m of the super code increases linearly with the number of users, the input alphabet and number of states increases exponentially with k and m. Thus, the complexity of the super-trellis grows exponentially with the number of users. For this reason, suboptimal detection using an iterative algorithm is necessary.

3.3 Iterative Multiuser Detection

Unlike the optimal detector that has a single decoder structure that operates on the super-trellis, the CFSK receiver with iterative detection is composed of two components, the metric computation and a list of component decoders. As shown in Figure 3.2, the metric computation works on the received channel signal $\bar{F}_t$ and *a priori* information of the users' transmitted symbols. Tentative information for the users' symbols is output to the component decoders via a channel metric. Each user's component decoder operates on the channel metric and finds the optimal estimate of the symbol $f_{j_i}^{(i)}$, the frequency f_{j_i} transmitted by user $U^{(i)}$. The soft information about the symbol $f_{j_i}^{(i)}$ is fed back to the metric computation as the *a priori* information for the next iteration.

For the multiuser channel metric given in (3.1), there are M^T channel metrics to be computed at each stage of the super-trellis since each user has M choices of frequencies and there are T users. This is obviously too complex for large system applications. The component decoder in the iterative multiuser detector, however, operates on a single user's component trellis. For this trellis the channel metric is the conditional probability of receiving the signal vector $\bar{F}_t$ given that user $U^{(i)}$ transmits frequency f_{j_i}, denoted by $P(\bar{F}_t|f_{j_i}^{(i)})$.

Let the set of users be

$$\mathcal{U} = \{U^{(0)}, U^{(1)}, \ldots, U^{(T-1)}\}.$$

Assume user $U^{(0)}$ chooses frequency $f_{j_0}^{(0)}$. The choices of the other $T-1$ users plus $f_{j_0}^{(0)}$ amount to the frequency combination

$$c_0 = (f_{j_0}^{(0)}, f_{j_1}^{(1)}, \ldots, f_{j_u}^{(u)}, \ldots, f_{j_{T-1}}^{(T-1)}).$$

If user $U^{(u)}$ chooses frequency $f_{j_u}^{(u)}$ with probability $P(f_{j_u}^{(u)})$, then the probability of the frequency combination c_0 given that user $U^{(0)}$ transmits on frequency $f_{j_0}^{(0)}$ is

$$P(c_0|f_{j_0}^{(0)}) = \prod_{u=1}^{T-1} P(f_{j_u}^{(u)}). \tag{3.2}$$

Given that user $U^{(0)}$ transmits $f_{j_0}^{(0)}$ and the frequency combination c_0 is transmitted by the other $T-1$ users, the multiplicity μ_j for frequency f_j can be easily computed.

For synchronous transmission, the distribution of the received energy ρ_j for f_j is given by (2.2). If $f_{j_0}^{(0)}$ and c_0 are known, the probability distribution of ρ_j given is

$$P(\rho_j|c_0, f_{j_0}^{(0)}) = \frac{1}{N_0} e^{\left(-\frac{(\mu_j\sqrt{E_s}-\sqrt{\rho_j})^2}{N_o}\right)}. \tag{3.3}$$

If each frequency is transmitted independently, the probability of receiving signal $\bar{F}_t$ given $f_{j_0}^{(0)}$ and c_0 is

$$P(\bar{F}_t|c_0, f_{j_0}^{(0)}) = \left(\frac{1}{N_o}\right)^M \prod_{j=0}^{M-1} e^{\left(-\frac{(\mu_j\sqrt{E_s}-\sqrt{\rho_j})^2}{N_o}\right)}. \tag{3.4}$$

Let the set of all possible frequency combinations be C_0. Then, the probability of the received frequency vector $\bar{F}_t$ given that $U^{(0)}$ transmits $f_{j_0}^{(0)}$ can be computed as

$$P(\bar{F}_t|f_{j_0}^{(0)}) = \sum_{c_0 \in C_0} P(c_0|f_{i_0}^{(0)}) P(\bar{F}|c_0, f_{j_0}^{(0)}). \tag{3.5}$$

By substituting the probabilities in (3.2) and (3.4) into (3.5), the channel transition probability of the CFSK channel with intensity information for synchronous transmission is found to be

$$P(\bar{F}_t|f_{j_0}^{(0)}) = \left(\frac{1}{N_o}\right)^M \sum_{i_1=0}^{M-1} \sum_{i_2=0}^{M-1} \cdots \sum_{i_{T-1}=0}^{M-1} \left[\prod_{u=1}^{T-1} P(f_{i_u}^{(u)}) \prod_{j=0}^{M-1} e^{\left(-\frac{(\mu_j \sqrt{E_s} - \sqrt{\rho_j})^2}{N_o}\right)} \right], \tag{3.6}$$

where i_u is the index of the frequency for the u^{th} user.

In Chapter 2, the mean of the received energy ρ_j for the noisy asynchronous channel is shown to be $\approx \mu_j E + N_o$. Thus, for noiseless case, the average value for $\sqrt{\rho_j}$ is given by $\sqrt{\mu_j E}$, and the probability $P(\rho_j|c_0, f_{j_0}^{(0)})$ can be approximated from (3.3) by

$$P(\rho_j|c_0, f_{j_0}^{(0)}) \approx \frac{1}{N_o} e^{\left(-\frac{(\sqrt{\mu_j E_s} - \sqrt{\rho_j})^2}{N_o}\right)}.$$

As a result, the channel transition probability of the CFSK channel with intensity information for asynchronous transmission is

$$P(\bar{F}_t|f_{j_0}^{(0)}) \approx \left(\frac{1}{N_o}\right)^M \sum_{i_1=0}^{M-1} \sum_{i_2=0}^{M-1} \cdots \sum_{i_{T-1}=0}^{M-1} \left[\prod_{u=1}^{T-1} P(f_{j_u}^{(u)}) \prod_{j=0}^{M-1} e^{\left(-\frac{(\sqrt{\mu_j E_s} - \sqrt{\rho_j})^2}{N_o}\right)} \right]. \tag{3.7}$$

3.3.1 MAP-Consensus Decoder

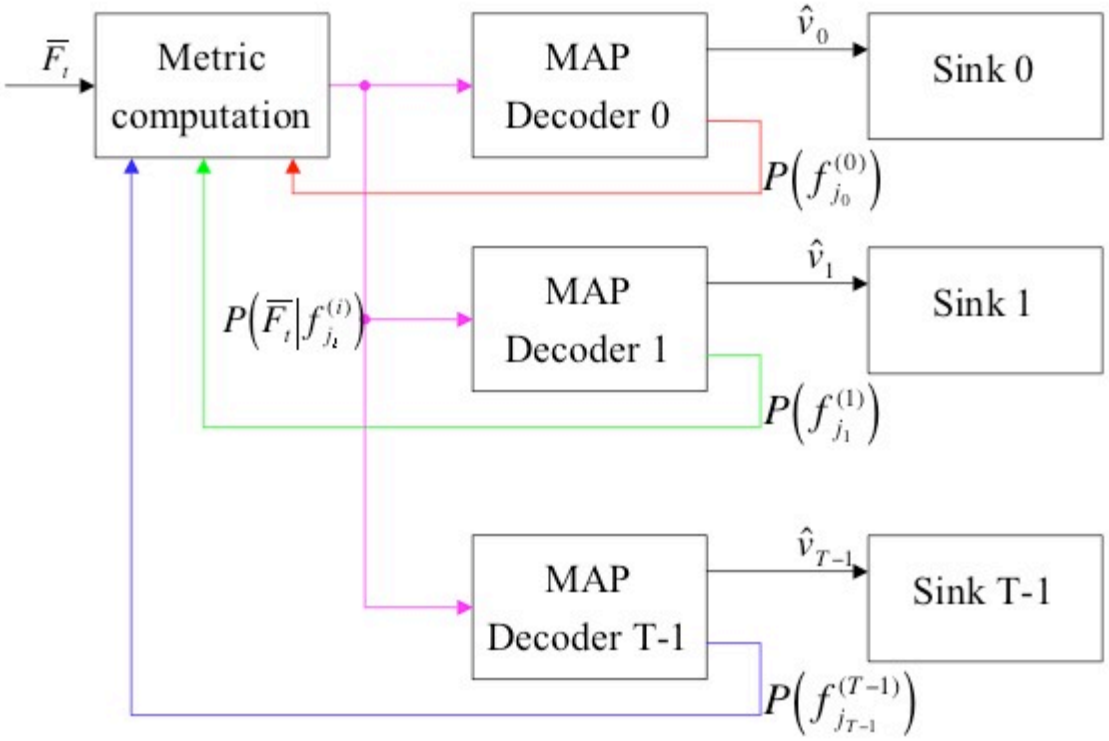

Figure 3.2: The consensus decoder.

The consensus decoder shown in Figure 3.2 was first introduced in [14] and is composed of the metric computation and a list of component decoders. The metric computation takes the *a priori* information $P(f_{j_i}^{(i)})$ and the channel signal $\bar{F}_t$ as input, and computes the channel metric using (3.6) or (3.7). Note that in the first iteration there is no available *a priori* information $P(f_{j_i}^{(i)})$ since the the component decoders have not decoded anything. In this situation, the probabilities $P(f_{j_i}^{(i)})$ are initialized

to $P(f_{j_i}^{(i)}) = \frac{1}{M}$.

The component decoders take the channel metric as input and operate on the corresponding user's trellis to obtain an estimate of the transmitted symbols and the information bits. In order to compute the soft information as the *a priori* information for the metric computation in the next iteration, a symbol-based maximum *a posteriori* (MAP) decoding algorithm is used for the component decoders [33]. N consecutive trellis sections are considered in the MAP algorithm. The received signal from time 0 to the current stage t is denoted by $\bar{F}_0^t$ and the current state of the trellis is denoted by S_t. The trellis branches are labeled with output symbols $f(t)$ at time t that takes the value f_j. The forward and backward recursions of the MAP algorithm are then

$$\begin{aligned} \alpha_t(m) &= P(S_t = m, \bar{F}_0^t) \\ &= \frac{\sum_{m'} \sum_{f_j} \gamma_{f_j}(\bar{F}_t, m', m)\alpha_{t-1}(m')}{\sum_m \sum_{m'} \sum_{f_j} \gamma_{f_j}(\bar{F}_t, m', m)\alpha_{t-1}(m')}, \end{aligned}$$

and

$$\begin{aligned} \beta_t(m) &= P(\bar{F}_{t+1}^{N-1} | S_t = m) \\ &= \frac{\sum_{m'} \sum_{f_j} \gamma_{f_j}(\bar{F}_{t+1}, m, m')\beta_{t+1}(m')}{\sum_m \sum_{m'} \sum_{f_j} \gamma_{f_j}(\bar{F}_t, m', m)\alpha_t(m')}. \end{aligned}$$

The branch transition probabilities, $\gamma_{f_j}(\bar{F}_t, m', m)$, can be calculated using

$$\begin{aligned} \gamma_{f_j}(\bar{F}_t, m', m) &= P(S_t = m, \bar{F}_t, f(t) = f_j | S_{t-1} = m') \\ &= P(\bar{F}_t | f(t) = f_j, S_{t-1} = m', S_t = m) Q(f(t) = f_j | S_{t-1} = m', S_t = m) \\ &\quad R(S_t = m | S_{t-1} = m'). \end{aligned}$$

At stage t, the joint probability of the previous state, the current state and the

received signal sequence is given by

$$\begin{aligned}\delta_t(m, m') &= P(S_{t-1} = m', S_t = m, \bar{F}_0^{N-1}) \\ &= \alpha_t(m')\gamma_{f_j}(\bar{F}_t, m', m)\beta_t(m).\end{aligned}$$

Note that the *a posteriori* probability of the symbols is

$$P(f(t) = f_j|\bar{F}_0^{N-1}) = \frac{P(f(t) = f_j, \bar{F}_0^{N-1})}{P(\bar{F}_0^{N-1})}.$$

By normalization, the value $P(\bar{F}_0^{N-1})$ is cancelled out from the above probability.

Finally, the *a posteriori* probabilities can be written as

$$\begin{aligned}P(f(t) = f_j|\bar{F}_0^{N-1}) &= \Lambda_t(f_j) \\ &= P(f(t) = f_j, \bar{F}_0^{N-1}) \\ &= \textstyle\sum_{(m',m)\in B(f_j)} \delta_t(m, m') \\ &= \textstyle\sum_{(m',m)\in B(f_j)} \alpha_t(m')\gamma_{f_j}(\bar{F}_t, m', m)\beta_t(m).\end{aligned}$$

The set $B(f_j)$ denotes the set of branch transitions from state m' to m with output symbol f_j. The final decision on the symbols is made by choosing the symbol f_j with the highest value for $\Lambda_t(f_j)$. For user $U^{(i)}$, the *a posteriori* information $P(f(t) = f_j|\bar{F}_0^{N-1})$ is fed back to the metric computation as the *a priori* information $P(f_{j_i}^{(i)})$ for the next iteration.

3.4 Metric Simplification

When computing the channel metric $P(\bar{F}_t|f_{j_0}^{(0)})$ given in (3.5), the summation is over the set C_0 of all possible frequency combinations. Since each of the $T-1$ other

users has M possible frequencies to choose from, there are M^{T-1} possible frequency combinations in the set C_0. Thus, the computational complexity of $P(\bar{F}_t|f_{j_0}^{(0)})$ is $O(M^{T-1})$, which increases exponentially with the number of users T. This computational complexity is impractical and a metric with a reduced complexity is critical to the implementation and application of the CFSK system.

To simplify the channel metrics of (3.6) and (3.7), a natural thought is to consider a subset of the combination set C_0. In general, the probabilities of most of the frequency combinations become small after many iterations . It is unlikely that omitting these combinations in the set C_0 will introduce serious errors into the metric. One method for simplifying the metric $P(\bar{F}_t|f_{j_0}^{(0)})$ is to only consider the $K(T)$ most probable frequency combinations in the set C_0, where $K(T)$ is a polynomial function of T.

Denote such a set of $K(T)$ combinations by C_0', then (3.5) becomes

$$P(\bar{F}_t|f_{j_0}^{(0)}) \approx \sum_{c_0 \in C_0'} P(c_0|f_{j_0}^{(0)}) P(\bar{F}_t|c_0, f_{j_0}^{(0)}). \tag{3.8}$$

When searching for the most probable combinations, if the channel measurement is given by

$$P_{\text{NSMP}} = \left(\frac{1}{N_o}\right)^M \prod_{u=1}^{T-1} P(f_{i_u}^{(u)}) \prod_{j=0}^{M-1} e^{\left(-\frac{(\mu_j\sqrt{E_s}-\sqrt{\rho_j})^2}{N_0}\right)}, \tag{3.9}$$

the simplified metric is called a "Narrow-Sense Most Probable" (NSMP) metric since it considers both the *a priori* probability of the combination and the distance between

the combination and the received signal. If the channel measurement is

$$P_{\text{WSMP}} = \prod_{u=1}^{T-1} P(f_{i_u}^{(u)}), \tag{3.10}$$

the simplified metric is called a "Wide-Sense Most Probable" (WSMP) metric since it ignores the channel information. For NSMP metric, a brute force computation that requires computation of all the M^{T-1} combinations is necessary. There are methods for computing the WSMP metric with polynomial complexity.

In both cases, the *a priori* probability $P(f_{i_u}^{(u)})$ is unavailable in the first iteration and is initialized to $\frac{1}{M}$. Thus, the *a posteriori* information output by the first iteration is suboptimal and the error propagates to later iterations. This results in poor performance for the iterative multiuser detector, especially when the system is highly loaded. To solve this problem, an NSMP metric can be applied in the first iteration. Since, as shown in Section 3.6, NSMP in the first iteration is computationally simple.

For the CFSK channel with intensity information, another simplified metric based on an entirely different philosophy can be derived. Due to the structure of the CFSK system, the metrics given in (3.6) and (3.7) are subject to the following constraint.

Constraint 1 *Each user can send one and only one frequency at a time.*

If this constraint is loosened and each user is allowed to transmit more than one frequency at a time, then a relaxed constraint is

Constraint 2 *There must be T and only T transmissions over all the frequencies at a time.*

Under this constraint there are more then M^{T-1} frequency combinations. A relaxation metric, which satisfies Constraint 2 but not Constraint 1, can be derived by considering the distributions of the users' *a priori* information.

In the following discussions, WSMP metrics with linear complexity are discussed first. Then, an NSMP metric based on (3.9) is proposed, which has low complexity in the first iteration. Finally, a relaxation metric is proposed that depends on the computation of *a priori* enumeration polynomials and the channel transition enumeration polynomials.

3.5 WSMP Metrics

The WSMP metrics are based on the approximation given in (3.8) and using the subset C_0' using the channel measurement P_{WSMP} given in (3.10). In this section, two methods are proposed to construct subsets C_0' that has a size linear with the number of users, T.

3.5.1 K-Most Probable Combinations Metric

In computing the K-Most Probable Combinations (K-MPC) metric, the subset of the frequency combinations, C_0', is of size K. In choosing C_0', the most probable combination occurs when all $T-1$ users choose their most probable frequency based on $P(f_{j_i}^{(i)})$. The other combinations in C_0' are formed by choosing the most probable frequency for $T-2$ users and the second most probable frequency for one user. To decide which user can choose the less probable frequency, all $T-1$ users are sorted according to their probabilities.

A combination is constructed by picking the first frequency from the list, which belongs to, say, user $U^{(i)}$. For the other $T-2$ users, the most probable frequency is chosen. For the second combination, the second frequency from the sorted list is chosen, which belongs to, say, user $U^{(j)}$. For the other $T-2$ users, the most probable frequency is chosen. This procedure is repeated until all K frequency combinations are obtained. Since there are M possible frequencies for each user, the list of the less probable frequencies can have at most $(T-1)(M-1)$ frequencies. So, the maximal value of K in the K-MPC metric is

$$K_{\max} = 1 + (T-1)(M-1). \tag{3.11}$$

In this case, M of each user's frequencies are considered in constructing the combinations.

When one of the users has several frequencies whose probabilities are higher than the highest probability of other users' frequencies, then the resulting combinations will be biased to this user. In this case, this metric will degrade the performance of the iterative detector. For example, an *a priori* probability distribution for 4 users is given in Table 3.1. We wish to find the $K = 4$ most probable combinations. To compute $P(\bar{F}_t|f_{j_0}^{(0)})$ for user $U^{(0)}$, the frequency combinations obtained using the 4-MPC metric are given in Table 3.2. From these results, it is found that four frequencies of $U^{(1)}$ are chosen while only one frequency is chosen for $U^{(2)}$ and $U^{(3)}$. This is because for $U^{(1)}$ frequencies f_0, f_1, f_3, and f_5 are much more probable than f_2, f_4, f_6, and f_7. As a result, the value of $P(\bar{F}_t|f_{j_0}^{(0)})$ is biased toward $U^{(1)}$. In other words, $U^{(1)}$ will interfere with the detection results of the other users.

Table 3.1: An a priori probability distribution for 4 users.

	$P(f_0^{(i)})$	$P(f_1^{(i)})$	$P(f_2^{(i)})$	$P(f_3^{(i)})$	$P(f_4^{(i)})$	$P(f_5^{(i)})$	$P(f_6^{(i)})$	$P(f_7^{(i)})$
$U^{(0)}$	0.2	0.2	0.1	0.1	0.2	0.1	0.1	0
$U^{(1)}$	0.25	0.27	0	0.23	0	0.25	0	0
$U^{(2)}$	0.2	0.1	0.06	0.15	0.13	0.17	0.1	0.1
$U^{(3)}$	0	0.15	0.3	0.22	0.1	0.08	0	0.15

3.5.2 k-Most Probable Frequencies Metric

In the k-Most Probable Frequencies (k-MPF) metric, k frequencies with the highest probabilities for each of the $T-1$ users are considered in constructing the set C_0'. One of the combinations in C_0' is the one where all $T-1$ users choose their most probable frequency. For other combinations, $T-2$ users choose their most probable frequency and the last user may choose the second, third, and up to the k^{th} most probable frequency. In the k-MPF metric, each of the $T-1$ users has $k-1$ chances to choose a frequency other than the most probable one. The relationship between the size of C_0' and T is

$$K(T) = 1 + (T-1)(k-1). \tag{3.12}$$

Note that when k is equal to the number of frequencies M, the k-MPF metric is the same as the K-MPC metric with K is equal to $K_{\max}$.

The k-MPF metric is not biased towards a particular user, since k frequencies for each user are considered. However, considering the channel measurement given in

Table 3.2: Combinations considered by the 4-MPC and 2-MPF for user $U^{(0)}$.

	c_0			c_1			c_2			c_3		
Users	$U^{(1)}$	$U^{(2)}$	$U^{(3)}$	$U^{(1)}$	$U^{(2)}$	$U^{(3)}$	$U^{(1)}$	$U^{(2)}$	$U^{(3)}$	$U^{(1)}$	$U^{(2)}$	$U^{(3)}$
4-MPC	f_1	f_0	f_2	f_0	f_0	f_2	f_5	f_0	f_2	f_3	f_0	f_2
2-MPF	f_1	f_0	f_2	f_0	f_0	f_2	f_1	f_5	f_2	f_1	f_0	f_3

(3.10), the combinations obtained using the k-MPF metric may not be the most probable combinations. Hence, when the same number of combinations are considered, the k-MPF metric will perform worse than the K-MPC metric.

When computing $P(\bar{F}_t|f_{j_0}^{(0)})$ for $U^{(0)}$ from the distribution given in Table 3.1, the frequency combinations obtained using the 2-MPF metric are given in Table 3.2. It can be observed that although $U^{(1)}$ has higher probabilities for frequencies f_0, f_1, f_3 and f_5, the C_0' is unbiased since each user has two distinct frequencies considered.

3.6 The NSMP Metric

The WSMP metrics described described in the previous section depend solely on the *a priori* information of the frequency combinations, and therefore introduce significant error in the first iteration since no *a priori* information is available. On the other hand, the NSMP metric is effective in the first iteration because the second product in (3.9) can provide a measurement for the most probable combinations. This measurement is given by

$$P_{\text{dist}} = \left(\frac{1}{N_0}\right)^M \prod_{j=0}^{M-1} e^{\left(-\frac{(\mu_j\sqrt{E_s}-\sqrt{\rho_j})^2}{N_0}\right)}, \tag{3.13}$$

which measures the distance between a particular frequency combination and the received signal.

Define the pattern of a frequency combination by the vector

$$\bar{\mu} = [\mu_0, \ldots, \mu_{M-1}],$$

where μ_j is the number of users that choose f_j. Assume that the pattern for the combination with the highest channel measurement P_{dist} is known. Denote this pattern by $\bar{\mu}_{\max}$ and let $C_{\bar{\mu}_{\max}}$ be the subset of all the combinations with the pattern $\bar{\mu}_{\max}$. Then, the size of $C_{\bar{\mu}_{\max}}$ is given by

$$\begin{aligned} |C_{\bar{\mu}_{\max}}| &= \binom{(T-1)}{\mu_0}\binom{(T-1-\mu_0)}{\mu_1}\cdots\binom{(T-1-\mu_0-\mu_1-\ldots-\mu_{M-1})}{\mu_{M-1}} \\ &= \frac{(T-1)!}{\mu_0!(T-1-\mu_0)!}\frac{(T-1-\mu_0)!}{\mu_1!(T-1-\mu_0-\mu_1)!} \\ &\quad \cdots\frac{(T-1-\mu_0-\mu_1-\ldots-\mu_{M-2})!}{\mu_{M-1}!(T-1-\mu_0-\mu_1-\ldots-\mu_{M-1})!} \\ &= \frac{(T-1)!}{\mu_0!\mu_1!\ldots\mu_{M-1}!}, \end{aligned} \tag{3.14}$$

where $(T-1-\mu_0-\mu_1-\ldots-\mu_{M-1})! = 0! = 1$. Thus, the channel metric computed using NSMP in the first iteration is given by

$$P(\bar{F}_t|f^{(0)}) = |C_{\bar{\mu}_{\max}}|P_{\text{NSMP}} = |C_{\bar{\mu}_{\max}}|\left(\frac{1}{M}\right)^{T-1}P_{\text{dist}}, \tag{3.15}$$

assuming that the *a priori* probabilities are initialized to $\frac{1}{M}$.

In order to find the pattern with the highest P_{dist}, a procedure where each of the $T-1$ users pick one of the the M possible frequencies is considered and there are M stages in this procedure. At the j^{th} stage, there are μ_j users that choose the frequency f_j. At each stage, if there are i users that have made their choices, then the procedure

is in state S_i. The procedure always starts from state S_0. There are at most $T-1$ users that choose a frequency in state S_0 since no user has made any choice yet. So, state S_0 can connect to any state between S_0 and state S_{T-1}. Similarly, in state S_i, there are at most $T-1-i$ users that choose a frequency. Hence, state S_i can connect to any state between S_i and S_{T-1}. For state S_{T-1}, since all the $T-1$ users have made their choices, no user can choose the frequency in the current stage and state S_{T-1} can only connect to state S_{T-1}.

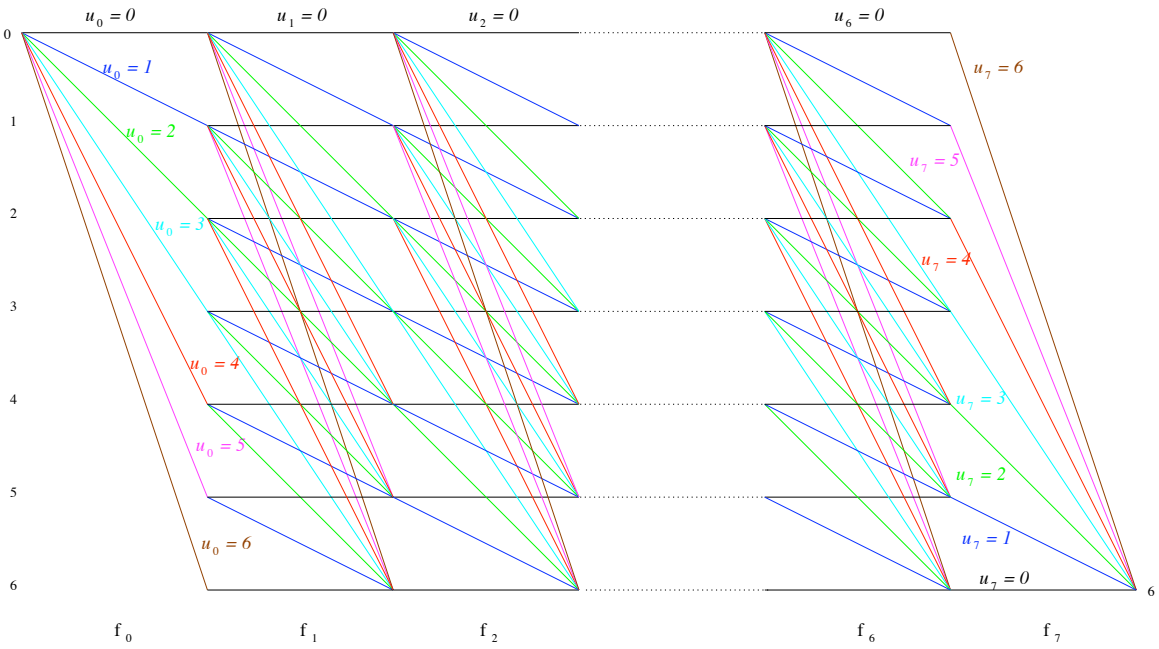

Figure 3.3: A trellis searching for the patterns of combinations with the highest P_{dist} in an 7-user, 8-frequency system.

With the states and stages defined above, a trellis can be constructed for the

frequency choosing procedure. In Figure 3.3, a trellis of an 7-user, 8-frequency system is shown. The purpose is to find the combination for computing (3.13) and (3.15). There are 7 states and 8 stages in Figure 3.3. At the j^{th} stage, if the state is S_i and μ_j users choose frequency f_j, then the next state is $S_{i+\mu_j}$. The trellis starts in state S_0 since no user has made a choice and the trellis ends up with state S_6 since all 6 users are supposed to have made their choices after considering all the M frequencies.

The goal is to use the trellis and the Viterbi algorithm [32] to find the combination, or path, with the highest P_{dist}. Note that P_{dist} can be rewritten as

$$\begin{aligned} P_{\text{dist}} &= \left\{ \frac{1}{N_o} e^{\left(-\frac{(\mu_0 \sqrt{E_s} - \sqrt{\rho_0})^2}{N_o} \right)} \right\} \left\{ \frac{1}{N_o} e^{\left\{ \frac{(\mu_1 \sqrt{E_s} - \sqrt{\rho_1})^2}{N_o} \right)} \right\} \\ &\quad \cdots \left\{ \frac{1}{N_o} e^{\left(-\frac{(\mu_{M-1} \sqrt{E_s} - \sqrt{\rho_{M-1}})^2}{N_o} \right)} \right\}. \end{aligned} \tag{3.16}$$

To compute $P(\bar{F}_t | f_{j_0}^{(0)})$, the branch metric for $\mu_j = \tau$ at the j^{th} stage is

$$m(j, \tau) = \frac{1}{N_o} e^{\left(-\frac{(\tau \sqrt{E_s} - \sqrt{\rho_j})^2}{N_o} \right)} \tag{3.17}$$

when $f_{j_0}^{(0)} \neq f_j$. Otherwise, the branch metric is computed as

$$m(j, \tau) = \frac{1}{N_o} e^{\left(-\frac{((\tau+1) \sqrt{E_s} - \sqrt{\rho_j})^2}{N_o} \right)}. \tag{3.18}$$

Figure 3.4 presents an example of the procedure on a trellis of a 4-user 8-frequency system. This procedure finds a path through the trellis with the highest P_{dist} so that the channel transition probability $P(\bar{F}_t | f_{j_0}^{(0)})$ given in (3.15) can be computed.

The Viterbi algorithm finds the path with the highest P_{dist} and the μ_j's corresponding to the branches of the path give the pattern of the combination. In Figure 3.4, the resulting pattern is

$$\bar{\mu}_{max} = \{0, 1, 1, 0, 0, 0, 1, 0\}. \tag{3.19}$$

By (3.14), the number of combinations with the pattern $\bar{\mu}_{\max}$ in (3.19) is 6. In the first iteration of the MAP-consensus decoder, the *a priori* probability $P(f_{i_u}^{(u)})$ is initialized to $1/M = 0.125$ and the $P(\bar{F}_t|f_{i_0}^{(0)})$ can be computed using (3.15).

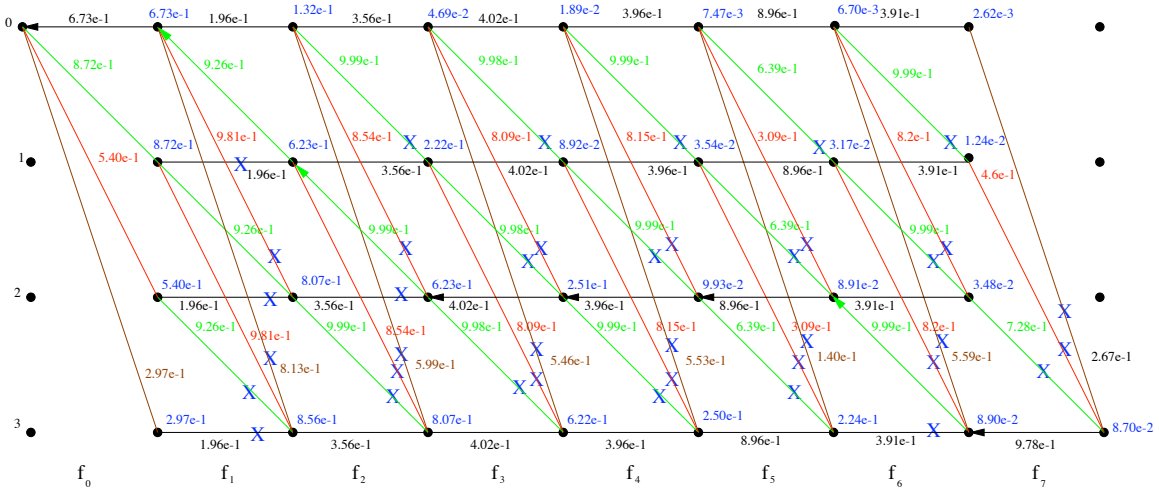

Figure 3.4: An example of the Viterbi algorithm in a 4-user, 8-frequency system.

For the trellis in Figure 3.4, the Viterbi algorithm requires $i+1$ multiplications and comparisons for each state S_i and there are $\sum_{i=1}^{T} i$ multiplications and comparisons

at each stage. Since there are M stages, the total computation needed for the NSMP is

$$N_{\text{NSMP}} = M \sum_{i=1}^{T} i = M \frac{T(T+1)}{2},$$

and the computational complexity is polynomial in T. This is also the computational complexity for NSMP in the first iteration.

To implement NSMP in later iterations, both the *a priori* information (P_{WSMP} in (3.10)) and the distance product (P_{dist} in (3.16)) of the combinations need to be considered in the construction of $C_{\bar{\mu}_{\max}}$, since the *a priori* probabilities $P(f_{j_i}^{(i)})$ are not uniformly distributed. When computing the NSMP metric using

$$P(\bar{F}_t | f_{j_0}^{(0)}) = \sum_{c_0 \in C_{\bar{\mu}_{\max}}} P_{\text{NSMP}} = \sum_{c_0 \in C_{\bar{\mu}_{\max}}} P_{\text{WSMP}} P_{\text{dist}}, \tag{3.20}$$

the subset $C_{\bar{\mu}_{\max}}$ needs to be constructed now requires one to check the patterns of all frequency combinations in the set C_0. As a result, the computational complexity is now $O(M^{T-1})$. Furthermore, the size of the subset $C_{\bar{\mu}_{\max}}$ very large. Due to the computational complexity of NSMP in later iterations is high it is recommended that K-MPC or k-MPF be used in subsequent iterations. These hybrid metrics are denoted by NSMP+K-MPC or NSMP+k-MPF.

3.7 The Relaxation Metric

The relaxation metric constructs a super-set, C_0'', of the set of all possible frequency combinations using Constraint 2. This is different from the NSMP and WSMP metrics that explicitly reduce the number of frequency combinations. Instead, the relaxation metric increases the number of combinations, but reduces the complexity of the associated computation. Constructing C_0'' is simplified through the use of *a priori* enumeration polynomials and channel transition enumeration polynomials. The simplified channel metric is

$$P(\bar{F}_t|f_{j_0}^{(0)}) \approx \sum_{c_0 \in C_0''} P(c_0|f_{j_0}^{(0)}) P(\bar{F}_t|c_0, f_{j_0}^{(0)}).$$

3.7.1 *a priori* Enumeration Polynomials

To compute the metric $P(\bar{F}_t|f_{j_0}^{(0)})$, all the $T-1$ other users need to be considered. For these users, define the *a priori* enumeration polynomial of frequency f_j by

$$V_j(D) = 1 + v_{j,1}D + \ldots + v_{j,T}D^{T-1},$$

where the coefficient $v_{j,u}$ denotes the *a priori* probability that there are u users that transmit frequency f_j. For each user, initialize a list of *a priori* enumeration polynomials $V_j^{(i)}(D)$, where

$$V_j^{(i)}(D) = 1 + P(f_j^{(i)})D. \tag{3.21}$$

Now, the polynomial $V_j(D)$ can be computed as

$$V_j(D) = \prod_{i=1}^{T-1} V_j^{(i)}(D). \tag{3.22}$$

This polynomial has degree $T-1$.

3.7.2 Channel Transition Enumeration Polynomials

Observing the product given in (3.4), the distance between the received signal and a frequency combination involving the j^{th} frequency is

$$m_j(u) = P(\rho_j | c_0, f_{j_0}^{(0)}) = \frac{1}{N_o} e^{\frac{(u\sqrt{E_s} - \sqrt{\rho_j})^2}{N_o}}.$$

When $j \neq j_0$, the channel transition enumeration polynomial for the j^{th} frequency is

$$T_j(D) = m_j(0) + v_{j,1} m_j(1) D + \ldots + v_{j,T-1} m_j(T-1) D^{T-1} \tag{3.23}$$

Otherwise, the enumeration polynomial is

$$T_j(D) = m_j(1) D + v_{j,1} m_j(2) D^2 + \ldots + v_{j,T-1} m_j(T) D^T. \tag{3.24}$$

For all M frequencies, the channel transition enumeration polynomial can be obtained by taking terms with degree T from the product $\prod_{j=0}^{M-1} T_j(D)$. Note that this product may contain terms with D^u for $u \neq T$. Based on Constraint 2, only T transmissions are allowed at each time and thus the enumeration polynomial should only contain terms with degree equal to T, i.e., $T(D)$ is of the form

$$T(D) = t_T D^T. \tag{3.25}$$

The relaxation metric is now simply

$$P(\bar{F}_t|f_{j_0}^{(0)}) \approx t_T. \tag{3.26}$$

A 3-user, 3-frequency system is considered here to illustrate this metric. The goal is to compute the channel metric $P(\bar{F}_t|f_{j_0}^{(0)})$, where $f_{j_0}^{(0)} = f_0$. To compute the *a priori* enumeration polynomials, the list of initial enumeration polynomials is first given in (3.21). Then, for frequency f_j, the convolution between $U^{(1)}$ and $U^{(2)}$ is given by

$$\begin{aligned} V_j(D) &= V_j^{(1)} \times V_j^{(2)} \\ &= \big(1 + P(f_j^{(1)})\big)\big(1 + P(f_j^{(2)})\big). \end{aligned}$$

This computation can be separated into three terms:

- Term 1: 1×1.
- Term 2: $1 \times P(f_j^{(2)}) + P(f_j^{(1)}) \times 1$.
- Term 3: $P(f_j^{(1)})P(f_j^{(2)})$,

and the result of the convolution is

$$V_j(D) = 1 + \big[P(f_j^{(1)}) + P(f_j^{(2)})\big]D + P(f_j^{(1)})P(f_j^{(2)})D^2.$$

The channel transition enumeration polynomial for frequency f_0 is computed using (3.24) which results in

$$\begin{aligned} T_0(D) &= m_0(1)D + \big[P(f_0^{(1)}) + P(f_0^{(2)})\big]m_0(2)D^2 \\ &\quad + P(f_0^{(1)})P(f_0^{(2)})m_0(3)D^3. \end{aligned}$$

For $j \neq 0$, the computation is given by (3.23) which results in

$$\begin{aligned} T_j(D) &= m_j(0) + \left[P(f_j^{(1)}) + P(f_j^{(2)})\right] m_j(1)D \\ &\quad + P(f_j^{(1)})P(f_j^{(2)})m_j(2)D^2. \end{aligned}$$

To compute $T(D)$ in (3.25), two convolutions are required. The first convolution is between $T_0(D)$ and $T_1(D)$. Ignoring terms with degree greater than 3, the result consists of three terms

- Term 1: $m_0(1) \times m_1(0)$.
- Term 2:
$$\begin{aligned} & m_0(1) \times \Big(P(f_1^{(1)}) + P(f_1^{(2)})\Big) m_1(1) \\ & + \Big(P(f_0^{(1)}) + P(f_0^{(2)})\Big) m_0(2) \times m_1(0). \end{aligned}$$
- Term 3:
$$\begin{aligned} & m_0(1) \times P(f_1^{(1)})P(f_1^{(2)})m_1(2) \\ & + \Big(P(f_0^{(1)}) + P(f_0^{(2)})\Big) m_0(2) \times \Big(P(f_1^{(1)}) + P(f_1^{(2)})\Big) m_1(1) \\ & + P(f_0^{(1)})P(f_0^{(2)})m_0(3) \times m_1(0). \end{aligned}$$

Since terms with degree greater than 3 in the above convolution will result in terms with degree greater than 3 in later convolutions, they are expurgated from the result.

The result of the expurgated convolution is

$$\begin{aligned} T_0(D) \times T_1(D) &= m_0(1)m_1(0)D + \Bigg(\Big(P(f_1^{(1)}) + P(f_1^{(2)}) \Big) m_0(1)m_1(1) \\ &\quad + \Big(P(f_0^{(1)}) + P(f_0^{(2)}) \Big) m_0(2)m_1(0) \Bigg) D^2 \\ &\quad + \Bigg(P(f_1^{(1)})P(f_1^{(2)}) m_0(1)m_1(2) \\ &\quad + \Big(P(f_0^{(1)})P(f_1^{(1)}) + P(f_0^{(1)})P(f_1^{(2)}) \\ &\quad + P(f_0^{(2)})P(f_1^{(1)}) + P(f_0^{(2)})P(f_1^{(2)}) \Big) m_0(2)m_1(1) \\ &\quad + P(f_0^{(1)})P(f_0^{(2)}) m_0(3)m_1(0) \Bigg) D^3. \end{aligned}$$

The second convolution is between $T_0(D) \times T_1(D)$ and $T_2(D)$. Since the suboptimal metric only needs the third term of $T(D)$, it is only necessary to compute

$$\begin{aligned} & m_0(1)m_1(0) \times P(f_2^{(1)})P(f_2^{(2)}) m_2(2) + \Bigg(\Big(P(f_1^{(1)}) + P(f_1^{(2)}) \Big) m_0(1)m_1(1) \\ & + \Big(P(f_0^{(1)}) + P(f_0^{(2)}) \Big) m_0(2)m_1(0) \Bigg) \times \Big(P(f_2^{(1)}) + P(f_2^{(2)}) \Big) m_2(1) \\ & + \Bigg(P(f_1^{(1)})P(f_1^{(2)}) m_0(1)m_1(2) + \Big(P(f_0^{(1)})P(f_1^{(1)}) \\ & + P(f_0^{(1)})P(f_1^{(2)}) + P(f_0^{(2)})P(f_1^{(1)}) + P(f_0^{(2)})P(f_1^{(2)}) \Big) m_0(2)m_1(1) \\ & + P(f_0^{(1)})P(f_0^{(2)}) m_0(3)m_1(0) \Bigg) \times m_2(0). \end{aligned}$$

Taking this term from this $T(D)$, the suboptimal metric is given by

$$
\begin{aligned}
&P(\bar{F}_t|f_0^{(0)}) \approx P(f_0^{(1)})P(f_0^{(2)})m_0(3)m_1(0)m_2(0) \\
&+P(f_1^{(1)})P(f_1^{(2)})m_0(1)m_1(2)m_2(0) + P(f_2^{(1)})P(f_2^{(2)})m_0(1)m_1(0)m_2(2) \\
&+\Big(P(f_1^{(1)})P(f_2^{(2)}) + P(f_1^{(2)})P(f_2^{(1)})\Big)m_0(1)m_1(1)m_2(1) \\
&+\Big(P(f_0^{(1)})P(f_2^{(2)}) + P(f_0^{(2)})P(f_2^{(1)})\Big)m_0(2)m_1(0)m_2(1) \\
&+\Big(P(f_0^{(1)})P(f_1^{(2)}) + P(f_0^{(2)})P(f_1^{(1)})\Big)m_0(2)m_1(1)m_2(0) \\
&+\Big(P(f_1^{(1)})P(f_2^{(1)}) + P(f_1^{(2)})P(f_2^{(2)})\Big)m_0(1)m_1(1)m_2(1) \\
&+\Big(P(f_0^{(1)})P(f_2^{(1)}) + P(f_0^{(2)})P(f_2^{(2)})\Big)m_0(2)m_1(0)m_2(1) \\
&+\Big(P(f_0^{(1)})P(f_1^{(1)}) + P(f_0^{(2)})P(f_1^{(2)})\Big)m_0(2)m_1(1)m_2(0).
\end{aligned}
$$

It is obvious that the sum of the first 6 terms in the above expression is equivalent to the optimal metric. The suboptimality comes from the last 3 terms, which satisfy Constrain 2 but do not satisfy Constraint 1. After a few iterations, most of the *a priori* information $P(f_j^{(i)})$ goes to 0 for the i^{th} user. The product $\prod_{j=m}^{n} P(f_j^{(i)})$ also goes to 0 for $m < n$, $m < M$ and $n < M$. Thus, the suboptimal metric will approach the optimal iterative metric after many iterations.

3.7.3 Computational Complexity

As the previous example shows, the products given in (3.22) and (3.25) can be implemented by a convolution of polynomials. For the *a priori* enumeration polynomial given in (3.22), each factor polynomial has 2 terms and the highest degree is 1. The

multiplication of these factor polynomials can be implemented by $T-2$ convolutions. In general, the i^{th} convolution results in $i+2$ steps. The first and the last step of each convolution only need 1 multiplication and no addition. For each of the other i steps, there are 2 multiplications and 1 addition. Thus, the number of multiplications required of the *a priori* enumeration polynomial (aPEP) $V_j(D)$ is

$$M_{\text{aPEP}} = \sum_{i=1}^{T-2}(1+1+2i) = (T+1)(T-2),$$

and the number of additions required is

$$N_{\text{aPEP}} = \sum_{i=1}^{T-2} i = \frac{(T-1)(T-2)}{2}.$$

Since there are M frequencies, we have to compute M polynomials as given in (3.22).

For the channel transition enumeration polynomial (CTEP) given in (3.25), there are M factors, and $M-1$ convolutions are required. All the factors have T terms, among which $M-1$ factors have highest degree $T-1$ and one factor has highest degree T. For the $M-1$ convolutions, the first $M-2$ will result in T terms since terms with degree higher than T do not have to be considered. For the i^{th} term, i multiplications and $i-1$ additions are required. Consider the result given in (3.25), the last convolution results in only one term, which has the degree T and T multiplications and $T-1$ additions are required. Thus, the number of multiplications required for all the convolutions is

$$M_{\text{CTEP}} = (M-2)\sum_{i=1}^{T} i + T = \frac{(M-2)(1+T)T}{2} + T,$$

and the number of additions required for all the convolutions is

$$\begin{aligned} N_{\text{CTEP}} &= (M-2)\sum_{i=1}^{T}(i-1)+T-1 \\ &= \tfrac{(M-2)(T-1)T}{2}+T-1. \end{aligned}$$

Finally, in order to compute the new metric given in (3.26), the total number of multiplications required is

$$\begin{aligned} M_{\text{metric}} &= M \times M_{\text{aPEP}} + M_{\text{CTEP}} \\ &= M(T+1)(T-2) + \tfrac{(M-2)(1+T)T}{2} + T, \end{aligned}$$

and the total number of additions required is

$$\begin{aligned} N_{\text{metric}} &= M \times N_{\text{aPEP}} + N_{\text{CTEP}} \\ &= M\tfrac{(T-1)(T-2)}{2} + \tfrac{(M-2)(T-1)T}{2} \\ &\quad +T-1. \end{aligned}$$

The complexity for the suboptimal relaxation metric is $O(MT^2)$, which is much lower than the complexity of the optimal metric ($O(M^{T-1})$).

3.8 Summary

A summary of the channel metrics discussed in this chapter and their properties is given in Table 3.3. The optimal metric will provide the best performance for the CFSK system but has the highest computational complexity. The simplified channel metrics provide a tradeoff between performance and computational complexity. In the

next chapter, the performance of these metrics is studied via analysis and computer simulation.

Table 3.3: Summary of channel metrics.

Metric Name	Metric Simplification	Set of Frequency Combinations	Computation Complexity
Optimal		The set of all possible frequency combinations, C_0, over the CFSK channel.	$O(M^{T-1})$
K-MPC	WSMP	Subset $C_0^{'} \subset C_0$ constructed according to the channel measurement $P_{\text{WSMP}} = \prod_{u=1}^{T-1} P(f_{i_u}^{(u)})$.	K
k-MPF	WSMP	Subset $C_0^{'} \subset C_0$ constructed according to the channel measurement $P_{\text{WSMP}} = \prod_{u=1}^{T-1} P(f_{i_u}^{(u)})$.	$1+(T-1)(k-1)$
NSMP		Subset $C_{\bar{\mu}_{\max}} \subset C_0$ constructed according to the channel measurement $P_{\text{NSMP}} = P_{\text{WSMP}} P_{\text{dist}}$ and $P_{\text{dist}} = \prod_{j=0}^{M-1} e^{\left(-\frac{(\mu_j \sqrt{E_s} - \sqrt{\rho_j})^2}{N_0}\right)}$.	$O(MT^2)$ in the 1st iteration, $O(M^{T-1})$ in subsequent iterations
NSMP+K-MPC	Hybrid	Subset $C_{\bar{\mu}_{\max}} \subset C_0$ constructed according to the channel measurement P_{NSMP} for the 1st iteration, $C_0^{'} \subset C_0$ constructed according to P_{WSMP} for subsequent iterations.	$O(MT^2)$ in the 1st iteration, K in subsequent iterations
NSMP+k-MPF	Hybrid	Subset $C_{\bar{\mu}_{\max}} \subset C_0$ constructed according to the channel measurement P_{NSMP} for the 1st iteration, $C_0^{'} \subset C_0$ constructed according to P_{WSMP} for subsequent iterations.	$O(MT^2)$ in the 1st iteration, $1+(T-1)(k-1)$ in subsequent iterations
Relaxation		Superset $C_0^{''} \supset C_0$ constructed according to Constraint 2	$O(MT^2)$

Chapter 4

Performance of Multiuser Detection

4.1 Induction

The performance of the multiuser detectors discussed in Chapter 3 is studied in this chapter, primarily via computer simulation. The distance of the super-trellis code is used as a metric to analyze the performance of the multiuser detectors. A comparison is made between MLSD and the optimal iterative detector based on this metric.

The performance of the simplified metrics derived in Chapter 3 is then studied using simulation results and the distance metric. Finally, EXIT chart analysis between the multiuser detector and the channel decoders is used for performance analysis and

code design.

4.2 Distance of the Super-Trellis Codes

The performance of the CFSK system is strongly influenced by the distance properties of the super-trellis code. In Section 3.2, a super-trellis code was given for an example of 2 users. In order to discuss the distance property of the super-trellis code, the notation introduced in Figure 4.1 are needed. The convolutional encoder CC_i takes the binary sequence $\bar{v}_i$ as inputs and outputs the binary sequence $\bar{u}_i$, where

$$\bar{v}_i = \{v_{i,0}, v_{i,1}, \ldots\},$$

and

$$\bar{u}_i = \{u_{i,0}, u_{i,1}, \ldots\},$$

for $0 \leq i \leq T-1$. Each code sequences is mapped to a sequence of M-ary FSK signals $\bar{f}^{(i)}$. Let the length of each coding block be N, then the transmitted signal sequence $\bar{f}^{(i)}$ is denoted as

$$\bar{f}^{(i)} = \{f_0^{(i)}, f_1^{(i)}, \ldots, f_{N-1}^{(i)}\},$$

where $f_t^{(i)}$ denotes the frequency in the i^{th} sequence at time t. For any integer q, assume that each q-tuple of coded bits is mapped to a frequency. Then, $M = 2^q$ and $f_t^{(i)}$ are over $GF(2^q)$ for $i \in \{0, \ldots, T-1\}$ and $0 \leq t \leq N-1$.

The adder in Figure 4.1 results in the super-trellis code sequence

$$\bar{R} = \{\bar{r}_0, \bar{r}_1, \ldots, \bar{r}_{N-1}\},$$

where $\bar{r}_t$ is an M-tuple

$$\bar{r}_t = [\mu_{t,0}, \mu_{t,1}, \ldots, \mu_{t,M-1}].$$

The value $\mu_{t,j}$ denotes the number of transmissions on frequency f_j by all users at time t, where $j \in GF(2^q)$. For a T-user system, $\sum_{j=0}^{M-1} \mu_{t,j} = T$. The set of all super-trellis code sequences is denoted by $\mathcal{R}$.

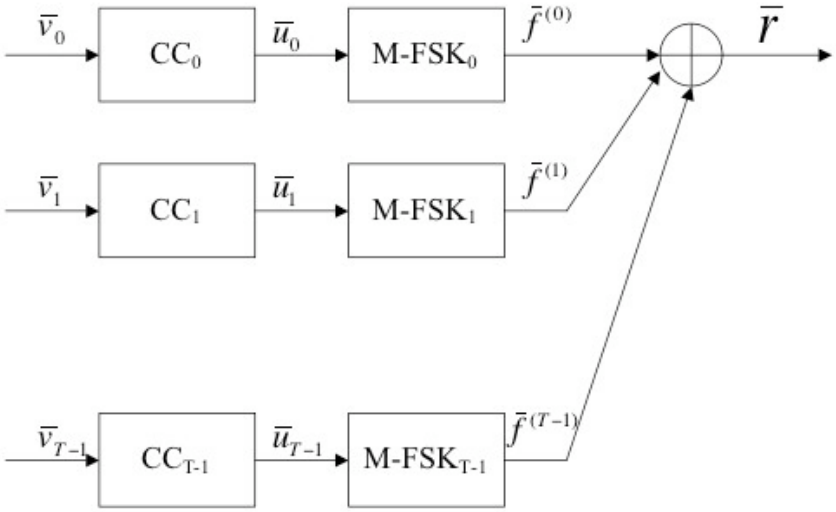

Figure 4.1: A T-user CFSK system.

Definition 1 *The hamming distance between two super-trellis code sequences $\bar{R}$ and $\bar{R}'$ is the number of positions in which $\bar{r}_t \neq \bar{r}'_t$. Note that $\bar{r}_t \neq \bar{r}'_t$ whenever $\mu_{t,j} \neq \mu'_{t,j}$*

for any $0 \leq j \leq M-1$.

The hamming distance of a super-trellis code is different from that of the convolutional codes in that the super-trellis code is nonlinear. Since the addition in Figure 4.1 is not over the Galois Field GF(2^q), the hamming distance between any two code sequences in $\mathcal{R}$ is not equal to the distance between the sum of these two sequences and the all zero sequence.

Definition 2 *The minimum distance* $d_{\min}$ *of a super-trellis code of length* N *is the minimum hamming distance between any two length* N *code sequences* $\bar{R}$ *and* $\bar{R}'$.

We can now introduce the notion of uniquely decodable codes for the CFSK system with intensity information.

Definition 3 *A uniquely decodable code maps a input sequence into a unique output sequence.*

Proposition 1 *The super-trellis code corresponding to the CFSK system with intensity information has* $d_{min} \neq 0$*, if and only if the super-trellis is* uniquely decodable.

Definition 4 *The distance enumerating function for a super-trellis code is*

$$A(W) = \sum_{d=d_{\min}}^{N} A_d W^d,$$

where A_d *is the number of code word pairs* $\bar{r}, \bar{r}' \in \mathcal{R}$ *with hamming distance between* $\bar{r}$ *and* $\bar{r}'$ *equal to* d.

According to Proposition 1, the super-trellis code is uniquely decodable if $A_0 = 0$.

4.3 Suboptimality of Iterative Multiuser Detection

The suboptimality of the iterative multiuser detector is measured relative to the optimal multiuser detector implemented with MLSD. The optimal iterative multiuser detector implements the metric computation given in (3.6). A 3-user, 4-frequency synchronous CFSK system with intensity information is simulated. The channel codes are randomly generated convolutional codes with rate 1/2 and memory 2. Each coding block is of length 12. Figure 4.2 shows the codes generated for the three users.

A careful study of the super-trellis code constructed from these component codes reveals that it is not uniquely decodable. For example, if the input to the super-trellis is

$$\bar{v}_0 = \{111101001110\},$$

$$\bar{v}_1 = \{110000010100\},$$

and

$$\bar{v}_2 = \{111111001110\},$$

then the output is

$$\bar{R} = \{[0012], [0021], [1011], [0120], [1110], [1002], [2100], [1110], [0111], [0021], [1011], [3000]\}. \tag{4.1}$$

The set of inputs

$$\bar{v}_0 = \{111101011010\},$$

$$\bar{v}_1 = \{110000010100\},$$

and

$$\bar{v}_2 = \{111111011100\},$$

also result in the transmitted sequence of (4.1). So, this super-trellis code is not uniquely decodable.

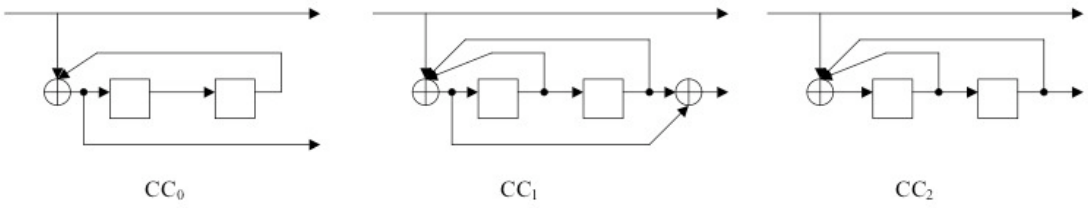

Figure 4.2: The random convolutional codes for 3 users.

This system was simulated and the results are shown in Figure 4.3. 5000 information bit errors are counted for each user. For the iterative detector, 16 iterations are used.

Both bit error rate (BER) curves shown in Figure 4.3 consist of a waterfall region and an error floor region. The suboptimality of the iterative multiuser detector is reflected in both the waterfall region and the error floor region. In the waterfall region, the iterative detector has a smaller slope, which results in a gap of about 1 dB when the BER is 10^{-1} and above 2 dB when the BER is 5×10^{-2}. The error floor of the iterative detector is much higher than that of MLSD.

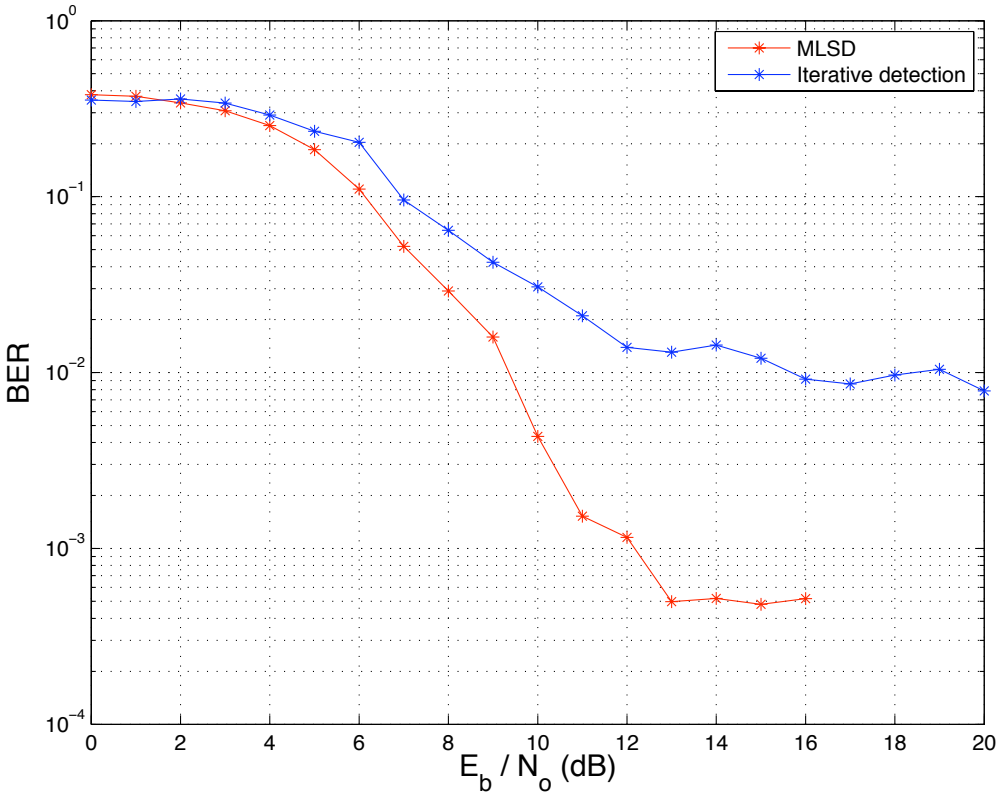

Figure 4.3: Average BER performance of the 3-user, 4-frequency synchronous system with component codes shown in Figure 4.2.

The BER performance of the MLSD provides a lower bound for the iterative detector and is closely related to the distance spectrum of the super-trellis code as described by the distance enumerating function $A(W)$. In [34], Pérez, et al., investigated the distance spectrum for turbo codes, and provided an explanation for the waterfall and error floor regions of their performance curves. A similar explanation exists for the CFSK system.

First, the error floor is caused by the low distance between codewords of the super-trellis code. The level of the error floor is decided by the value of $A_{d_{\min}}$. If the A_d's for small distances have large values, then the error floor is relatively high. When the super-trellis code is not uniquely decodable, $d_{\min} = 0$ and $A_0 \neq 0$. In this case, an error floor exists in the BER performance of the CFSK system because there are two paths through the super-trellis with the same transmitted sequence $\bar{R}$. The larger A_0 is, the higher the error floor will be. In Figure 4.3, it can be observed that the error floor of MLSD has a slope approaching zero since the super-trellis code is not uniquely decodable. The fact that the error floor occurs at $\approx 4 \times 10^{-4}$ implies that A_0 has a relatively small value.

The waterfall region is a consequence of the density of the distance spectrum. If the distance spectrum of the super-trellis code is sparse for low and moderate distances, then the waterfall is steep. A sparse distance spectrum means that the A_d's have small values for small values of d. On the other hand, the distance spectrum is dense when

A_d's have large values. The waterfall region for MLSD in Figure 4.3 has a relatively small slope, which implies that the distance spectrum is likely to be dense. This suggests that choosing component codes that result in a sparse distance spectrum may result in better performance in the waterfall region. In subsequent discussions on channel interleavers and code design, this observation is shown to be correct.

It is a somewhat surprising that the error floor for the iterative detector is so much higher than that of MLSD, since the two BER curves are based on the same distance spectrum and the level of the error floor is largely determined by $A_{d_{\min}}$. The reason for this difference is that multiuser interference is introduced during the iterative detection. For the initial iterations, the soft information on the symbols is not accurate, and this information is exchanged among the users, which leads to multiuser interference. This amounts to introducing an additional noise into the system.

4.3.1 Channel Interleavers

In [35], the random channel interleavers were introduced to reduce the level of correlation among the users' channel codes for a Trellis-Coded Multiple-Access (TCMA) system similar to the CFSK system. In an attempt to improve the distance properties of the super-trellis code, symbol-based pseudorandom channel interleavers, denoted by Π_i, are introduced for each user after the M-FSK modulator. The interleavers

randomly permute the symbols within a block of length N. At the receiver, the users' component decoders need to be modified, as shown in Figure 4.4, so that the component decoder knows all the users' interleavers.

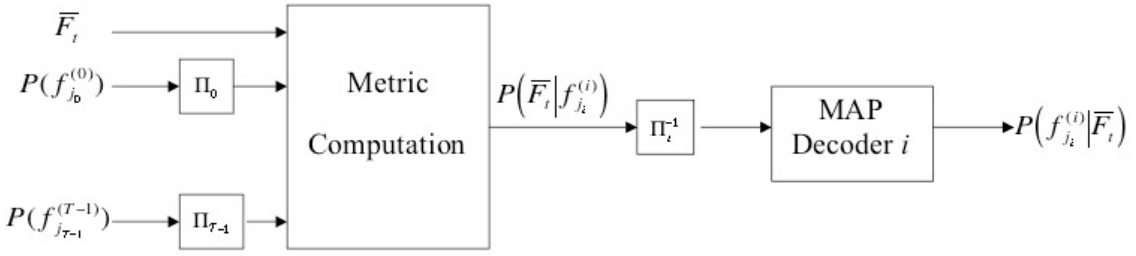

Figure 4.4: Component decoder for the i^{th} user with channel interleavers.

In general, the size of the interleaver equals the length of the coding block, N, but interleaver size can affect performance. In Figure 4.5, the performance of the synchronous 3-user, 4-frequency system is shown with different interleaver sizes. As the size of the interleaver increases, the BER performance improves.

From the distance spectrum perspective, the interleavers make the distance spectrum of the super-trellis code sparse, and reduce the multiplicities A_d for small distances. Thus, the BER curve becomes steeper in the waterfall region and the error floor is lowered. At some point, increasing the size of the interleaver does not continue to improve performance. In Figure 4.5, when the interleaver size is increased from 1000 to 10000, the performance improvement is negligible, in contrast to the significant improvement that occurs when the interleaver size is increased from 250

to 1000.

The use of channel interleavers also increases the memory of the super-trellis by a factor of N, the size of the interleaver, and makes the implementation of MLSD impractical. Thus, the performance of the MLSD with channel interleavers is not shown in Figure 4.5. It is interesting that the performance of the iterative detector with channel interleavers is better than the performance of MLSD without interleavers. Channel interleavers are used for the remainder of this work.

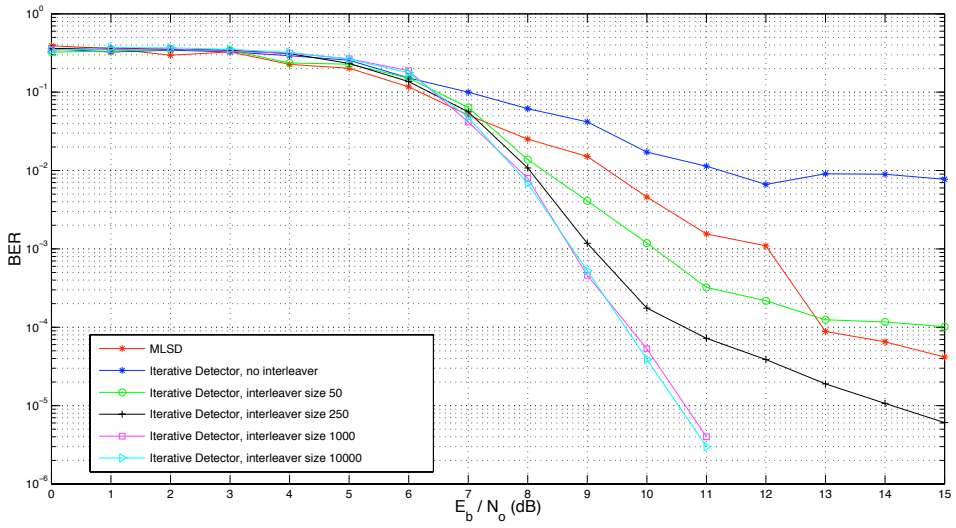

Figure 4.5: Performance of the synchronous 3-user, 4-frequency system with channel interleavers and the component codes shown in Figure 4.2.

4.4 Performance of Simplified Metrics

The BER performance of the K-MPC and k-MPF metrics is now studied in a synchronous system using rate 1/3 codes with memory 6 and 8 frequencies. The number of users is varied from 1 to 4, and the corresponding spreading factor changes from 8 to 2, respectively. The code block length is 250 symbols and 16 iterations are used. Figure 4.6 shows the results for a two-user system and it is clear that 2-MPC and 2-MPF have the same performance since the frequency combinations considered by these two metrics are exactly the same.

For the 4-user system, 22 combinations are used for K-MPC and k-MPF. Since T is 4 and M is 8. $K_{\max}$ is 22 according to (3.11) and this is the maximum number of combinations. From (3.12), $k = 8$ should be used when $K = 22$. Since $K = K_{\max}$, K-MPC and k-MPF are exactly the same. Thus, 22-MPC and 8-MPF have the same performance for the 4-user case. To compare K-MPC and k-MPF further, results are shown in Figure 4.7 for synchronous 8-frequency systems with rate 1/3, memory 3 codes. The results show that the performance of K-MPC and k-MPF are very similar when the number of frequency combinations considered by the two metrics is the same. For this reason, only K-MPC will be considered in later discussions.

In general single-user performance provides a lower bound for the performance of multiuser detection systems and the single-user performance is shown in Figure 4.6. The performance of the iterative detector with the optimal metric is also given. For

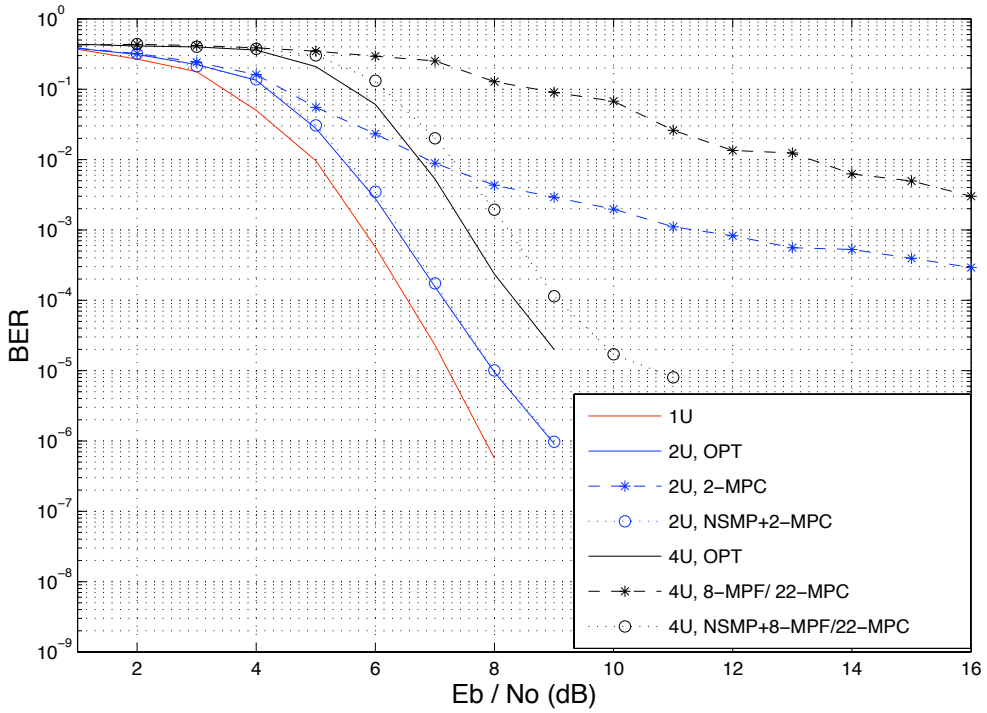

Figure 4.6: Average BER performance of a synchronous 8-frequency system with rate 1/3, memory 6.

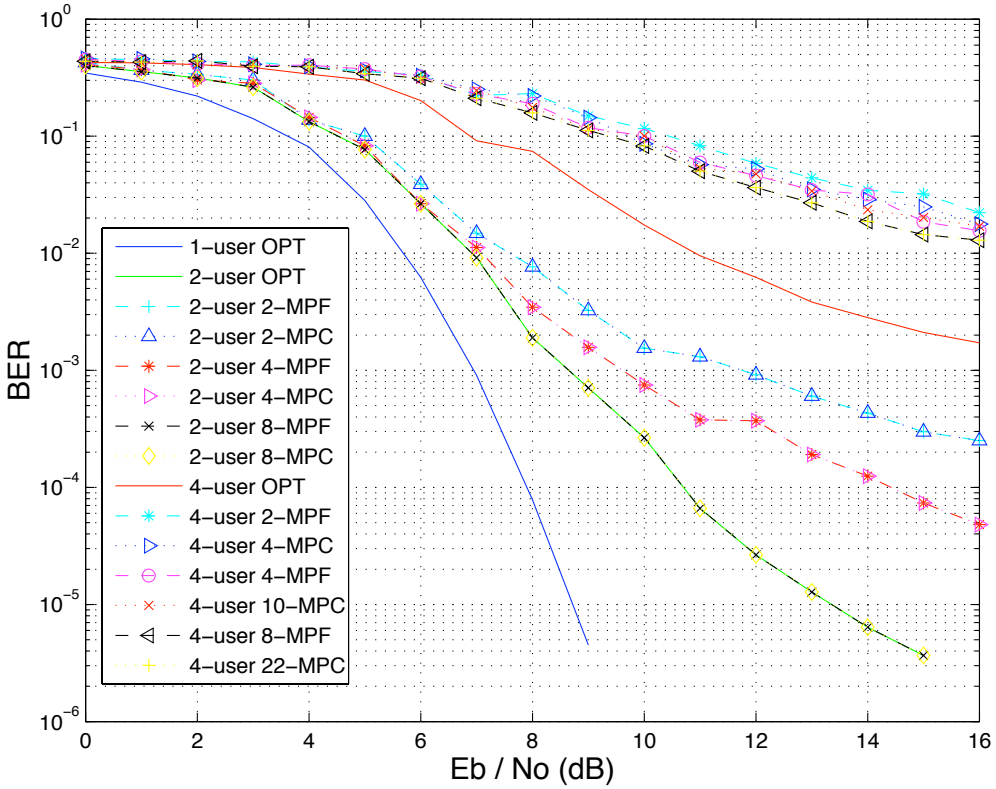

Figure 4.7: The average BER performance of a synchronous 8-frequency system with rate 1/3, memory 3 codes as a function of SNR.

the 2-user case, the iterative detector with the optimal metric is within 1dB of the single-user performance. For the 4-user case, the optimal iterative detector is 2dB worse than the single-user performance. In both systems, no error floor is observed in the simulation results. Compared with the optimal iterative multiuser detector, K-MPC and k-MPF are highly suboptimal and the waterfall region can hardly be distinguished from the error floor. In order to improve this performance, the NSMP metric is used in the first iteration. For the 2-user case, the performance of NSMP+2-MPC is the same as the optimal metric. For the 4-user case, the performance of NSMP+22-MPC is improved to within 1dB of the optimal metric. In both cases, no error floor is observed.

In order to investigate the improvement due to the use of the NSMP metric in the first iteration in a more detailed manner, the convergence behavior of the iterative detector is studied for the 2-user, 8-frequency system with rate 1/3, memory 6 codes at 7 dB. The convergence behavior of this system is shown in Figure 4.8. In the first iteration, the BER of 2-MPC and 2-MPF is much higher than the BER of the optimal metric. The poor performance in first iteration of the 2-MPC and 2-MPF metrics results in significant multiuser interference in subsequent iterations, and limits the performance. When the NSMP metric is used in the first iteration, the BER converges to that given by the optimal metric and the convergence is faster than the system without using NSMP metric.

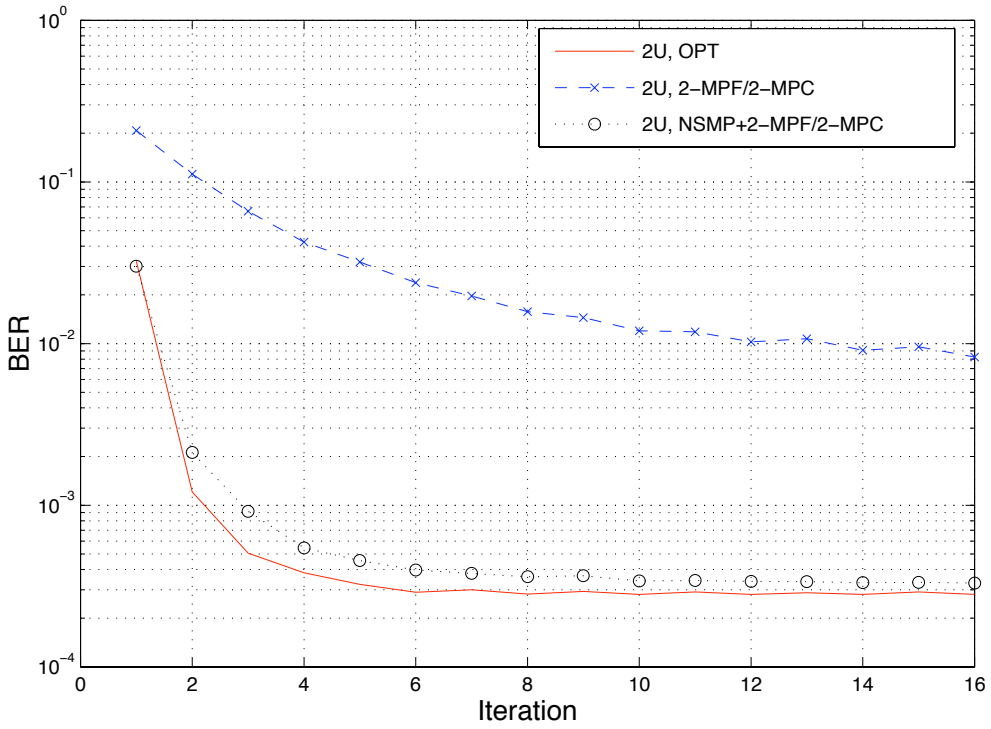

Figure 4.8: The convergence of 2-user iterative detection with rate 1/3, memory 6 codes at 7 dB.

To investigate the performance of the simplified metrics under high loads, a 3-user, 4-frequency system is simulated with rate 1/2, memory 2 convolutional codes. This results in a spreading factor of 1.33. Figure 4.9 shows the performance of this system with different metrics, including the relaxation metric. The results show that the relaxation metric has performance very close to the optimal metric. For both the optimal metric and the relaxation metric, the performance is within 1dB of the single user performance. For the 3-MPC metric, the iterative detector diverges and the performance is flat. This behavior is explained by the EXIT chart analysis in Section 4.5. The NSMP+3-MPC detector has an error floor above 10^{-3}. If NSMP is used in all the iterations, there is a 4dB loss compared to the optimal metric.

The relaxation metric still performs well for an overloaded system with 8 users 4 frequencies as shown in Figure 4.10. In this simulation, the code rate is 1/6 and 2 coded bits are mapped to a frequency. The resulting spreading factor is 0.5. The performance of the optimal iterative detector cannot be simulated due to its complexity. The performance of the relaxation detector approaches the single user performance, which implies that the performance is close to the optimal metric. The performance using the NSMP metric in all the iterations is also given in Figure 4.10 and is more than 3dB worse than the single user performance. The sum rate for this simulation is 2.67 bits per channel use, where the sum rate is defined by

$$R_{\text{sum}} = T\frac{k}{n}\log_2 M, \tag{4.2}$$

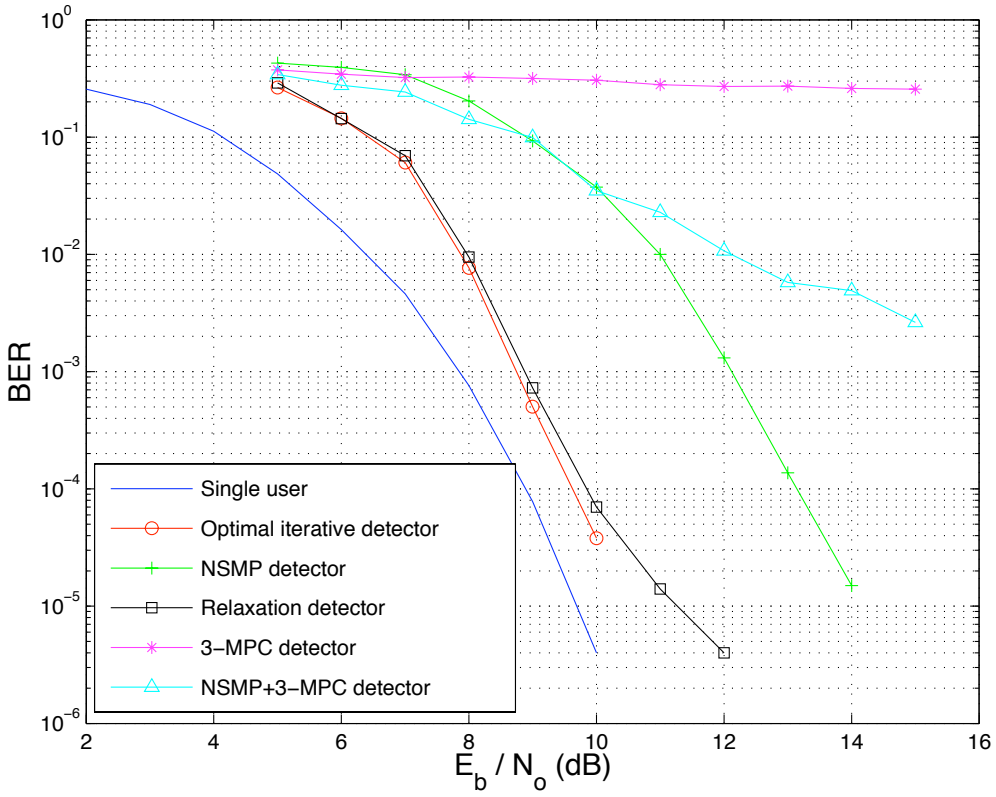

Figure 4.9: Performance of a 3-user 4-frequency system with rate 1/2, memory 2 codes and different metrics.

where k/n is the rate of the convolutional codes. This is 35% of the channel capacity[13] and is higher than all known results for DS/CDMA systems with iterative multiuser detection [36, 28, 29, 30, 37, 38, 27, 31, 5, 6]. In Chapter 6, detailed rate comparisons will be made between the CFSK system and CDMA systems.

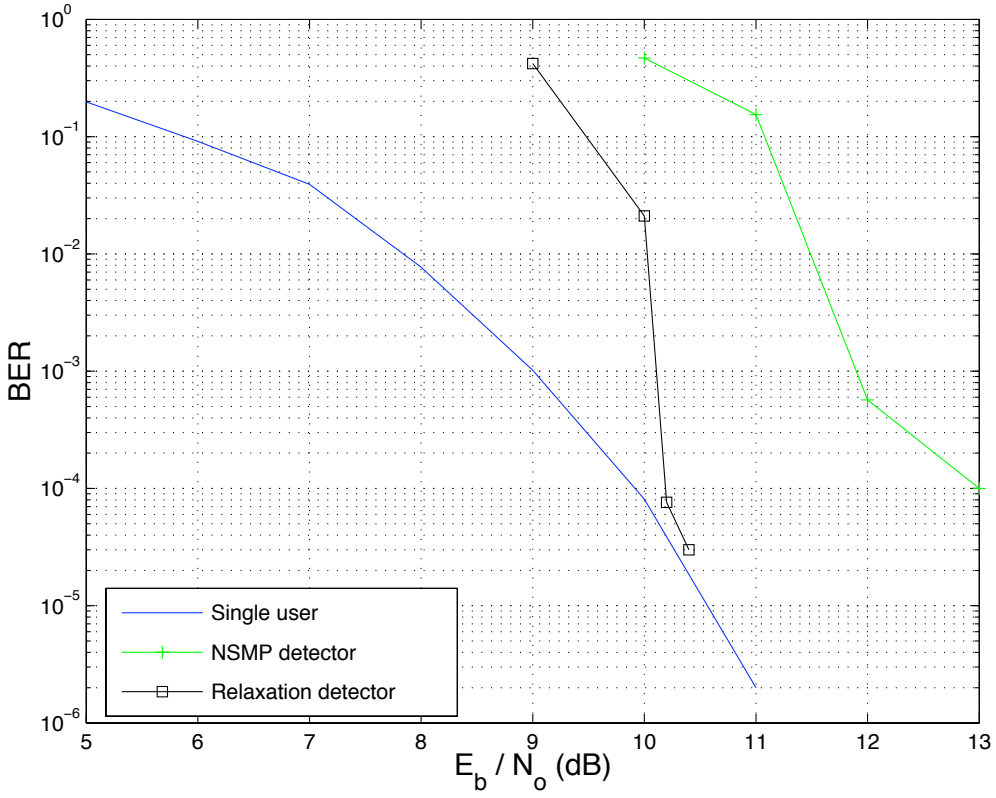

Figure 4.10: Performance of a 8-user 4-frequency system with rate 1/6, memory 4 codes.

4.5 EXIT Chart Analysis

Extrinsic information transfer chart (EXIT chart) analysis, first proposed by ten Brink [39, 40, 41], is known to be an effective approach for predicting the convergence behavior of iterative decoders, including the SNR convergence threshold and the onset of the waterfall region. This approach has been successfully extended to DS/CDMA [42, 43] and TCMA systems [44] to predict the convergence of different iterative multiuser detectors and to provide direction for code design.

The non-binary nature of the CFSK system limits the application of the EXIT chart analysis because the statistics and computation of the multi-dimensional extrinsic information is fairly complex. In [45], Grant proposed a feasible approach to analyze non-binary iterative decoding of serial concatenated convolutional codes using EXIT charts. This approach is adopted here for the EXIT chart analysis of iterative multiuser detection in the CFSK system. For a system with a small number of users and frequencies, simulation results show that this approach is precise in predicting the performance of the iterative detector.

The system model for the EXIT analysis of the CFSK system is shown in Figure 4.11. At the transmitter, user $U^{(i)}$ transmits symbol $f_j^{(i)}$ that results in the received signal $\bar{F}$. The *a priori* information of the transmitted symbols of user $U^{(i)}$ is given

in the vector of probabilities

$$A_1^{(i)} = [p(f_0^{(i)}), p(f_1^{(i)}), \ldots, p(f_{M-1}^{(i)})],$$

where the subscript "1" denotes that this *a priori* information is input to the metric computation block in Figure 4.11. The metric computation uses this *a priori* information to compute the extrinsic information. For user $U^{(i)}$, the extrinsic information is given by the vector

$$E_1^{(i)} = [p(\bar{F}|f_0^{(i)}), p(\bar{F}|f_1^{(i)}), \ldots, p(\bar{F}|f_{M-1}^{(i)})], \tag{4.3}$$

where the subscript "1" denotes that this extrinsic information is output from the metric computation. Similarly, the *a priori* information input to the i^{th} MAP decoder is denoted by $A_2^{(i)}$ and the output extrinsic information from the i^{th} MAP decoder is denoted by $E_2^{(i)}$. Assuming that random symbol-based channel interleavers and deinterleavers with very long interleaving blocks are placed between the metric computation and the MAP decoders, as shown in Figure 4.11, then $A_1^{(i)}$ is independent of E_2^i and $A_2^{(i)}$ is independent of $E_1^{(i)}$.

Let $A_1^{(i)} \in A_1$, where A_1 is the ensemble of $A_1^{(i)}$'s for $i \in \{0, 1, \ldots, T-1\}$. Let $f_{j_i}^{(i)} \in \mathcal{F} = \{f_0, \ldots, f_{M-1}\}$. Then, the mutual information between A_1 and $\mathcal{F}$, $I(\mathcal{F}, A_1)$, depends on the joint distribution $\psi_{\mathcal{F},A_1}(f, a)$. The mutual information can be computed as

$$IA_1 = I(\mathcal{F}, A_1) = \sum_{f \in \mathcal{F}} \int_{a \in A_1} \psi_{\mathcal{F},A_1}(f, a) log \frac{\psi_{\mathcal{F},A_1}(x, a)}{\sum_{u \in \mathcal{F}} \psi_{\mathcal{F},A_1}(u, a) \int_{\alpha \in A_1} \psi_{\mathcal{F},A_1}(f, \alpha) d\alpha} da.$$

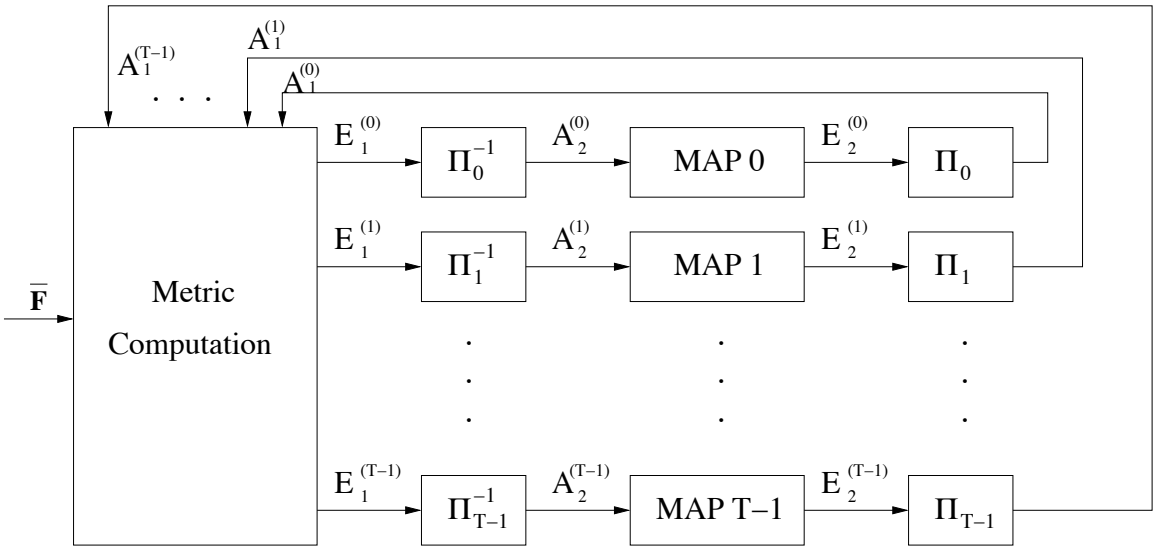

Figure 4.11: Extrinsic information transfer analysis of the CFSK system.

Let $E_1^{(i)} \in E_1$, where E_1 is the ensemble of $E_1^{(i)}$'s for $i \in \{0, 1, \ldots, T-1\}$. Then, the mutual information between E_1 and the transmitted symbol is computed as

$$IE_1 = I(\mathcal{F}, E_1) = \sum_{f \in \mathcal{F}} \int_{e \in E_1} \psi_{\mathcal{F},E_1}(f,e) log \frac{\psi_{\mathcal{F},E_1}(f,e)}{\sum_{u \in \mathcal{F}} \psi_{\mathcal{F},E_1}(u,e) \int_{\epsilon_1 \in E_1} \psi_{\mathcal{F},E_1}(f,\epsilon) d\epsilon} de, \tag{4.4}$$

where $\psi_{\mathcal{F},E_1}(f,e)$ is the joint distribution of $\mathcal{F}$ and E_1. As a result, the mapping between IA_1 and IE_1 satisfies

$$IE_1 = \eta(IA_1),$$

which is known as the extrinsic information transfer function. The plot of IE_1 versus IA_1 is the EXIT chart for the metric computation. Likewise, the EXIT chart of the

MAP decoders is defined by

$$IE_2 = \eta(IA_2),$$

which shows the relationship between $IA_2 = I(\mathcal{F}, A_2)$ and $I(\mathcal{F}, E_2)$.

To compute the mutual information $I(\mathcal{F}, A_1)$, the distribution of the values of $p(f_j^{(i)})$ needs to be known. Discussions in [41, 45] show that this distribution can be controlled to generate different levels of IA_1. The approach is based on the assumption that the coded bit symbols are independent within each coding block, and their probabilities follow the Gaussian distribution. Using symbol-based interleavers, this assumption can be satisfied asymptotically.

The probabilities $P(f_j^{(i)})$ are generated in the following manner. Suppose $f_j^{(i)} = f_j$ is transmitted, then a q-tuple binary sequence $\bar{b}_j$ is obtained through naturally binary mapping of the frequency index j. After adding Gaussian noise to each bit of $\bar{b}_j$, an observation of $\bar{b}_j$ over the binary-input Gaussian channel is generated. The probability $P(f_j^{(i)})$ is then computed by measuring the Euclidean distance between $\bar{b}_j$ and its observation. Over the binary channel, the level of the Gaussian noise is controlled using the relationship $\sigma_A = J^{-1}(I_A)$ [41]. For the CFSK system, $I_A = I(\mathcal{F}, A_1)/q$ and σ_A is computed as

$$\sigma_A = J^{-1}(I(\mathcal{F}, A_1)/q). \tag{4.5}$$

With $P(f_j^{(i)})$ as inputs the corresponding mutual information $I(\mathcal{F}, E_1)$ can be measured at the output of the metric computation using (4.4).

This requires a measurement of the joint distribution $\psi_{\mathcal{F},E_1}(f,e_1)$ where $e_1 \in E_1$ has the form of (4.3) and is multi-dimensional. It is extremely complicated to compute the integral in (4.4). In [45], a function, $\mathcal{S}:\Lambda^M \mapsto \Xi$, is introduced to map a vector of real numbers to a scalar where $\Lambda \subset \mathbb{R}$ is the set of real numbers between 0 and 1 and Ξ is a subset of integers. The function $\mathcal{S}$ requires Q-level quantization over each dimension of e_1 such that the quantized level of the j^{th} dimension is Q_j. Then, the mapping is defined as

$$S(e_1) = \sum_{j=0}^{M-1} Q^j \lfloor Q_j \rfloor, \tag{4.6}$$

The map $\mathcal{S}$ is nearly one-to-one given enough quantization levels. $I(\mathcal{F},E_1)$ can then be approximated by $I(\mathcal{F},\Xi)$. Since $S(e_1)$ is a scaler, it is simple to obtain the joint distribution $\psi_{\mathcal{F},\Xi}(f,S(e_1))$ and to compute $I(\mathcal{F},S(e_1))$ using

$$IE_1 \approx I(\mathcal{F},\Xi) = \sum_{f\in\mathcal{F}}\sum_{s\in\Xi} \psi_{\mathcal{F},\Xi}(f,s) log \frac{\psi_{\mathcal{F},\Xi}(f,s)}{\sum_{u\in\mathcal{F}}\psi_{\mathcal{F},\Xi}(u,s)\sum_{\xi\in\Xi}\psi_{\mathcal{F},\Xi}(f,\xi)}, \tag{4.7}$$

The number of possible values of $S(e_1)$ given in (4.6) increases exponentially as the number of frequencies M increases. Thus, to obtain sufficient statistics on $S(e_1)$, such that the joint distribution $\psi_{\mathcal{F},\Xi}(f,S(e_1))$ is precise enough, requires the length of the coding block to increase exponentially with M. Thus, later discussions will be limited to systems with a small number of frequencies so that the EXIT chart analysis is precise.

A 4-user, 4-frequency CFSK system with rate 2/6 and memory 6 random convolutional codes is now analyzed. For FSK modulation, 2 coded bits are mapped to a

frequency. From (4.6), a large value of Q results in a more precise mapping but will also increase the complexity and lead to the choice of a long coding block. 15-level quantization is considered here, and the length of each coding block is 60000.

In Figure 4.12, the EXIT curves of the optimal iterative multiuser detector and the relaxation detector are shown for an SNR of 8 dB. The results show that the EXIT curve of the code crosses with the EXIT curves of both detectors. This implies that the two detectors do not converge at 8 dB. In Figure 4.13, the EXIT curves of the two detectors at 9 dB do not cross with the curve of the code. Thus, the two detectors converge at 9 dB. The BER performance of the system is shown in Figure 4.14 and it is clear that the optimal iterative detector and the relaxation detector converge after 8 dB.

An interesting result in the EXIT charts in Figure 4.12 is that the relaxation detector is even better than the optimal iterative detector when the input *a priori* information is poor. To observe this, the BER performance of the optimal iterative detector and the relaxation detector between 8 dB and 9 dB is shown in Figure 4.15. This figure shows that the relaxation detector converges starting at 8.1dB, whereas the optimal iterative detector starts to converge at 8.5 dB.

In Figure 4.13, the EXIT curve of the NSMP detector is also given and it can be seen to be worse than those of the optimal iterative detector and the relaxation detector. The results in Figure 4.13 show that NSMP detector does not converge at 9

dB. When the SNR is increased to 10 dB, the EXIT chart given in Figure 4.16 shows that NSMP will converge. This result is consistent with the BER performance given in Figure 4.14, where the waterfall region of the NSMP detector starts after 9 dB.

The EXIT curve of the 4-MPC detector given in Figure 4.16 shows that the 4-MPC detector does not converge at 10 dB. When the SNR keeps increasing, the improvement of the 4-MPC detector is small as shown in Figure 4.17. Thus, the 4-MPC detector never converges even when the SNR $\geq$ 16 dB. If NSMP is used in the first iteration, the values of IE_1 is shown as triangles in Figure 4.17. At 11 dB, the value of IE_1 for NSMP in the first iteration is higher than the intersection of the 4-MPC curve and the code curve. Thus, the NSMP+4-MPC detector converges after 11 dB. The BER performance for NSMP+4-MPC in Figure 4.14 is consistent with the EXIT analysis.

Finally, the complexity of the convolutional codes is investigated using the EXIT chart analysis. In Figure 4.18, the EXIT curves of codes with rate 2/6 and memory 4, memory 6 and memory 8 are compared. The results show that large memory codes have small values for IE_2 when the input *a priori* information IA_2 is small. For high IA_2 values, the codes with large memories have large values for IE_2. Thus, a system using large memory codes is less likely to converge than one with small memory codes. This is consistent with the conclusions given in [41, 45]. In later discussions on code design in Chapter 5, this problem is investigated in detail.

4.6 Conclusion

The simulation results in this chapter show that the relaxation metric provides the best performance among the simplified metrics. The BER performance of the relaxation metric is close to that of the optimal iterative metric. With the NSMP metric in the first iteration, the performance of the WSMP metrics is significantly improved. NSMP+K-MPC and NSMP+k-MPF metrics have low complexity and can be used when the code rate is low. EXIT chart analysis is an effective method to predict the convergence of the iterative detectors.

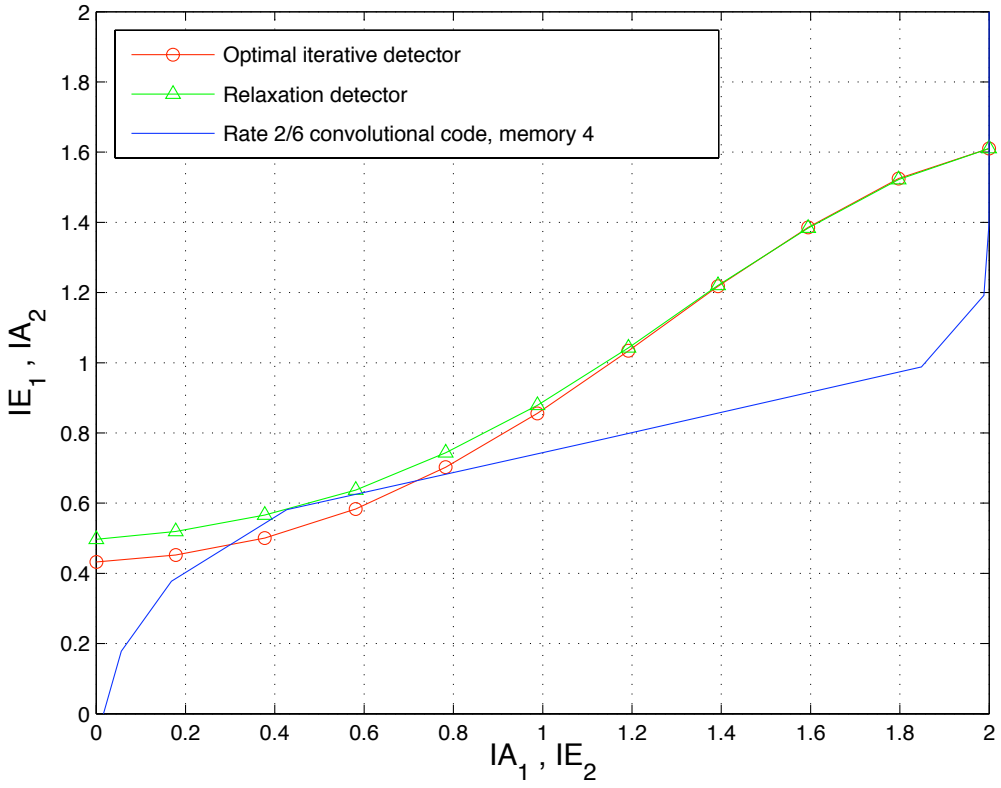

Figure 4.12: EXIT chart at 8 dB for optimal iterative detector and relaxation detector with rate 2/6, memory 4 convolutional codes.

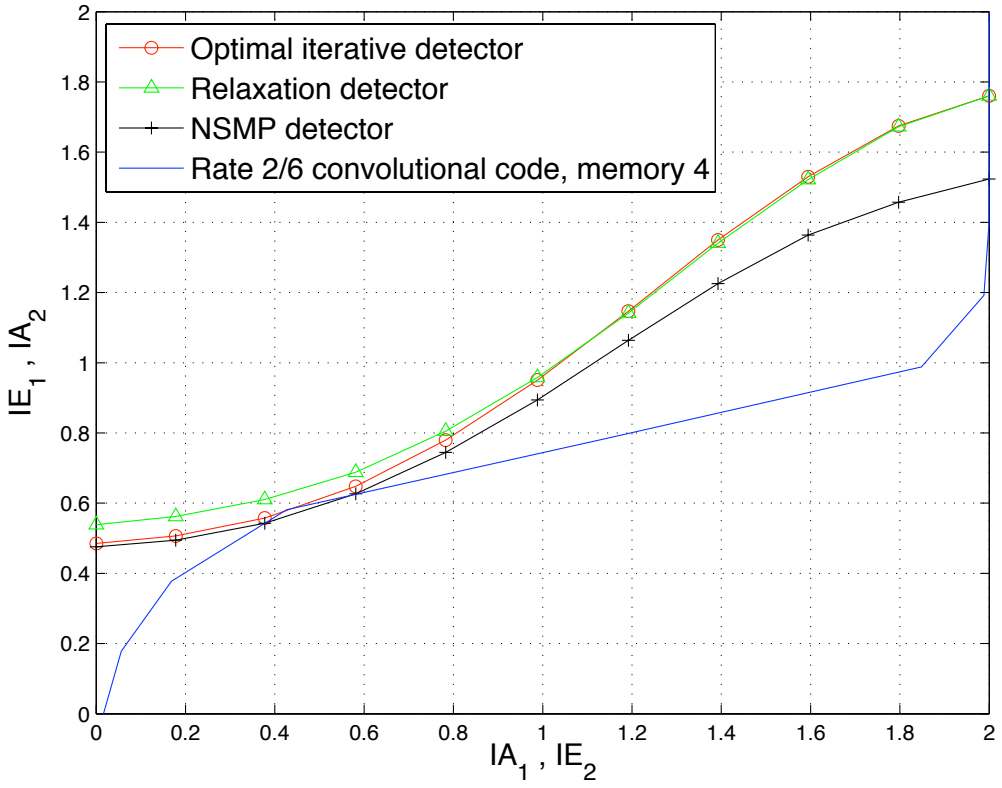

Figure 4.13: EXIT chart at 9 dB for optimal iterative detector, relaxation detector and NSMP detector with rate 2/6, memory 4 convolutional codes.

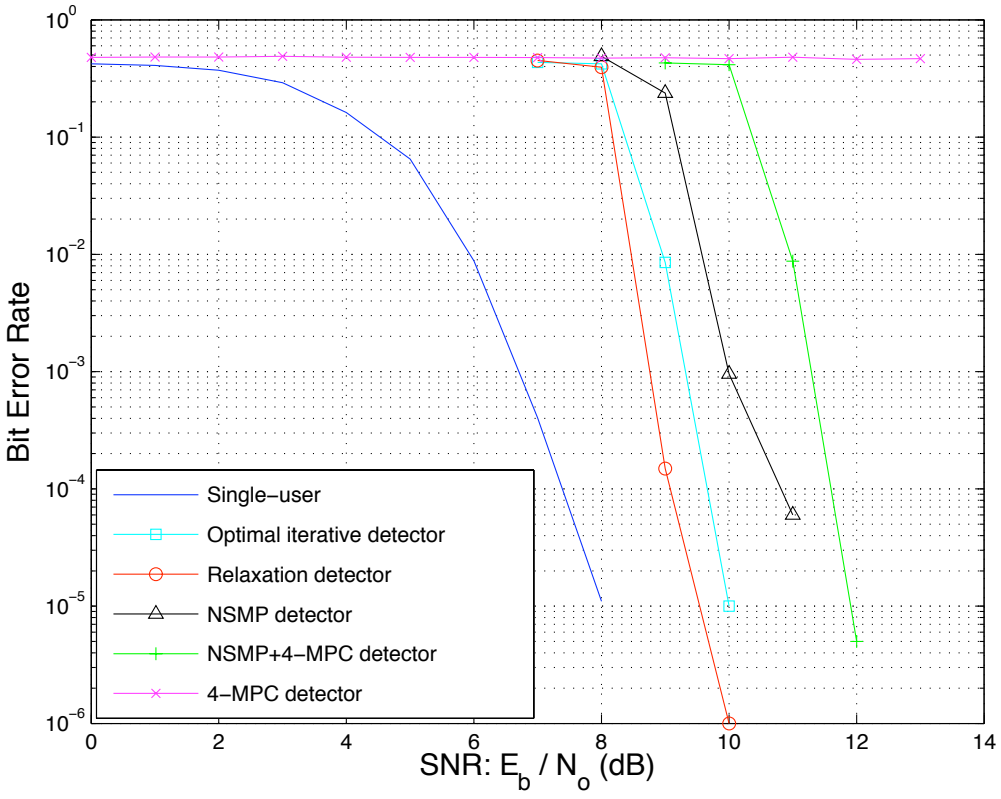

Figure 4.14: BER performance of 4-frequency 4-user system with rate 2/6, memory 4 convolutional codes.

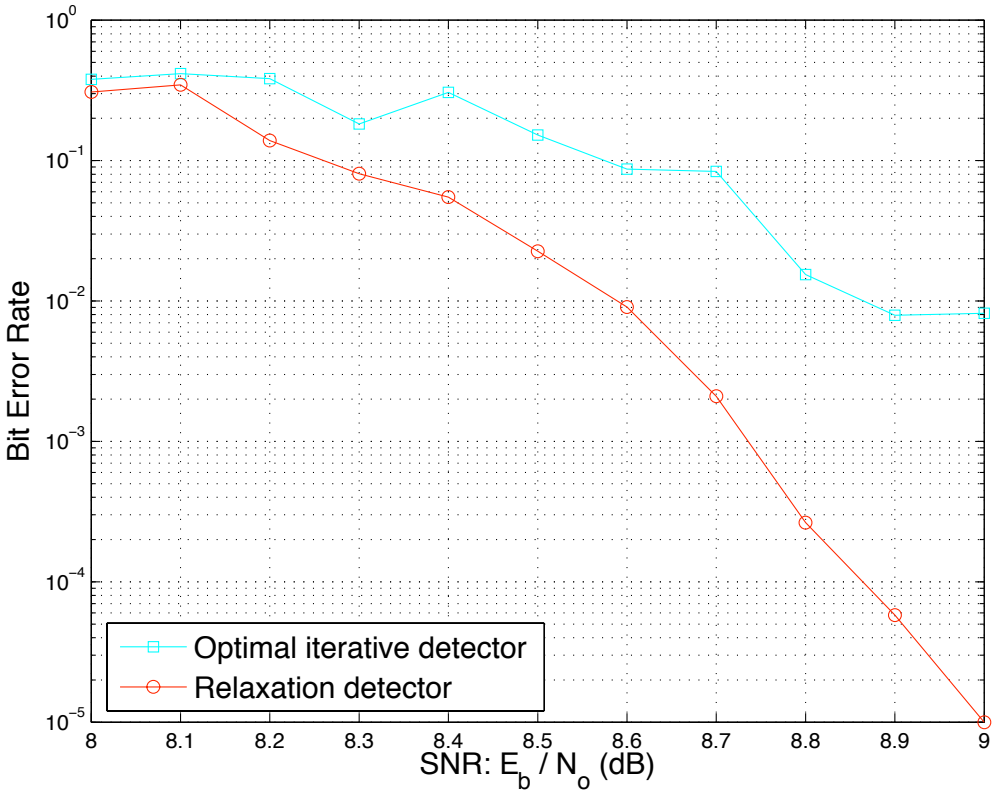

Figure 4.15: BER performance of optimal iterative detector and relaxation detector between 8 dB and 9 dB for 4-frequency 4-user system with rate 2/6, memory 4 convolutional codes.

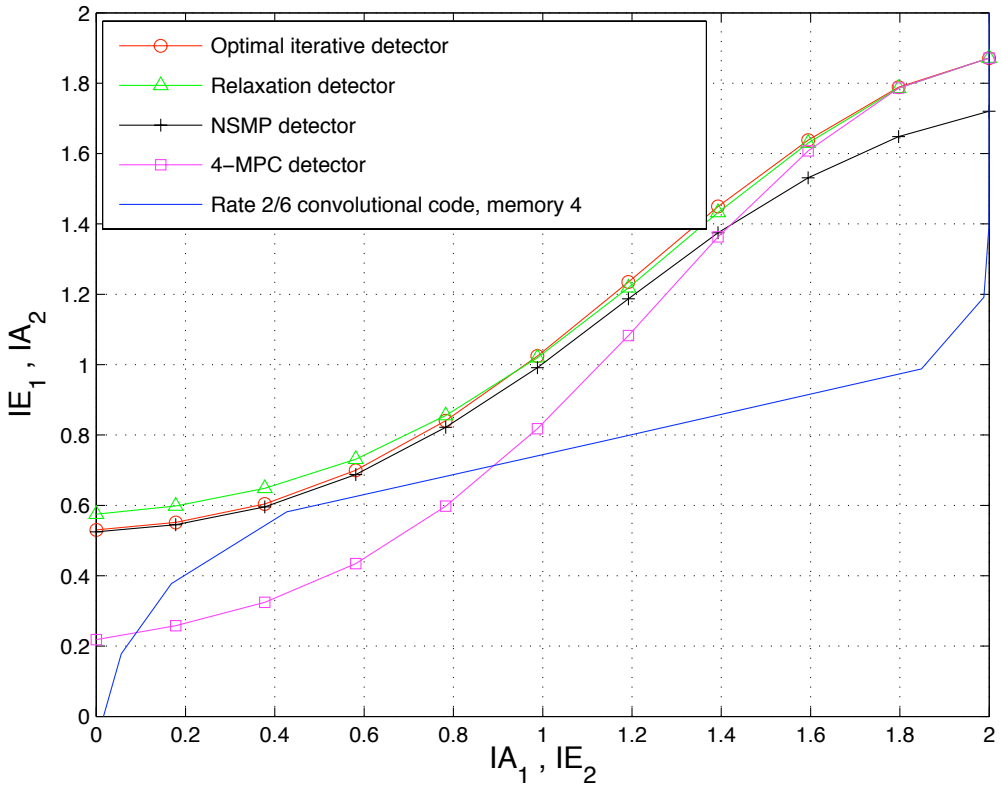

Figure 4.16: EXIT chart at 10 dB for optimal iterative detector, relaxation detector, NSMP detector and 4-MPC detector with rate 2/6, memory 4 convolutional code.

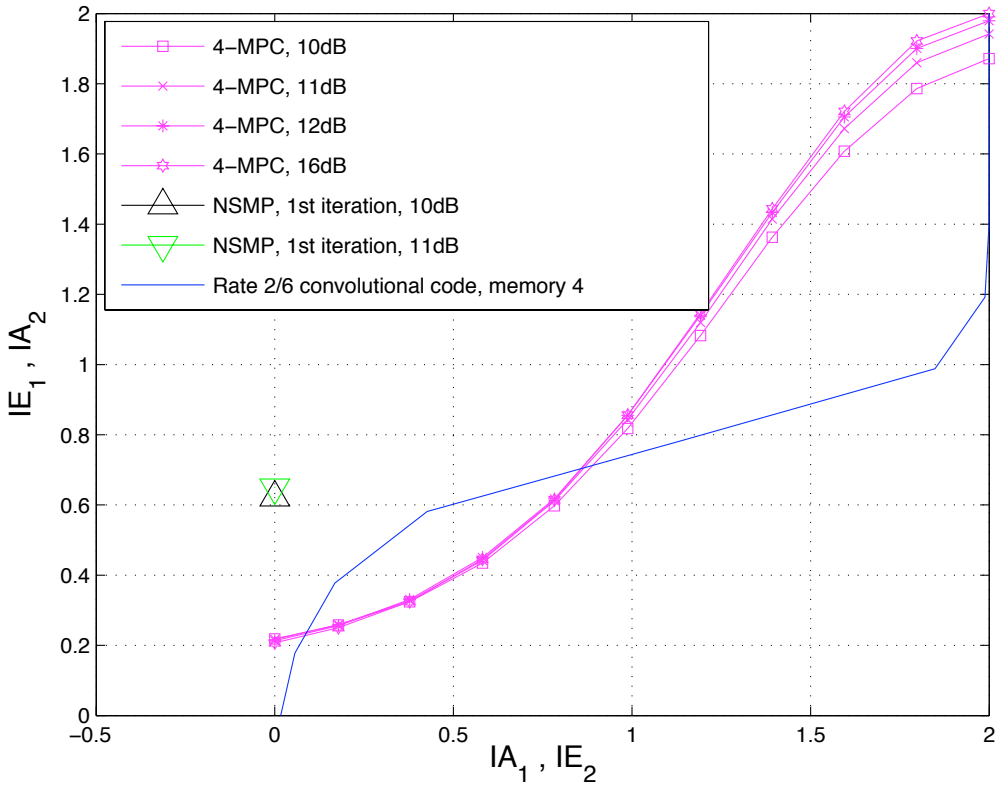

Figure 4.17: EXIT chart for NSMP+4-MPC detector with rate 2/6, memory 4 convolutional codes when SNR $\geq$ 11dB.

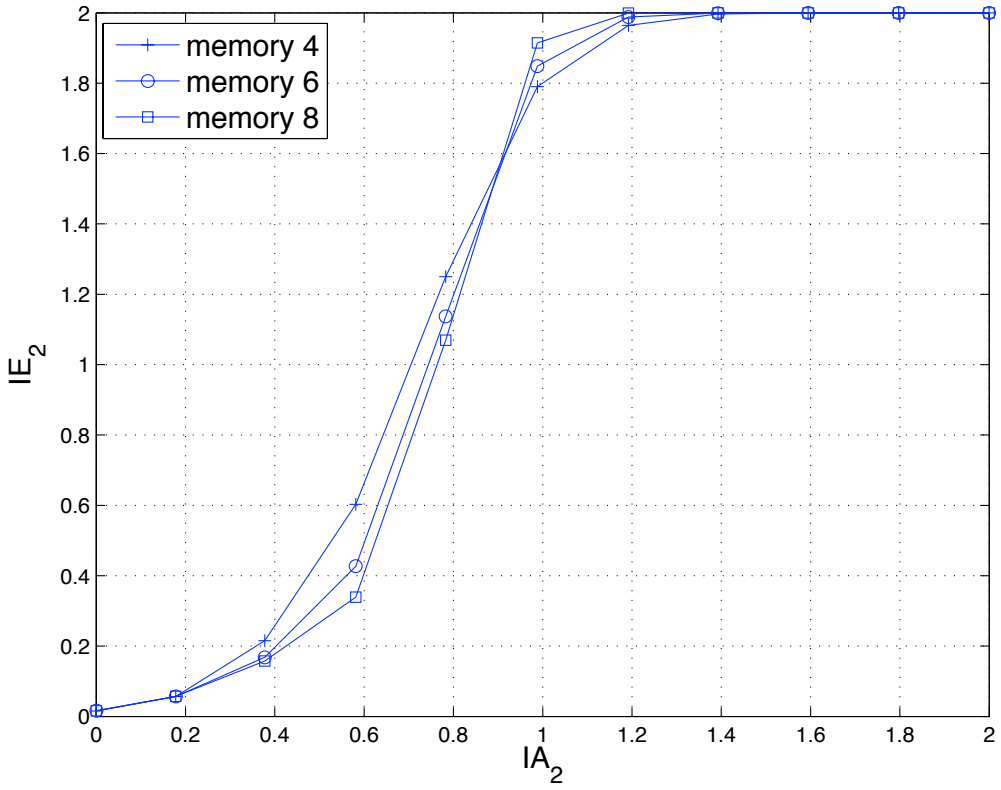

Figure 4.18: EXIT chart for rate 2/6 random convolutional codes with memory 4, 6 and 8.

Chapter 5

Code Design for the CFSK System

5.1 Introduction

An important aspect in the design of the CFSK system is the choise of the users' codes. These codes provide diversity so that the users can be distinguished at the receiver when collisions happen on the channel. Based on the discussion of the distance spectrum of the super-trellis code in Chapters 3 and 4, it is desirable that the codes be uniquely decodable. The earliest definition of uniquely decodable codes can be found in [18]-[20] for the binary adder channel. Subsequently, there have been many constructions of uniquely decodable codes for the binary adder and real adder channels [46]-[55]. Most of these efforts focus on improving the sum rates, R_{sum}, achieved by the multiuser code, though some efforts were also made to improve the error correcting

capability of the codes [46, 49, 51]. Strong error correcting ability generally requires sacrificing the sum rates of the codes ,and, in generally it is very difficult to achieve both high sum rate and strong error correcting ability.

Due to the M-ary FSK modulator, non-binary codes may be of more interest for the CFSK system. However, the construction of non-binary uniquely decodable codes is more complicated. The constructions for binary channels can be extended to the non-binary channel [13, 56, 50, 57], but these constructions usually require a special decoder structure, which is not compatible with iterative multiuser detectors. An alternative is to ask if there are random codes that are not uniquely decodable, but for which the error floor introduced by the non-unique decodability is low enough for practical applications. Random codes with these properties will be called uniquely decodable codes.

Code design for the CFSK system begins with the uniquely decodable block codes constructed by Chang and Wolf [13]. This construction is of interest since the sum rate of this construction approaches the capacity bound of the CFSK channel with intensity information as the spreading factor approaches 0. The weakness of these codes is that they cannot be decoded by the iterative detector and $d_{\min} = 1$ for any block length. In order to use these codes in the iterative multiuser detector and to improve the overall error correction capability, a coding scheme is proposed that concatenates convolutional codes with Chang and Wolf's codes. A comparison

between this concatenation scheme and random codes shows that it is possible for the random codes to achieve nearly unique decodability. The random codes have additional superior properties compared to uniquely decodable block codes. This leads to a search of the encoding parameters for random codes such that the code set is nearly uniquely decodable and high spectral efficiency is achieved.

5.2 Uniquely Decodable Block Codes

In [46], Chang and Weldon proposed an iterative construction for uniquely decodable block codes (UDBC) on the binary memoryless T-user adder channel. Chang and Wolf [13] extended this construction to nonbinary UDBC's on the T-user, M-frequency channel with intensity information. The iterative construction begins with the binary case, where the codes are expressed in the form of a difference matrix $\tilde{D}$. Before the construction, the difference matrix is initialized as $\tilde{D}_0 = [1]$. The iteration is then

$$\tilde{D}_i = \begin{bmatrix} \tilde{D}_{i-1} & \tilde{D}_{i-1} \\ \tilde{D}_{i-1} & -\tilde{D}_{i-1} \\ I_{i-1} & O_{i-1} \end{bmatrix}, \tag{5.1}$$

where the matrix $\tilde{D}_i$ has 2^i columns. In (5.1), I_{i-1} and O_{i-1} are the identity matrix and zero matrix, respectively, with dimension $2^{i-1} \times 2^{i-1}$. As a result, $\tilde{D}_i$ has $(i+2)2^{i-1}$ rows. Each element of $\tilde{D}_i$ belongs to $\{0, 1, -1\}$. For the binary case, each row of $\tilde{D}_i$ represents the difference vector of two codewords from a user's code. For example,

the second row of D_1 is $(1, -1)$ and two codewords, $(1, 0)$ and $(0, 1)$ result in this difference vector. Thus, the matrix $\tilde{D}_i$ represents a set of codes for $(i+2)2^{i-1}$ users, and each code contains two codewords. In [46], it was proven that this set of codes is uniquely decodable.

The extension of $\tilde{D}_i$ to the non-binary case is straightforward. Let $P_i = (i+2)2^{i-1}$ be the number of rows in $\tilde{D}_i$. Choose any value a such that $a \geq P_i(M-1)+1$, where M is the size of the alphabet, i.e., the number of frequencies in CFSK. Then, as shown in [13], the matrix D_i is the difference matrix of a uniquely decodable code set for $P_i(M-1)$ users with block length 2^i, where

$$D_i = \begin{bmatrix} \tilde{D}_i \\ a\tilde{D}_i \\ a^2\tilde{D}_i \\ \cdots \\ a^{M-2}\tilde{D}_i \end{bmatrix}.$$

As an example, a set of uniquely decodable codes for a 6-user, 3-frequency system is

constructed from $\tilde{D}_1$ by choosing $a = 7$. The result is

$$\left\{\begin{array}{rcl} C_0 &=& \{(1,1),(0,0)\}, \\ C_1 &=& \{(1,0),(0,1)\}, \\ C_2 &=& \{(1,0),(0,0)\}, \\ C_3 &=& \{(7,7),(0,0)\}, \\ C_4 &=& \{(7,0),(0,7)\}, \\ C_5 &=& \{(7,0),(0,0)\} \end{array}\right\}.$$

To use this code set in the CFSK system, the signal mapping

$$\left\{\begin{array}{rcl} 0 &\rightarrow& f_0, \\ 1 &\rightarrow& f_1, \\ 7 &\rightarrow& f_2 \end{array}\right\}$$

is used which results in following nonbinary UDBC

$$\left\{\begin{array}{rcl} C_0 &=& \{(f_1,f_1),(f_0,f_0)\}, \\ C_1 &=& \{(f_1,f_0),(f_0,f_1)\}, \\ C_2 &=& \{(f_1,f_0),(f_0,f_0)\}, \\ C_3 &=& \{(f_2,f_2),(f_0,f_0)\}, \\ C_4 &=& \{(f_2,f_0),(f_0,f_2)\}, \\ C_5 &=& \{(f_2,f_0),(f_0,f_0)\} \end{array}\right\}. \tag{5.2}$$

The uniquely decodable code set given in (5.2) does not offer significant error correction capability since, for example, the Hamming distance for C_5 is only 1.

Practical applications require strong error correction capability for each user's channel code to combat the multiuser interference introduced by the suboptimal multiuser detectors. Also, iterative detectors work better with codes with a trellis structure that cannot be provided by the above construction. This suggests a concatenation a convolutional code with the UDBC as shown in Figure 5.1.

The coded sequence from the convolutional code is encoded by the UDBC. Since there are two codewords in each user's UDBC and each codeword can represent 1 bit, each bit of the coded sequence output by the convolutional code is mapped to a codeword in the UDBC set. In Figure 5.1, an example is given for the code C_0. The encoding rule for the UDBC is that 0 is mapped to the codeword $(1, 1)$ and 1 is mapped to the codeword $(0, 0)$. For M-FSK modulation, the symbol 1 is mapped to frequency f_1 and 0 is mapped to frequency f_0. Note that the symbol-based interleaver is optional. The "symbol" here is defined by the coded bits output by the convolutional encoder, which corresponds to a sequence of 2^i frequencies. Hence, the interleaver operates on the unit of 2^i-tuple frequencies. This guarantees that the sequence of frequencies is uniquely decodable. Given that the convolutional code is

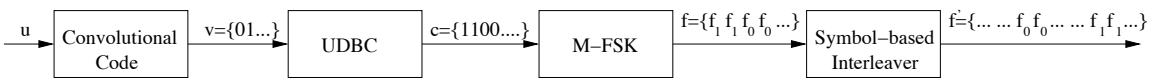

Figure 5.1: CFSK transmitter with a binary convolutional code concatenated with a UDBC.

rate k/n, the rate of the concatenated code is $k/n2^i$.

The concatenated code defined above can be regarded as a non-binary trellis code that is non-linear due to the non-linearity of the UDBC. Its performance is decided by the distance properties of the super-trellis defined in Chapter 4. Since, by construction, the code is uniquely decodable, the super-trellis must have the property that $d_{min} > 0$ and $A_0 = 0$. Thus, it can be anticipated that the BER performance will have a low error floor. The waterfall region is decided by the first several terms of the code's distance spectrum. A theoretical analysis of the distance spectrum is extremely difficult for these codes due to the non-binary nature and the large number of users. In the following discussions, the performance of this scheme is investigated through simulation and a comparison is made between the concatenated codes and random convolutional codes.

5.2.1 Performance of UDBC's

In order to investigate the performance of the UDBC's in the concatenated scheme, a 2-frequency, 7-user system is simulated. To generate the UDBC from the iterative construction, 2 iterations are used which results in a length of 4. Rate 1/2, memory 3 convolutional codes are used for the inner codes and the overall concatenated codes have rate 1/8. Details about the concatenated codes are given in Table 5.1. Random channel interleavers with a block length of 4000 symbols are also used. The iterative

detector uses 32 iterations with the relaxation metric. The results, shown in Figure 5.2, manifest no error floor and the waterfall region spans SNR's from 6 dB to 14 dB. This implies that the distance spectrum of the super-trellis code is not sparse.

Table 5.1: Rate 1/8 concatenated codes for a 2-frequency 7-user system.

	Convolutional code output			
	0		1	
	UDBC output	2-FSK output	UDBC output	2-FSK output
User 0	1111	$f_1f_1f_1f_1$	0000	$f_0f_0f_0f_0$
User 1	1010	$f_1f_0f_1f_0$	0101	$f_0f_1f_0f_1$
User 2	1010	$f_1f_0f_1f_0$	0000	$f_0f_0f_0f_0$
User 3	1100	$f_1f_1f_0f_0$	0011	$f_0f_0f_1f_1$
User 4	1001	$f_1f_0f_0f_1$	0110	$f_0f_1f_1f_0$
User 5	1000	$f_1f_0f_0f_0$	0001	$f_0f_0f_0f_1$
User 6	1000	$f_1f_0f_0f_0$	0000	$f_0f_0f_0f_0$

For comparison, the BER performance for a 2-frequency, 7-user system with rate 1/8, memory 3 random convolutional codes is also shown in Figure 5.2. In this case, each coded bit is mapped to a frequency and the rate of the system is 1/8. All others parameters are the same as those for the concatenated scheme. The waterfall region

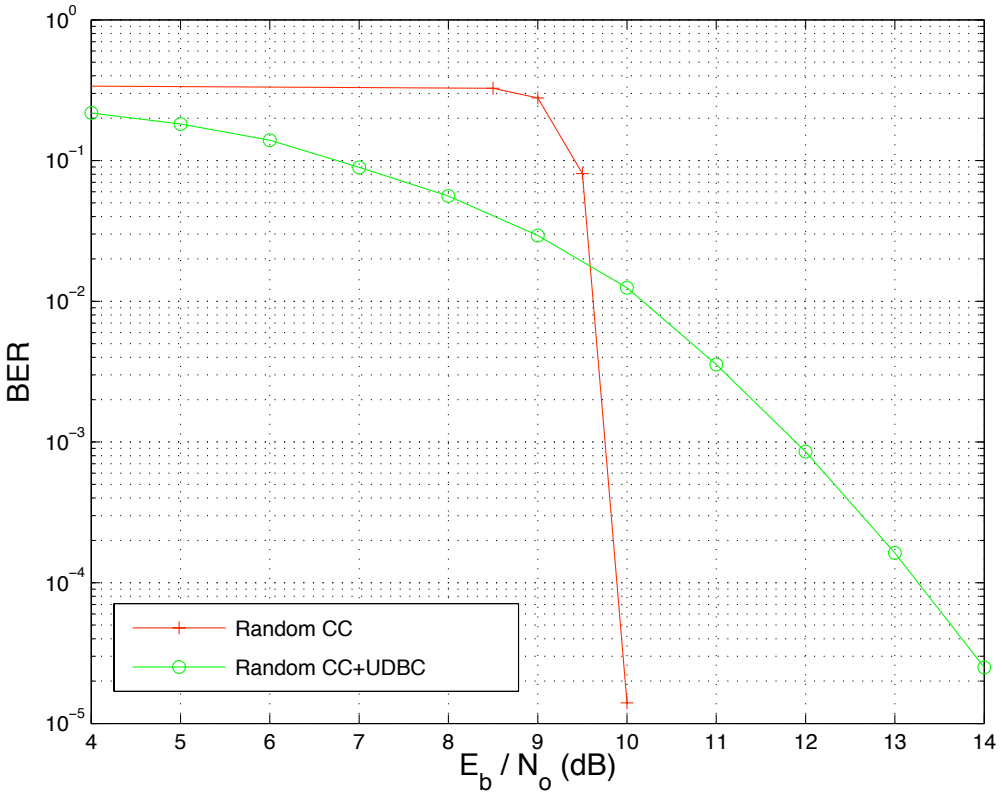

Figure 5.2: Performance comparison between UDBC and random convolution codes in a CFSK system with 2 frequencies, 7 users and transmission rate 1/8 bits/symbol.

of this scheme is sharp, though it starts later than the concatenated scheme and no error floor can be observed. This implies that the distance spectrum of the random codes has some superior properties compared with the concatenated scheme.

First, random codes with low rates can provide very low A_d values for the super-trellis code when d is small. This results in a low error floor comparable to the UDBC scheme. Second, random codes generally have a sparse distance spectrum that results in a sharp waterfall region. Thus, random codes generally have much better BER performance than the concatenated scheme for low and moderate SNR's. Additionally, the most efficient application of Chang and Wolf's codes is in low spreading factor, highly loaded systems. The reason for this is that the rate of the code for each user is extremely low $(1/2^i)$ and a high sum rate can only be achieved by accommodating a large number of users in the system. On the other hand, for random codes, high efficiency can be achieved for any spreading factor given the proper choice of the code parameters. It is possible to achieve high sum rates and approach the capacity bound of the CFSK channel with the random codes over a wide range of spreading factors.

Motivated by the superiority of the random codes over the concatenation scheme using UDBC's, the remainder of this chapter investigates the application of random codes in the CFSK system. Since the random codes are not constructed, the study emphasizes the choice of the code parameters that achieves the highest spectral efficiency.

5.3 Spectral Efficiency of the CFSK System

Let R be the rate of the convolutional codes used in the CFSK system, and let R_c be the transmission rate of the system in bits/symbol. Then, the bandwidth expansion factor of the system is defined (similar to that of CDMA systems [43]) as

$$\Omega = \frac{M}{R_c}, \tag{5.3}$$

in chips×symbols/bit. In the CFSK system, the number of chips is the number of frequencies. For a fixed bandwidth expansion factor Ω and transmission rate R_c, it is possible to find the maximal number of users that can be accommodated in the system. Denote this maximal number of users by $T_{\max}(\Omega, R_c)$, then the spectral efficiency of the system is given by

$$\mathcal{K} = \frac{T_{\max}(\Omega, R_c)}{\Omega} = \frac{T_{\max}(\Omega, R_c)R_c}{M},$$

in bits/symbol/chip.

To calculate the spectral efficiency of the system, the maximal number of users, $T_{\max}(\Omega, R_c)$, needs to be found for a given Ω and M. With fixed Ω and M values, the transmission rate R_c can be computed by (5.3). In Table 5.2, specific Ω and M values, and the corresponding R_c values are given, where each $q = \log_2 M$ coded bits are mapped to a frequency. The rates for the corresponding convolutional codes, R, can be computed as

$$R = \frac{R_c}{q}.$$

In Table 5.2, the R value is given in parenthesis below the corresponding transmission rate R_c. In order to determine the effects of code memory on the performance of the multiuser detector, both memory 4 and 8 codes were simulated.

Table 5.2: Transmission rates as a function of Ω and M.

Ω	$M=2$	$M=4$	$M=8$	$M=16$	$M=32$	$M=64$	$M=128$
8	1/4 (1/4)	1/2 (1/4)	1 (1/3)	2 (2/4)	4 (4/5)		
16	1/8 (1/8)	1/4 (1/8)	1/2 (1/6)	1 (1/4)	2 (2/5)	4 (4/6)	
32	1/16 (1/16)	1/8 (1/16)	1/4 (1/12)	1/2 (1/8)	1 (1/5)	2 (2/6)	4 (4/7)

One approach to determine the maximal number of users $T_{\max}$ is through the EXIT chart analysis discussed in Chapter 4. However, EXIT chart analysis can only provide information about the convergence of the iterative detector. The maximal number of users determined in this manner only provides an upper bound on the number of users for which the detector will converge. When there are many users, the super-trellis code may have a low $d_{\min}$ and thus a very high error floor. In order to observe the convergence and error floor simultaneously, a better approach is to find $T_{\max}$ by setting a threshold on the error floor and simulating the BER performance

with increasing numbers of users and fixed Ω and R_c values.

In order to be able to observe the error floor, the SNR should be set high, since the error floor has small slope and always extends to the high SNR region. In searching for $T_{\max}$, the SNR is set to 16 dB. A BER of 10^{-3} is chosen as the threshold delineating whether or not the iterative multiuser detector converges with a low error floor. Random channel interleavers are used for each user. The spectral efficiency $\mathcal{K}$ can then be computed from Ω and $T_{\max}$ and the relationship between the spectral efficiency $\mathcal{K}$ and the rates R_c is determined. This relationship provides insight for choice of the code parameters and detector approaches.

5.4 Choice of Code Parameters

The choice of code rates affects the convergence of the iterative detector and thus the water fall region. The choice of the code memory affects convergence. EXIT chart analyses in the Section 4.5 showed that increasing the memory of the component codes makes the convergence of iterative decoding more difficult and delays convergence. In Figure 5.3, the BER performance of codes with transmission rate 1/8 are given for different memories and number of frequencies. The 7-user system converges after 8 dB with 2 frequencies and code memory 4. However, when the code memory is increased to 8, the convergence is delayed to 16 dB.

Convergence is also be related to the number of frequencies. For example, as shown

in Figure 5.3, when the number of frequencies is increased from 2 to 4, convergence begins several dB earlier. Using more frequencies also improves convergence and the waterfall region for system with rates of 1 and 4 as shown in Figures 5.4 and 5.5, respectively.

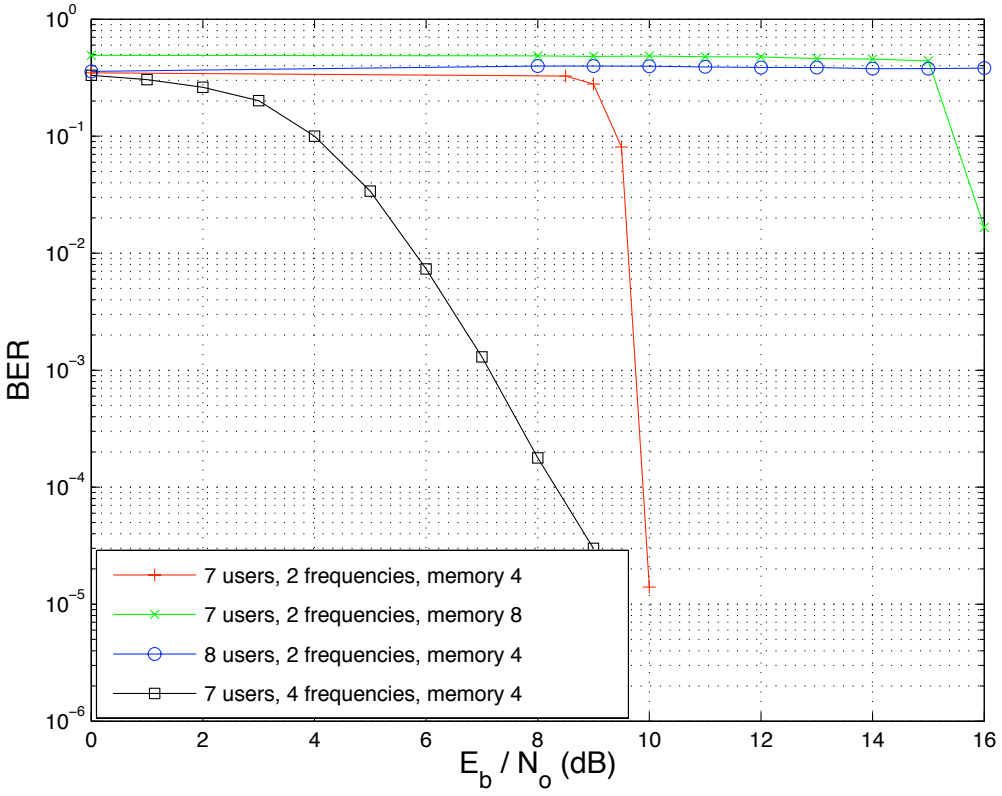

Figure 5.3: BER performance for codes with transmission rate 1/8 bits/symbol.

The level of the error floor is decided by the multiplicities A_d values for small d's, especially A_0. Intuitively, a larger alphabet can improve the distance properties

of the super-trellis code since the chance that two paths though the trellis have the same output sequence is reduced by using a larger alphabet. Thus, for a given rate, increasing the number of frequencies may also lower the error floor. An example of this is shown in Figure 5.5, for a system with a transmission rate of 4. For the 3-user system with 64 frequencies and code memory 4, the error floor is around 4×10^{-3}. When the number of frequencies is increased to 128, the error floor is lowered to 1.2×10^{-3}.

Increasing the code memory negatively affects the convergence of the detector, due to the huge increase in the number of code paths through the super-trellis, but distance properties are improved. Thus, the error floor can be lowered by increasing the code memory provided the iterative detector converges. Figure 5.5 shows that the convergence for code memory 8 begins at 6 dB, which is much later than the 2 dB convergence for code memory 4. However, the error floor for the memory 8 codes is so much lower than that of the memory 4 codes that it cannot be observed in the simulation.

It is clear that tradeoffs are involved in the choice of code parameters to achieve high spectral efficiency. To investigate these tradeoffs further, transmission rates are divided into three regions. The low rate region is for rate below 0.5 and the results in Figure 5.3 belong to this region. The middle rate region is for rates between 0.5 and 2 and the results in Figure 5.4 belong to this region. The high rate region is for

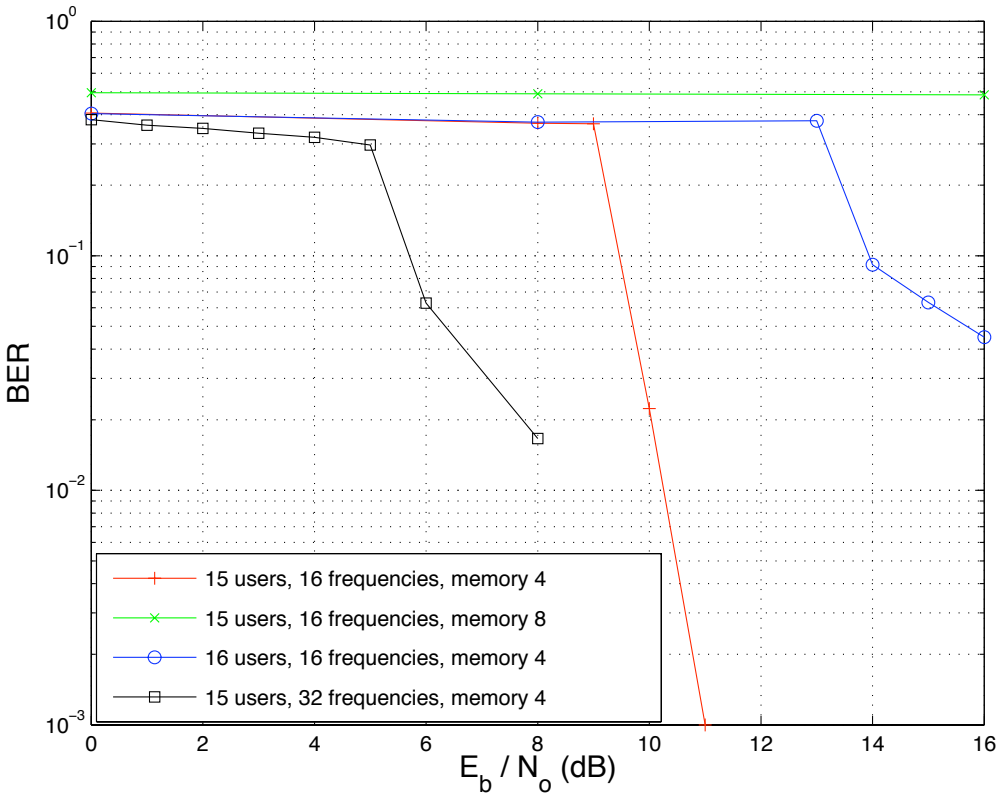

Figure 5.4: BER performance for codes with transmission rate 1.

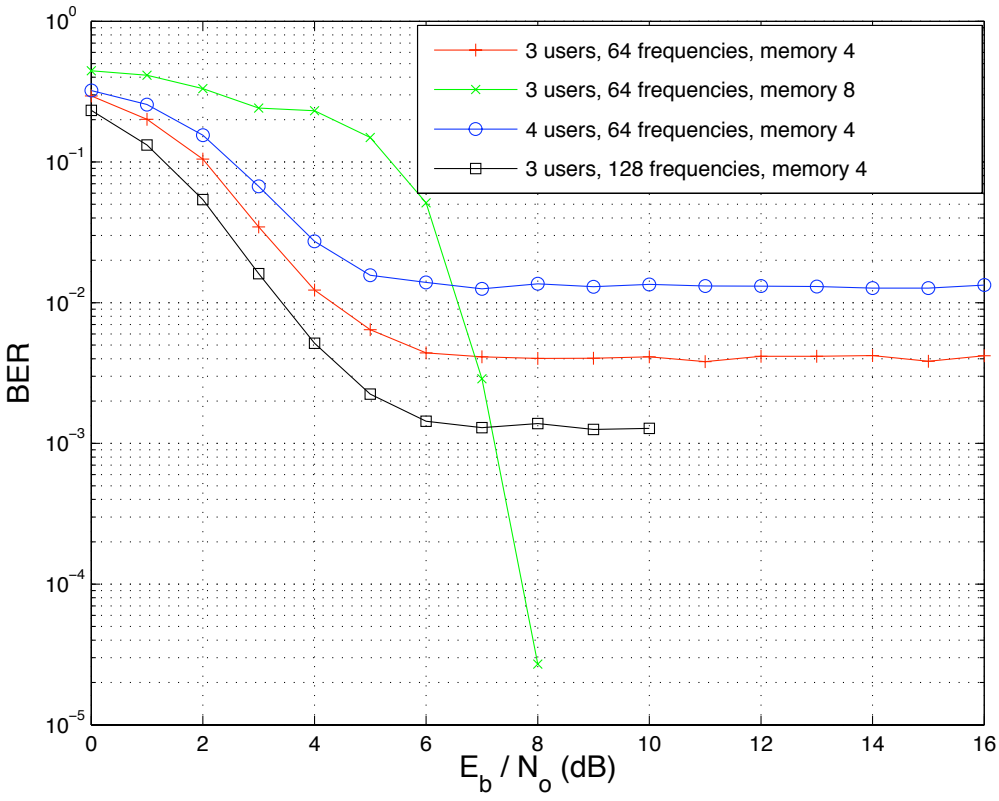

Figure 5.5: BER performance for codes with transmission rate 4.

rate above 2 and the results in Figure 5.5 belong to this region.

As previously defined, the value $T_{\max}$ is the largest number of users that achieves a BER below 10^{-3}. Let T_{conv} be the largest number of users for which the the iterative detector converges, as determined through EXIT chart analysis. The relationship between $T_{\max}$ and T_{conv} in the three rate regions is different. For low transmission rates, as shown in Figure 5.3, the error floor is low enough that it is difficult to observe in the simulations and the system performance is dominated by the convergence of the iterative detector.Thus, we conjecture that in the low rate region $T_{\max} = T_{\text{conv}}$. From the simulations, when the number of users is increased to 8, the iterative detector does not converge so $T_{\max} = T_{\text{conv}} = 7$ in this case.

When the transmission rate is in the middle region, both the error floor and detector convergence will affect the performance. In Figure 5.4, the BER is shown for several systems with a transmission rate 1. With 16 frequencies and codes of memory 4, increasing the number of users is increased from 15 to 16 introduces an error floor above 10^{-2}. Obviously, the value of T_{conv} for this rate is no less than 16. However, since the error floor for the 16-user system is higher than 10^{-3}, the $T_{\max} < 16$ and we conclude that $T_{\max} = 15$. Thus, in this region of transmission rates, it is possible that $T_{\max} < T_{\text{conv}}$.

When the transmission rate is high enough, the error floor will dominate the system performance. In this case, the number of users can be fairly high and the

detector will still converge, but the error floor may also be high. In this region, $T_{\max} < T_{\text{conv}}$. In Figure 5.5, the 4-user system converges at low SNR, which implies that $T_{\text{conv}} > 4$. However, the error floor is higher than 10^{-2} for 4 users so the value of $T_{\max}$ has to be less than 4. The 3-users system has an error floor around 10^{-3}, and we conclude that $T_{\max} = 3$.

5.4.1 Choice of Iterative Multiuser Detectors

In Figure 5.6, the spectral efficiency $\mathcal{K}$ is compared for different detector approaches for codes with memory 4. It can be observed that the relaxation approach has the highest spectral efficiency and the K-MPC approach has the lowest spectral efficiency. By using NSMP in the first iteration, the system performance is slightly improved over the K-MPC metric. The gap between the curves is the largest for moderate transmission rates. For very low or high transmission rates, the differences between the detectors are small. When the transmission rate tends to zero, the increase in the number of users cannot compensate for the rate loss and the spectral efficiency tends to zero for all of the detectors. For high transmission rates, the user diversity provided by the codes becomes weak since A_d is high for small values of d. The error floor dominates the system performance in this case and the system can only allow a small number of users. High transmission rates can be achieved by using a large set of frequencies, but the spectral efficiency of the system will tend to zero for all

detectors.

The highest spectral efficiency is achieved using the relaxation metric in the middle region of the transmission rates. For R_c between 0.1 and 0.3 bits / symbol, the performance of the NSMP+K-MPC metric is very close to that of the relaxation metric. Considering the increased computational complexity of the relaxation metric, NSMP+K-MPC is recommended in this rate region. For extremely high transmission rates, since all the detectors perform similarly, K-MPC is the best choice due to its low complexity.

5.4.2 Choice of Bandwidth Expansion Factors

In Figure 5.7, the spectral efficiency for the relaxation metric is compared for $\Omega = 8$, $\Omega = 16$ and $\Omega = 32$. In the low rate region that $R_c < 0.5$, there is a tendency for the spectral efficiency of high Ω values to be higher than that of low Ω values. Note that, for a given transmission rate, higher Ω values are achieved by increasing the number of frequencies. The increase in frequencies improves the convergence of the iterative detector. In the low rate region, convergence dominates the system performance and increasing the number of frequencies will increase T_{conv}. As discussed previously, this increase in the number of users will not introduce a high error floor for these rates and $T_{\max} = T_{\text{conv}}$. As a result, the increase of $T_{\max}$ is even faster than the increase in the number of frequencies and the spectral efficiency is increased.

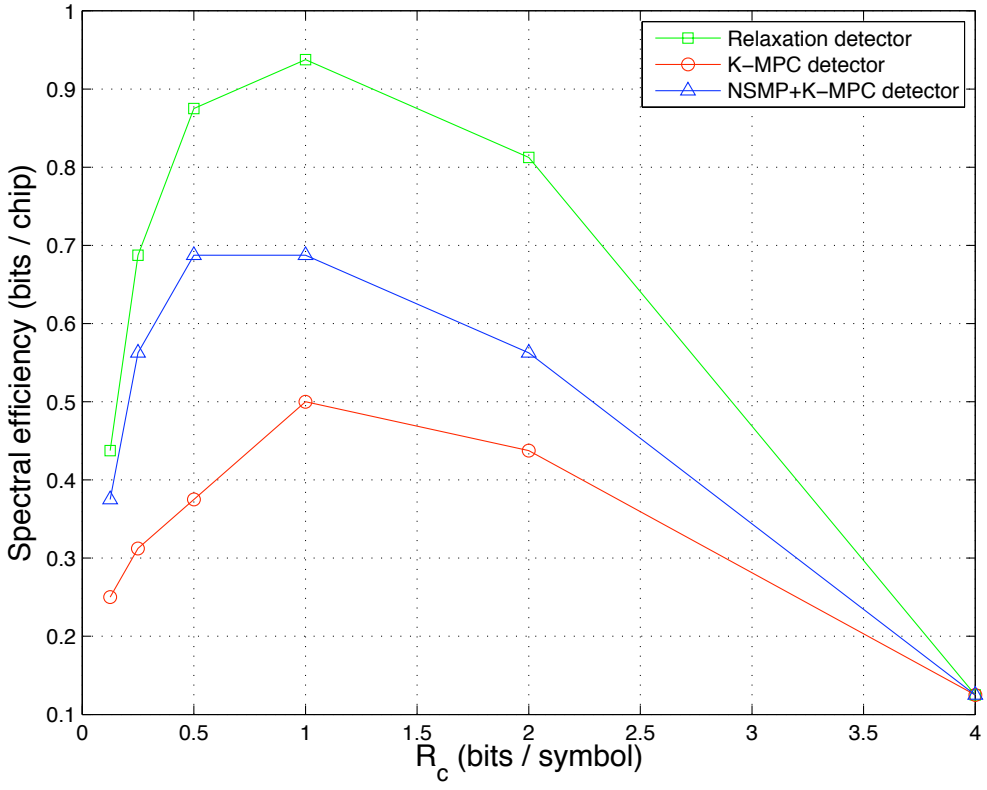

Figure 5.6: Comparison of spectral efficiencies for different detectors. The coding scheme has $\Omega = 16$ chips-symbo/bit, memory 4.

For moderate transmission rates that $0.5 < R_c < 1.5$, it can be observed that the spectral efficiency for high Ω values is lower than that for low Ω values. This implies that with the same transmission rate, the increase in $T_{\max}$ is slower than the increase in the number of frequencies. As a result, the spectral efficiency decreases as the number of frequencies increases. The reason behind this is that both convergence and the error floor affect the system performance. Thus, the increase in the number of users will increase the error floor, which cancels the improvement obtained by increasing the number of frequencies.

For very high transmission rates that $R_c > 2$, spectral efficiency with high Ω values is also higher. This is because the error floor dominates the system performance in this region. Increasing the number of frequencies may lower the error floor significantly and allow more users in the system. Note that $T_{\max} < T_{\text{conv}}$ in this region and as long the number of users is less than T_{conv}, $T_{\max}$ will increase. Moreover, increasing in the number of frequencies may also increase T_{conv}. Thus, the increase in $T_{\max}$ is faster than the increase in the number of frequencies and the spectral efficiency is improved.

5.4.3 Choice of Code Memory

To investigate the influence of code memory on the iterative detector, comparisons are made between memory 4 codes and memory 8 codes in Figures 5.8, 5.9 and 5.10,

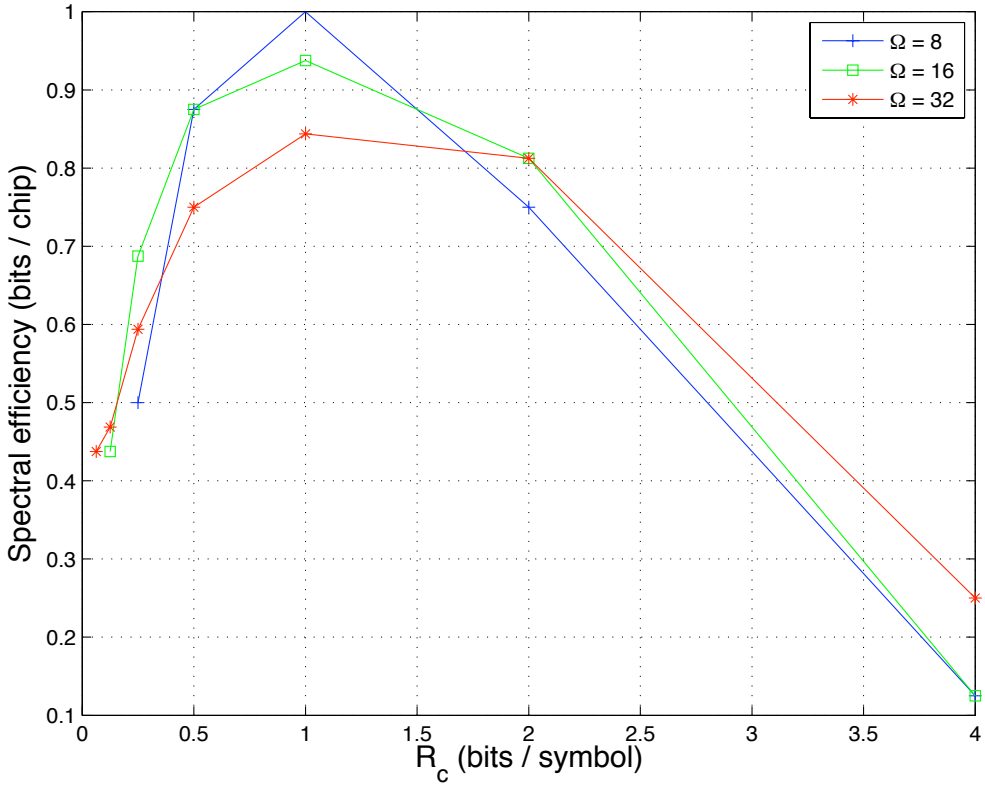

Figure 5.7: Spectral efficiencies for different bandwidth expansion factors with the relaxation detector and memory 4 codes.

for $\Omega = 8$, $\Omega = 16$ and $\Omega = 32$, respectively.

In Figure 5.8, it can be seen that the spectral efficiency is lower for higher code memory unless $R_c > 4$. For $R_{c<4}$, convergence will dominate the system performance due to the small value of Ω and thus $T_{\max} = T_{\text{conv}}$. Since increasing code memory decreases the value of T_{conv}, $T_{\max}$ is also decreased and the sprectral efficiency is lowered. For very high transmission rates, the error floor starts to dominate the system performance and increasing code memory helps lower the error floor. Thus, $T_{\max}$ can be increased, provided it is lower than T_{conv}, to increase the spectral efficiency.

When Ω increases, the rate region dominated by convergence will shift to lower rates. When $\Omega = 16$, Figure 5.9 shows that the gap between the memory 4 and the memory 8 curves becomes smaller. This implies that convergence becomes less dominant in the moderate rate region that $0.5 < R_c < 1.5$. On the other hand, the error floor starts to affect the performance in this region. If Ω is increased to 32, increasing the code memory may even increase the spectral efficiency for moderate transmission rates. This is reasonable since the error floor already dominates the system performance in this region.

5.5 Conclusions

Due to the difficulty in constructing uniquely decodable codes for the CFSK system with a large number of users, the performance of randomly generated convolutional

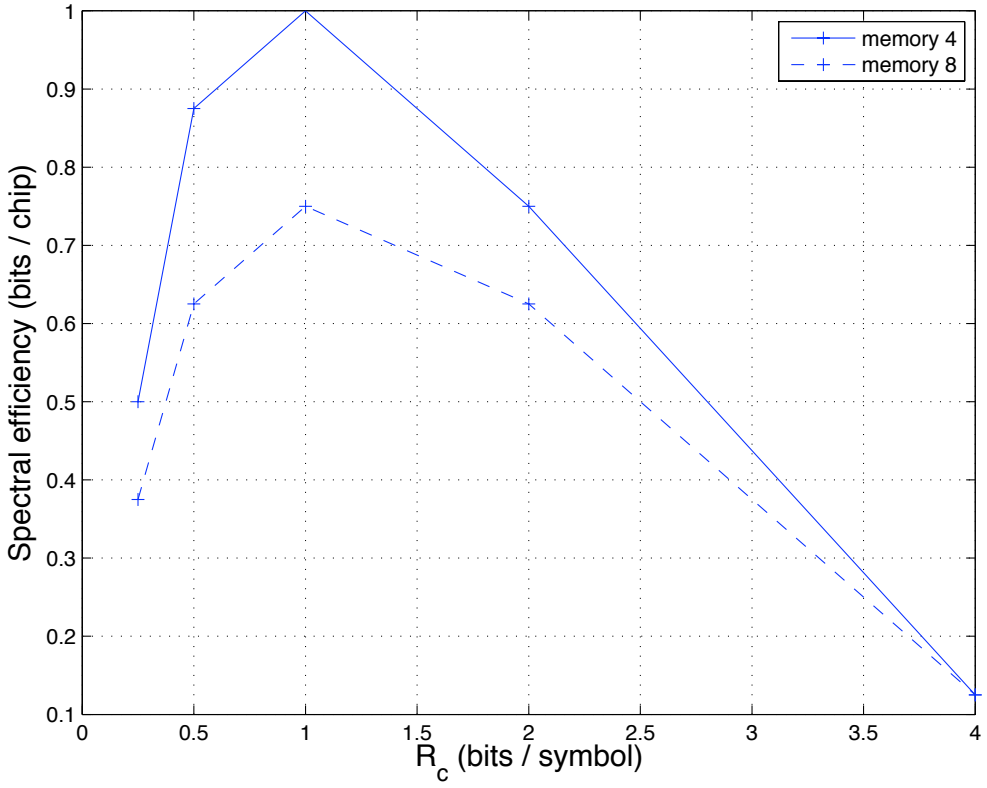

Figure 5.8: Comparison of spectral efficiencies for memory 4 and memory 8 codes with relaxation detector when $\Omega = 8$.

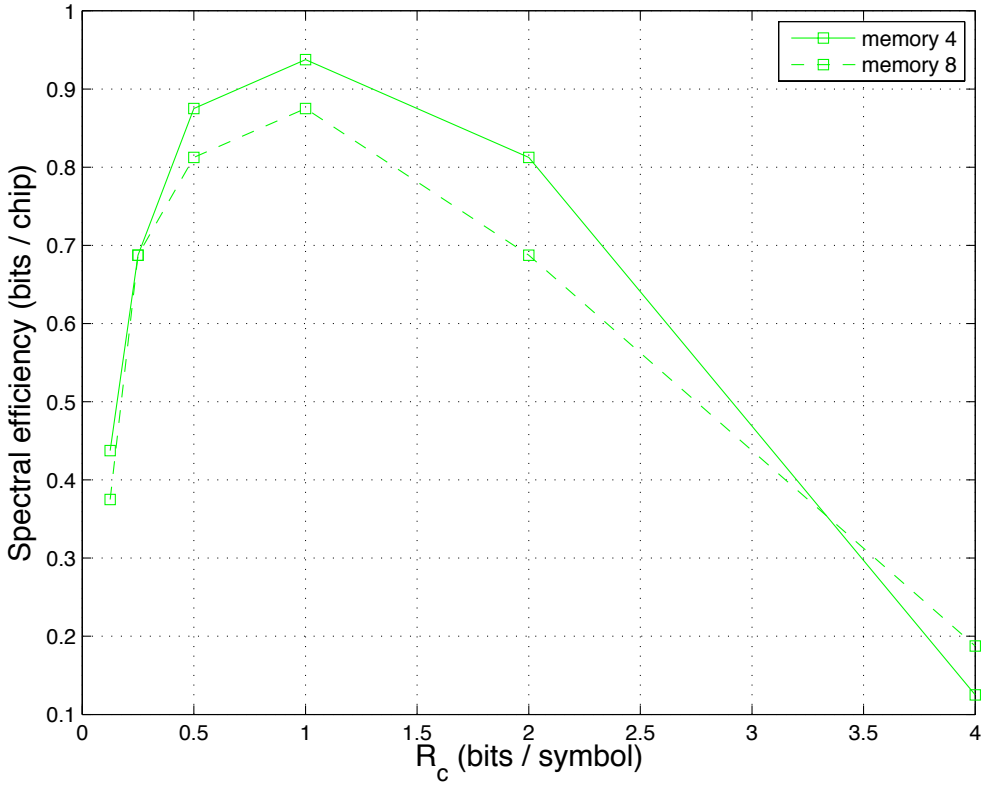

Figure 5.9: Comparison of spectral efficiencies for memory 4 and memory 8 codes with relaxation detector when $\Omega = 16$.

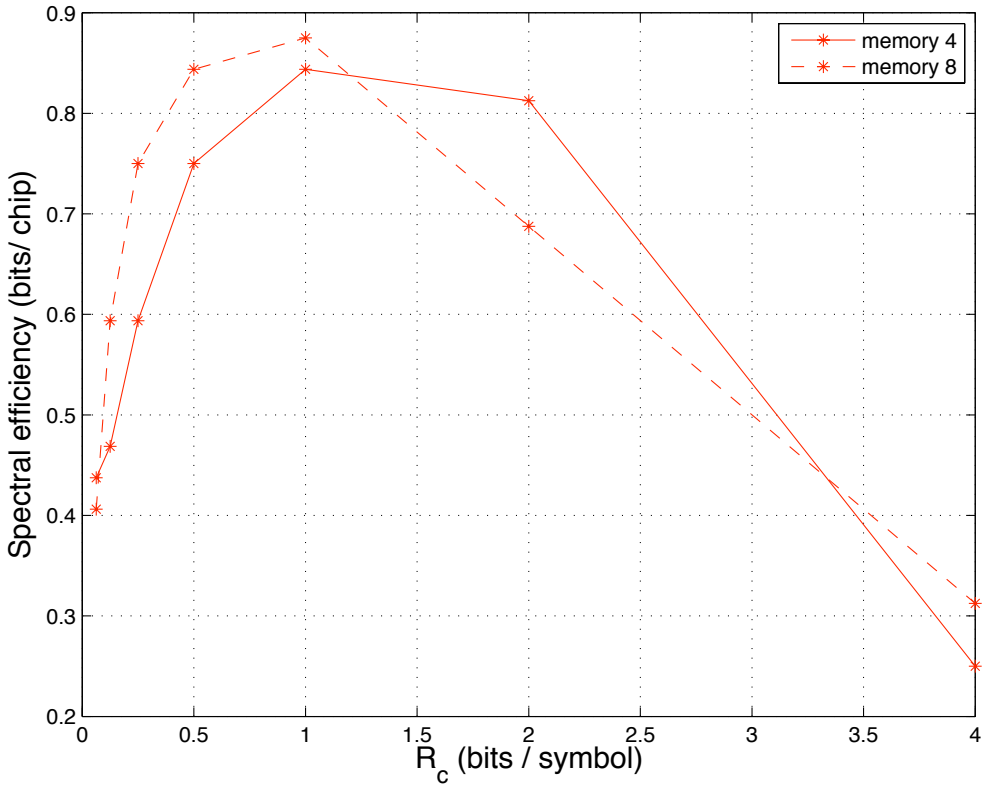

Figure 5.10: Comparison of spectral efficiencies for memory 4 and memory 8 codes with relaxation detector when $\Omega = 32$.

codes was studied. Based on spectral efficiency, it can be concluded that coding schemes with a large number of frequencies improve the convergence of the iterative detector. Also, simulation results show that the error floor can be lowered by using more frequencies. However, the spectral efficiency will be reduced due to the increase in the number of frequencies. It was also shown that increasing the code memory lowers the error floor at the expense of increasing the difficulty of convergence.

In general, for low transmission rates, coding schemes with a large number of frequencies and large code memories will increase the spectral efficiency. For moderate transmission rates, increasing the number of frequencies and the code memory becomes less efficient and coding schemes with a small frequency set and code memory are recommended. For high transmission rates, coding schemes with a large number of frequencies and large code memory become efficient again.

The conclusion with respect to code memory is significant since it makes it possible to use the most powerful channel codes, such as turbo codes [58] and Low Density Parity Check (LDPC) codes [59]. It is well known that these codes can achieve near capacity performance on the AWGN channel. However, due to their large memory, it is hard for the iterative detector to converge even when the system is not heavily loaded. As proposed in Figure 5.10, when a large number of frequencies is used, it is still possible for large memory codes to converge for moderate and high rates. The use of turbo codes and LDPC codes in the CFSK system needs further study.

Chapter 6

Conclusion

This dissertation investigates capacity bounds, detection techniques and code design for the CFSK system. Capacity bounds show that, for synchronous transmission, the CFSK system with intensity information is superior to both the CFSK system without intensity information and CDMA systems. For the asynchronous case, the simulations show that the two CFSK system perform similarly and the capacity of the CFSK system with intensity information tends to a constant level when the system is overloaded. A comparison between the CFSK system and CDMA systems shows that the CFSK system is superior for almost all system parameters and configurations. This result is the primary motivation for investigating the CFSK system with intensity information. Despite its theoretical advantages, practical CFSK implementations have been elusive.

The capacity results for the CFSK systems clearly show that multiuser detection is the key to system performance. Here, attention is focused on the system with intensity information due to its increased capacity. The optimal multiuser detector has a computational complexity that increases exponentially with the number of users and thus is impractical for real applications. For this reason, suboptimal multiuser detection methods with iterative techniques are investigated.

The optimal iterative multiuser detector is based on an iterative channel metric with complexity $O(M^{T-1})$, which is still impractical and further simplification approaches are proposed. The K-MPC and K-MPF metrics simplify the channel metric by considering a subset of the possible frequency combinations with high *a priori* information. The complexity of these metrics is linear with the number of users, and are thus appealing for real applications. However, since no channel information is considered in these metrics, their use leads to serious performance degradation. An improvement to these metrics is to consider both the *a priori* information of the frequency combinations and the channel information. This is called the narrow sense most probable combinations (NSMP) approach.

Further improvement is achieved by using the relaxation metric that considers an enlarged set of frequency combinations by assuming a relaxed constraint on the frequency combinations possible over the CFSK channel. This metric has low complexity and the performance of the relaxation metric is very close to that of the

optimal iterative metric.

Simulation results show that the iterative multiuser detectors raise the BER error floor. By using random symbol-based channel interleavers, the error floor can be lowered. The performance of the various detectors is also studied using the EXIT chart analysis. This analysis shows that the relaxation approach converges faster than the optimal iterative detector. EXIT analysis gives some insights into code design as well. For example, large code memory prevents convergence and low code rate improves convergence.

With respect to the channel codes in the CFSK system, random convolutional codes are compared to the uniquely decodable codes. Simulation results show that for low transmission rates, the BER performance of random codes is significantly better than Chang and Wolf's uniquely decodable block codes.

The coding parameters for the random codes is studied by considering spectral efficiency. The highest spectral efficiency can be achieved for both low transmission rates and high transmission rates by using large memory codes and a large number of frequencies. For moderate transmission rates, it is better to use small code memory and a small number of frequencies. With respect to complexity, the relaxation approach should be used for moderate transmission rates, the NSMP+K-MPC approach should be used for low transmission rates and the K-MPC approach should be used for high transmission rates.

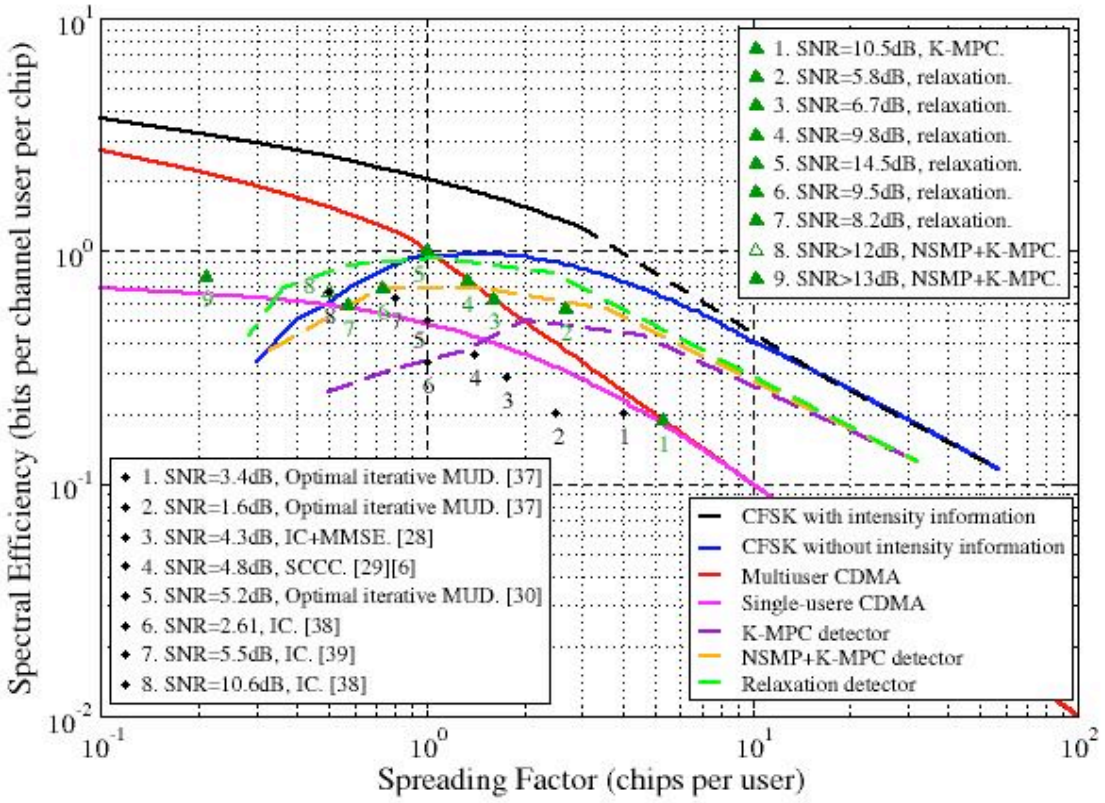

Figure 6.1: Achieved spectral efficiency at a BER of 10^{-4} for the CFSK system and a variety of CDMA systems.

The final question is how the CFSK system compares to other multiple access systems. In Figure 6.1, the highest spectral efficiencies achieved in simulations by different detectors for the CFSK system are compared with the normalized capacity bounds. This figure shows that all of the CFSK detectors achieve spectral efficiencies higher than the normalized capacity of multiuser CDMA systems when the spreading factor is greater than 2 chips/user. When the spreading factor is between 0.6 and 1.5 chips/user, the relaxation detector and the NSMP detector have higher spectral efficiencies than the normalized capacity of the single-user CDMA system.

A series of simulations were performed for the CFSK system, and are shown in Figure 6.1 as green triangles. Details on these points are given in the Table 6.1. For comparison, actual rates achieved by DS/CDMA systems with iterative multiuser detection are shown in Figure 6.1 as black dots [5]-[6], [27]-[31], [36]-[38]. The results show that the spectral efficiency achieved by DS/CDMA systems is lower than those achieved by the CFSK system. To achieve a BER of 10^{-4}, DS/CDMA systems generally require a lower SNR than that required by the CFSK system. The high spectral efficiency achieved by the CFSK systems using practical iterative detector makes it an attractive alternative for some systems.

Table 6.1: Code schemes for simulations of the CFSK system given Figure 6.1.

number	T	M	code	spreading factor	R_{sum}	percent of capacity
1	12	64	rate 1 $GF(2) \rightarrow GF(64)$ C	5.30	12.00	24.05%
2	3	8	rate 1/2 $GF(8) \rightarrow GF(8)$ CC	2.67	4.50	57.13 %
3	5	8	rate 1/2 $GF(4) \rightarrow GF(8)$ CC	1.60	5.00	47.82 %
4	3	4	rate 1 $GF(1) \rightarrow GF(4)$ CC	1.33	3.00	49.00 %
5	8	8	rate 1 $GF(2) \rightarrow GF(8)$ CC	1.00	2.67	51.87 %
6	11	8	rate 1/2 $GF(2) \rightarrow GF(8)$ CC	0.73	5.50	38.09 %
7	7	4	rate 1/3 $GF(2) \rightarrow GF(4)$ CC	0.57	2.33	36.73 %
8	6	3	rate 2/3 binary CC + length 2 UDBC	0.50	2.00	46.49 %
9	14	3	rate 2/3 binary CC + length 4 UDBC	0.21	2.33	42.18 %

Bibliography

[1] J. G. Proakis and M. Salehi, *Communication Systems Engineering.* Upper Saddle River, NJ: Prentice Hall, 1994.

[2] J. G. Proakis, *Digital Communications, Fourth Edition.* McGraw-Hill, 2001.

[3] S. Verdu, *Multiuser Detection.* Cambridge University Press, 1998.

[4] T. R. Giallorenzi and S. G. Wilson, "Multiuser ML sequence estimator for convolutionally coded asynchronous DS-CDMA systems." *IEEE Trans. Comm.*, pp. 997–1008, August 1996.

[5] P. D. Alexander, L. K. Rasmussen, and C. B. Schlegel, "A linear receiver for coded multiuser CDMA." *IEEE Trans. Comm.*, vol. COM-45, pp. 605–610, May 1997.

[6] M. C. Reed, C. B. Schlegel, P. D. Alexander, and J. A. Asenstorfer, "Iterative multiple detection for CDMA with FEC: near-single user performance." *IEEE*

Trans. Comm., pp. 1693–1699, December 1998.

[7] U. Timor, "Improved decoding scheme for frequency-hopped multilevel FSK system." *Bell Syst. Tech. J.*, pp. 1839–1855, December 1980.

[8] T. Mabuchi, R. Kohno, and H. Imai, "Multiuser detection scheme based on canceling cochannel interference for MFSK/FH-SSMA system." *IEEE J. Select. Areas Commun.*, pp. 539–604, May 1994.

[9] A. J. Grant, "Multi-user information theory and coding." Ph.D. dissertation, University of South Australia, Mobile Communications Research Centre, Warrendi Rd. The Levels SA 5095, Australia, May 1996.

[10] J. L. Massey and P. Mathys, "The collision channel without feedback." *IEEE Trans. Inform. Theory*, pp. 192–204, March 1985.

[11] T. Aulin and R. Espineira, "Trellis coded multiple access (TCMA)." in *Proc. Int. Conf. Commun. (ICC99)*, Vancouver, BC, Canada, June 1999, pp. 1177–1181.

[12] F. N. Brännström, "Trellis coded multiple access (TCMA)-detectors and capacity considerations." Ph.D. dissertation, Chalmers University of Technology, Department of Computer Engineering, Göteborg, Sweden., November 2000.

[13] S. Chang and J. K. Wolf, "On the T-user M-frequency noiseless multiple-access channel with and without intensity information." *IEEE Trans. Inform. Theory*, pp. 41–48, January 1981.

[14] A. J. Grant and C. Schlegel, "Collision-type multiple-user communications." *IEEE Trans. Inform. Theory*, vol. 43, pp. 1725–1736, September 1996.

[15] J. Hui, "Throughput analysis for code division multiple accessing of the spread spectrum channel." *IEEE J. Select. Areas Commun.*, vol. SAC-2, pp. 482–486, July 1984.

[16] M. Rupf and J. L. Massey, "Optimum sequence multisets for synchronous code-division multiple-access channels." *IEEE Trans. Inform. Theory*, pp. 1261–1266, July 1994.

[17] D. M. Arnold, C. Schlegel, and L. C. Pérez, "Iterative multiuser detection of a multiple access FSK system." in *Proceedings of the 1997 IEEE International Symposium on Information Theory*, Ulm, Germany, July 1997.

[18] T. Kasami and L. S, "Coding for a multiple-access channel." *IEEE Trans. Inform. Theory*, pp. 129–137, March 1976.

[19] M. A. Deaett and J. K. Wolf, "Non-binary convolutional codes for turbo coding." *Electronics Letters*, pp. 39–40, Jan. 1993.

[20] R. Peterson and J. D. J. Costello, "Binary convolutional codes for a multiple-access channel." *IEEE Trans. Inform. Theory*, pp. 101–105, January 1979.

[21] T. M. Cover and J. A. Thomas, *Elements of Information Theory.* New Yark: Wiley, 1991.

[22] J. Luo, S. Ulukus, and A. Ephremides, "Optimal sequences and sum capacity of symbol asynchronous CDMA systems." *IEEE Trans. Inform. Theory*, pp. 2760–2769, August 2005.

[23] M. V. Hegde and W. E. Stark, "Capacity of frequency-hop spread-spectrum multiple-access communication systems." *IEEE Trans. Comm.*, vol. 38, pp. 1050–1059, July 1990.

[24] J. G. Goh and S. V. Marić, "The capacities of frequency-hopped code-division multiple-access channels." *IEEE Trans. Inform. Theory*, vol. 44, pp. 1204–1211, May 1998.

[25] S. Verdú, "Minimum probability of error for asynchronous Gaussian multiple-access channels." *IEEE Trans. Inform. Theory*, pp. 85–95, Jan 1986.

[26] ——, "Computational complexity of optimum multiuser detection." *Algorithmica*, pp. 303–312, 1989.

[27] M. Moher, "An iterative multiuser decoder for near-capacity communication." *IEEE Trans. Commun.*, pp. 870–880, July 1998.

[28] X. Wang and V. H. Poor, "Iterative (Turbo) soft interference cancellation and decoding for coded CDMA." *IEEE Trans. Commun.*, pp. 1046–1061, July 1999.

[29] P. D. Alexander, M. C. Reed, J. A. Asenstorfer, and C. B. Schlegel, "Iterative multiuser interference reduction: Turbo CDMA." *IEEE Trans. Comm.*, vol. 47, pp. 1008–1014, 1999.

[30] A. B. Reid, A. J. Grant, and P. D. Alexander, "List detection for multi-access channels." vol. 2, pp. 1083–1087, November 2002.

[31] H. E. Gamal and E. Geraniotis, "Iterative multiuser detection for coded CDMA signals in AWGN and fading channels." *IEEE Journal on Selected Areas in Communications.*, vol. 18, pp. 30–41, January 2000.

[32] A. J. Viterbi, "Error bounds for convolutional codes and an asymptotically optimum decoding algorithm." *IEEE Trans. Inform. Theory*, pp. 260–269, April 1967.

[33] P. Robertson, "Illuminating the structure of code and decoder of parallel concatenated recursive systematic (Turbo) codes." in *Proc. CLOBECOM'94*, vol. 3, Dec. 1994, pp. 1298–1303.

[34] L. C. Pérez, J. Seghers, and D. J. C. Jr., "A distance spectrum interpretation of Turbo codes." *IEEE Trans. Inform. Theory*, pp. 1698–1709, November 1996.

[35] F. N. Brännström, T. M. Aulin, and L. K. Rasmussen, "Iterative multi-user detection of trellis code multiple access using a posteriori probabilities." in *Proc. Int. Conf. Commun. (ICC2001)*, Helsinki, Finland, June 2001.

[36] Z. Tang and W. E. Ryan, "Achievable information rate, and the coding-spreading tradeoff in finite-sized synchronous CDMA systems." in *Proc. IEEE CLOBECOM'03*, vol. 3, December. 2003, pp. 1877–1881.

[37] Z. Shi and C. Schlegel, "Joint iterative decoding of serially concatenated error control coded CDMA." *IEEE Trans. Comm.*, pp. 1646–1653, August 2001.

[38] A. J. Grant and P. D. Alexander, "Convergence analysis for iterative multiuser decoding." in *Proc. IEEE PIMRC'2000*, September 2000, pp. 519–523.

[39] S. ten Brink, "Convergence of iterative decoding." *IEE Electron. Lett.*, vol. 35, pp. 806–810, May 1999.

[40] ——, "Design of serially concatenated codes based on iterative decoding convergence." in *2nd International Symposium on Turbo Codes and Related Topics*, Brest, France, 2000.

[41] ——, "Convergence behavior of iterative decoded parallel concatenated codes." *IEEE Trans. Commun.*, vol. 49, pp. 1727–1737, October 2001.

[42] A. Tarable, G. Montorisi, and S. Benedetto, "A linear front end for iterative soft interference cancellation and decoding in coded CDMA." in *Proc. IEEE Int. Conf. Commun.*, vol. 1, Helsinki, Finland, June 2001, pp. 1–5.

[43] K. Li and X. Wang, "EXIT chart analysis of Turbo multiuser detection." *IEEE Trans. Wireless Commum.*, pp. 300–311, January 2005.

[44] F. N. Brännström, T. M. Aulin, L. K. Rasmussen, and A. J. Grant, "Convergence analysis of iterative detectors for narrow-band multiple access." in *Proc. IEEE GLOBECOM'02*, Helsinki, Finland, June 2002.

[45] A. J. Grant, "Convergence of non-binary iterative decoding." in *Proc. IEEE GLOBECOM'01*, San Antonio, Texas, USA, November 2001, pp. 1058–1062.

[46] S. Chang and J. E. J. Weldon, "Coding for T-user multiple-access channels." *IEEE Trans. Inform. Theory*, pp. 684–691, November 1979.

[47] P. R. Chevillat, "N-user trellis coding for a class of multiple-access channels." *IEEE Trans. Inform. Theory*, pp. 114–120, January 1981.

[48] P. A. B. M. C. V. D. Braak and H. C. A. V. Tilborg, "A family of good uniquely decodable codes pairs for the two-access binary adder channel." *IEEE Trans. Inform. Theory*, pp. 3–9, January 1985.

[49] J. H. Wilson, "Error-correcting codes for a T-user binary adder channel." *IEEE Trans. Inform. Theory*, pp. 888–890, July 1988.

[50] B. L. Hughes and A. B. C. III, "Nearly optimal multiuser codes for the binary adder channel." *IEEE Trans. Inform. Theory*, pp. 387–398, March 1996.

[51] V. P. Telang and M. A. Herro, "Error control coding for the N-user mod-2 multiple-access channel." *IEEE Trans. Inform. Theory*, pp. 1632–1642, July 1998.

[52] P. Mathys, "A class of codes for a T active users out of N multiple-access communication system." *IEEE Trans. Inform. Theory*, pp. 1206–1219, November 1990.

[53] G. H. Khachatrian and S. S. Martirossian, "Code construction for the T-user noiseless adder channel." pp. 1953–1957, September 1998.

[54] W. H. Kautz and R. C. Singleton, "Nonrandom binary superimposed codes." *IEEE Trans. Inform. Theory*, pp. 363–377, April 1964.

[55] T. Ericson and V. I. Levenshtein, "Superimposed codes in the Hamming Space." *IEEE Trans. Inform. Theory*, pp. 1882–1893, November 1994.

[56] P. Z. Fan, M. Darnell, and B. Honary, "Superimposed codes for the multiaccess binary adder channel." *IEEE Trans. Inform. Theory*, pp. 1178–1182, July 1995.

[57] J. Cheng and Y. Watanabe, "A multiuser k-ary code for the noisy multiple-access adder channel." *IEEE Trans. Inform. Theory*, vol. 47, pp. 2603–2607, Sept. 2001.

[58] C. Berrou, A. Glavieux, and P. Thitimajshima, "Near Shannon limit error-correcting coding: Turbo codes." *Proc. 1993 IEEE International Conference on Communications, Geneva, Switzerland*, pp. 1064–1070, May 1993.

[59] R. G. Gallager, "Low-density parity check codes." *IEEE Trans. Inform. Theory*, vol. 8, pp. 21–28, Jan 1962.